WH2 domains and actin variants as multifunctional organizers of the actin cytoskeleton

Dissertation
der Fakultät für Biologie der
Ludwig-Maximilians-Universität München
zur Erlangung des akademischen Grades
„Doktor der Naturwissenschaften"
(Dr. rer. nat.)

vorgelegt von

Julia Gallinger

München, 2013

Eidesstattliche Erklärung

Ich versichere hiermit an Eides statt, dass die vorgelegte Dissertation von mir selbständig und ohne unerlaubte Hilfe angefertigt ist.

München, den 11. Juli 2013
Julia Gallinger

Ort der Durchführung

Der experimentelle Teil dieser Dissertation wurde von Juli 2009 bis Juni 2013 im Labor von Prof. Dr. Michael Schleicher am Institut für Anatomie und Zellbiologie der Ludwig-Maximilians-Universität München ausgeführt.

1. Gutachter:	Prof. Dr. Michael Schleicher
2. Gutachter:	Prof. Dr. Barbara Conradt
Eingereicht am:	11. Juli 2013
Tag der mündlichen Prüfung:	16. September 2013

Publications

Journal

2013 Peche VS, Holak TA, Burgute BD, Kosmas K, Kale SP, Wunderlich FT, Elhamine F, Stehle R, Pfitzer G, Nohroudi K, Addicks K, Stockigt F, Schrickel JW, **Gallinger J**, Schleicher M, Noegel AA (2013) Ablation of cyclase-associated protein 2 (CAP2) leads to cardiomyopathy. *Cellular and molecular life sciences : CMLS 70: 527-543*

2011 Sitar T[1], **Gallinger J**[1], Ducka AM, Ikonen TP, Wohlhoefler M, Schmoller KM, Bausch AR, Joel P, Trybus KM, Noegel AA, Schleicher M, Huber R, Holak TA (2011) Molecular architecture of the Spire-actin nucleus and its implication for actin filament assembly. *Proceedings of the National Academy of Sciences of the United States of America 108: 19575-19580*
[1]T.S. and J.G. contributed equally to this work.

Talk

07/2012 Annual International *Dictyostelium* Conference, 2012, Madrid, Spain
Title: Filactin - a primadonna among actin variants.

Poster Presentations

04/2011 Ishikawa-Ankerhold HC, **Gallinger J**, Schleicher M, Characterization of protein rod formation in *Dictyostelium* nuclei, Annual Meeting of the German Society for Cell Biology, 2011, Bonn, Germany

12/2010 **Gallinger J**, Sitar T, Ducka AM, Ishikawa-Ankerhold HC, Holak TA, Schleicher M, The WH2 Domains of Spire Sever Actin Filaments and Show Only Marginal Nucleation Activity, ASCB 50th international meeting, 2010, Philadelphia, PA (Muziol et al)

09/2010 **Gallinger J** and Schleicher M, Actin Variants in *Dictyostelium* Amoebae - Is filactin involved in the ESCRT pathway?, EMBO annual meeting 2010, Barcelona, Spain

09/2010 **Gallinger J** and Schleicher M, Actin Variants in *Dictyostelium* Amoebae - Is filactin involved in the ESCRT pathway?, Actin Dynamics, International meeting of the German Society for Cell Biology, 2010, Jena, Germany

Table of Content

Summary

Actin is one of the most abundant proteins in eukaryotic cells and regulation of the microfilament system is crucial for a wide range of cellular functions including cell shape, cell motility, cell division and membrane dynamics. The aim of this thesis was (1) to gain a better understanding of the function of distinct actin binding domains in the regulation of the actin cytoskeleton and (2) to elucidate the role of actin variants.

WH2 domains (WH2, Wiskott-Aldrich syndrome protein homology 2) are ubiquitous multifunctional regulators of actin dynamics. The protein Spire contains four central WH2 domains A-B-C-D with about 20 amino acids each and the cyclase-associated protein CAP2 contains only one WH2 domain. Under certain conditions, they can (1) nucleate actin polymerization, (2) disintegrate actin filaments and (3) sequester actin monomers. Here, the influence of selected *Drosophila melanogaster* Spire-WH2 and *Mus musculus* CAP2-WH2 domain constructs on actin dynamics was tested *in vitro*. To act as a filament nucleator, at least two WH2 domains are required, and nucleation of actin polymerization was only observed at substoichiometric concentrations of WH2 domains over actin. At higher concentrations, the sequestering activity of WH2 domains takes over. Preformed and purified SpireWH2-actin complexes act as extremely efficient nuclei for actin polymerization, even at superstoichiometric WH2 concentrations, under which free WH2 domains would sequester actin. All analyzed constructs, including these with only a single WH2 domain, sequester actin as well as they can disrupt filaments. This latter and most peculiar behavior of WH2 domains was observed in fluorometric, viscometric and TIRF assays. The WH2 domains seem to have such a high affinity for actin that they can forcefully sequester monomers even from filaments and filament bundles, thus breaking the whole structures. Taken together, the data clearly show that SpireWH2-actin complexes are the intermediates that account for the observed nucleating activity, whereas free WH2 domains can disrupt filaments and filament bundles within seconds, again underlining the intrinsic versatility of this regulator of actin dynamics. These data have been confirmed by crystallography in collaboration with the groups of Prof. Dr. Tad Holak and Prof. Dr. Robert Huber (Martinsried, Germany).

Besides the well-studied conventional actins many organisms harbor actin variants with unknown function. The model organism *Dictyostelium discoideum* comprises an actinome of a total of 41 actins, actin isoforms and actin-related proteins. Among them is filactin, a highly conserved actin with an elongated N-terminus. The 105 kDa protein has a distinct domain organization and homologs of this protein are present in other *Dictyosteliidae* and in some pathogenic *Entamoebae*. Here, the functions of filactin were studied *in vivo* and

in vitro. Immunofluorescence studies in *D. discoideum* localize endogenous and GFP-filactin in the cytoplasm at vesicle-like structures and in cortical regions of the cell. A most peculiar behavior is the stress-induced appearance of full length filactin in nuclear actin rods. To perform *in vitro* analyses recombinant filactin was expressed in Sf9 cells. Fluorescence studies with the filactin actin domain suggest that it interferes with actin polymerization by sequestering G-actin or even capping filaments. Gel filtration assays propose a tetrameric structure of full length filactin. Protein interaction studies suggest that filactin is involved in the ESCRT (endosomal sorting complexes required for transport) pathway which is responsible for multivesicular body formation. The data on filactin suggest that only the conventional actins are the backbone for the microfilamentous system whereas less related actin isoforms have highly specific and perhaps cytoskeleton-independent subcellular functions.

Zusammenfassung

Aktin ist als Bestandteil des Zytoskeletts eines der häufigsten Proteine in allen eukaryontischen Zellen. Eine genaue Regulation des Mikrofilamentsystems ist essentiell für Zellform, Zellmigration, Zellteilung und Membrandynamik. Ziel dieser Arbeit war (1) die Funktion von ausgewählten Aktin Bindedomänen in der Regulation des Aktin Zytoskeletts zu untersuchen und (2) die Funktion von Aktinvarianten zu verstehen.

WH2 Domänen (WH2, Wiskott-Aldrich Syndrom Protein Homologie 2) sind kurze, konservierte Sequenzmotive (ca. 20 Aminosäuren), welche bevorzugt monomere Aktinmoleküle binden. Von besonderem Interesse waren *Drosophila melanogaster* Spire-WH2 und *Mus musculus* CAP2-WH2 Konstrukte. Das Protein Spire enthält vier WH2 Domänen (A-B-C-D) wohingegen CAP2 (Cyclase-assoziiertes Protein 2) nur eine WH2 Domäne besitzt. Diese WH2 Domänen können unter bestimmten Bedingungen (1) die Aktinpolymerisation stimulieren, (2) Aktinfilamente zerstückeln und (3) Aktinmonomere sequestrieren. Für die Nukleation der Aktinpolymerisation müssen mindestens zwei hintereinander angeordnete WH2 Domänen vorhanden sein und unterstöchiometrische Mengen an WH2 Domänen im Vergleich zur Aktinkonzentration vorliegen. Bei höheren WH2 Konzentrationen überwiegt die Sequestrierungsaktivität. Polymerisationsexperimente mit vorgefertigten SpireWH2-Aktin Komplexen bestätigen, dass diese Komplexe für die beobachtete Nukleation der Aktinpolymerisation verantwortlich sind. Im Gegensatz zu ungebundenen WH2 Domänen sind diese WH2-Aktin Komplexe selbst bei überstöchiometrischen WH2 Konzentrationen äußerst effiziente Nukleatoren. Alle untersuchten WH2 Konstrukte zeigen die bereits bekannte Bindung an G-Aktin, können aber auch vorgeformte Aktinfilamente sogar auseinanderreißen. Diese letztere und besonders auffällige Eigenschaft von WH2 Domänen wurde in fluorometrischen, viskometrischen und TIRF Experimenten nachgewiesen. Anscheinend ist die Affinität der WH2 Domänen zu Aktinmonomeren so stark, dass sie diese aus den Filamenten entfernen können und damit ganze Filamente und Filamentbündel zerstückeln. Für die Multifunktionalität der analysierten konservierten WH2 Domänen spricht zusammenfassend, dass sie neben der Aktinfilament Nukleation auch Filamente und Filamentbündel innerhalb von Sekunden fragmentieren können. Diese Daten wurden in Kollaboration mit den Gruppen Prof. Dr. Tad Holak und Prof. Dr. Robert Huber (Martinsried) durch kristallographische Versuchsansätze bestätigt.

Neben den gut untersuchten konventionellen Aktinisoformen liegen oft auch Aktinvarianten vor, deren Funktion bisher unbekannt ist. Der Modellorganismus *Dictyostelium discoideum* besitzt mit seinen 41 Aktinen und Aktin-verwandten Proteinen ein umfangreiches

„Aktinom". Dazu gehört auch das Protein Filaktin (105 KDa), eine besonders außergewöhnliche Aktinvariante, die neben der konservierten Aktin-ähnlichen Domäne zusätzlich einen verlängerten N-Terminus mit einer definierten Domänenstruktur besitzt. Homologe von Filaktin wurden bisher in Dictyosteliden und einigen pathogenen Entamoeben identifiziert. Im zweiten Teil dieser Arbeit wurden die Funktionen von Filaktin *in vivo* und *in vitro* analysiert. Immunfluoreszenz Experimente zeigen, dass Filaktin mit konventionellem Aktin kolokalisiert und zusätzlich im Zytoplasma an Vesikel-artigen Strukturen zu sehen ist. Ein besonderes Merkmal von Filaktin ist zudem, dass es Teil von Stress-induzierten, intranukleären, stäbchenförmigen Proteinaggregaten, sogenannten „nuclear rods" ist. Für umfassende *in vitro* Experimente wurden rekombinante Filaktin Konstrukte mithilfe von Sf9 Insektenzellen exprimiert. Die Ergebnisse von fluorometrischen und viskometrischen Experimenten deuten darauf hin, dass die Aktin Domäne von Filaktin Aktinmonomere sequestrieren oder sogar Aktinfilamente verkappen kann. Gelfiltrationsexperimente ergaben zusätzlich, dass Filaktin wohl als Tetramer vorliegt. Außerdem verbinden Protein-Interaktionsstudien Filaktin mit dem ESCRT Signalweg (Endosomal Sorting Complexes Required for Transport), der unter anderem bei der Entstehung von multivesikulären Körpern wichtig ist. Zusammengefasst besteht das Mikrofilamentsystem vermutlich hauptsächlich aus konventionellen Aktinen, wohingegen spezielle Aktinvarianten andere zusätzliche und sogar Zytoskelett-unabhängige Funktionen übernehmen können.

1. Introduction

1.1 The actin cytoskeleton

The three major components of the cytoskeleton in eukaryotic cells are (1) microfilaments, (2) microtubules and (3) intermediate filaments. The filaments provide the cell with structure, shape, internal transport tracks and enable cell movement as well as cell division. Actin constitutes the microfilament system and is a highly conserved and abundant protein, making up to 5 – 10 % of the total cell protein. It was initially isolated from frog muscle (Halliburton, 1887) and purified, named and described by Straub (Straub, 1942). Actin is a protein of about 42 kDa with a characteristic structure of four subdomains and an ATP binding cleft between the main-domains one and two. Actin is present in two forms, as (1) monomeric, globular actin (G-actin) and as (2) polymeric, filamentous actin (F-actin). The filaments consist of two helical, interlaced strands of monomeric actin subunits resulting in a right handed helix with a diameter of about 7-9 nm. *De novo* formation of actin filaments requires an actin 'nucleus' which is essentially an actin trimer. The formation of such a nucleus is kinetically unfavorable, but once it is formed, further monomers elongate the filament spontaneously (figure 1).

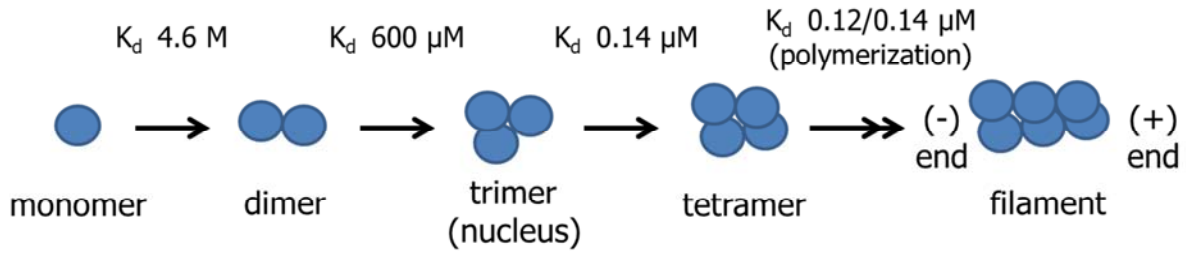

Figure 1: The process of spontaneous actin polymerization. Spontaneous actin assembly is highly inefficient as the formation of actin dimers and trimeric 'nuclei' is kinetically unfavorable as represented by the calculated dissociation constants (Sept & McCammon, 2001). Once a nucleus is formed, addition of further actin molecules is accelerated by more than three orders of magnitude. Therefore, *in vivo* initiation of actin polymerization from free actin monomers requires nucleation factors that help to overcome this lag phase.

In vitro, actin polymerization continues until almost all G-actin is consumed attaining the so-called steady state. In this situation, the system reaches a balance between actin assembly and disassembly, which occurs in an asymmetric way: ATP-loaded monomers are preferentially added at the 'barbed'/plus end of the filament and ADP-actin monomers dissociate from the 'pointed'/minus end. This happens since the minimal concentration of G-actin required for addition of monomers (critical concentration) is lower at the plus end (ca. 0.1 µM) than at the minus end (ca. 0.8 µM). The ATP-loaded actin which is incorporated into

the filament releases the phosphate a short time after addition and remains as ADP-actin in the filament. Therefore, filaments are polar not only because of the structural asymmetry of monomers they are built of but also because the growing plus end is marked by newly added ATP-actin, whereas the minus end consists of ADP-actin subunits.

In vivo, the average actin concentration is about 100 µM and due to intracellular Mg^{2+} and K^{+} concentrations the entire actin would polymerize spontaneously. However, all steps in actin dynamics are regulated by actin binding proteins. The nucleation of filaments is triggered by proteins like the ARP2/3 complex, formins or WH2 domain containing nucleators like Spire, which will be discussed below. Profilin or β-thymosins control the pool of available, non-filamentous actin by sequestering G-actin. Furthermore, profilin also ensures the efficient exchange of ADP for ATP in the actin molecule. ADP-actin stretches within filaments are preferred targets for severing or disassembling proteins, like gelsolin, severin or cofilin. Finally, there are proteins that can 'cap' the plus or the minus end of a filament, thereby inhibiting polymerization or protecting the filament from depolymerization. Tropomodulin capping the minus end thus stabilizes F-actin and CapZ by binding to the plus end of the filament prevents further elongation.

The number of actin genes among eukaryotes is highly variable. *Saccharomyces cerevisiae* possesses only one gene that encodes conventional actin, *Arabidopsis thaliana* contains 10, and *M. musculus* has 35 genes that code for actin proteins (Joseph et al, 2008; McKinney & Meagher, 1998). In humans, actins are classified based on cell type and location: there are specific actins in cardiac, skeletal or smooth muscle tissues or only present in the cytoplasm (McHugh et al, 1991; Vandekerckhove & Weber, 1978). It is still unknown why almost identical isoforms are so different in their localization and furthermore, what the functions of other, yet uncharacterized actin isoforms are.

There are many diseases associated with defective actin dynamics in the cell, including muscular, neurological, immunological, vascular diseases and even cancer (Cleuren & Boonstra, 2012). A dysfunction of actin protein can lead to nemaline myopathies in mammals. The intranuclear rod myopathy (IRM) is in the majority of cases a result of a Val163Leu mutation in ACTA1, the actin gene expressed in skeletal muscle (Domazetovska et al, 2007; Kaimaktchiev et al, 2006; Sparrow et al, 2003; Vandebrouck et al, 2010). This mutation results in the accumulation of rod-shaped protein aggregates in the nuclei and the cytoplasm of the muscle cells (figure 2).

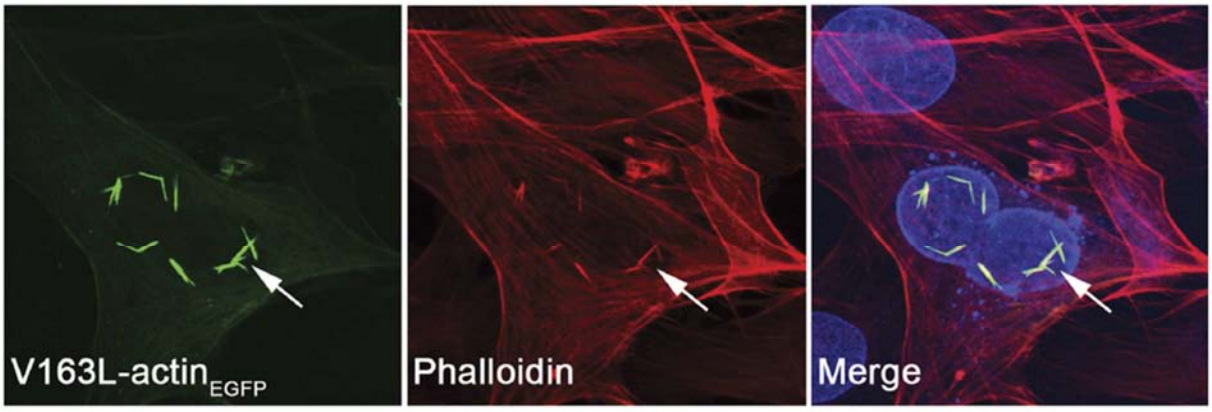

Figure 2: Intranuclear rods as a result of a mutation in the α-skeletal muscle actin protein (Vandebrouck et al, 2010). Intranuclear rods were induced by the transfection of V163L-actin$_{EGFP}$ in C2C12 myoblasts. Actin was stained with TRITC-phalloidin (red) and nuclei were labeled with emerin (blue). The arrows accentuate the intranuclear rods, which can be stained with phalloidin, indicating that they are formed by filamentous actin.

The symptoms of the patients with this congenital disease comprise a delay in speech and walking development, early-onset hypotonia, hyporeflexia, generalized muscle weakness, absent tendon reflexes, feeding difficulties, or respiratory insufficiency (Kaimaktchiev et al, 2006). The nemaline bodies comprise mutated actin, nebulin, cofilin, troponin and tropomyosin but the exact composition, formation and biophysics of these rods are yet unknown. Possibly, due to continuous muscle contraction, the chromatin of the cell is harmed by the rod-shaped aggregates in the nucleus, finally leading to cell death (Hutchinson et al, 2006; Nowak et al, 1999; Sparrow et al, 2003).

1.2 The WH2 domain containing proteins Spire and CAP2

The Wiskott-Aldrich-Syndrome protein homology domain 2 (WH2) is a 17–27 amino acid long actin binding motif found in a number of different proteins. WH2 domains are intrinsically disordered and adopt an α-helical form upon binding to actin (Czisch et al, 1993). The main structural element for actin binding is a conserved N-terminal amphipathic helix of variable length (Chereau et al, 2005). The C-terminal part contains the consensus motif L++V/T, with '+' representing basic amino acids. As the fourth amino acid, threonine or valine, but also alanine or serine are found very often. The proteins Spire and CAP2 contain four and one WH2 domain, respectively.

Spire was identified in *D. melanogaster* as a factor required for dorsal-ventral and anterior-posterior patterning of the embryo (Manseau & Schupbach, 1989) and was described as a WH2 domain containing actin nucleator (Quinlan et al, 2005). Figure 3 A shows the domain structure of *D. melanogaster* Spire. The KIND domain (the kinase

noncatalytic C-lobe domain, residues 90–328 in *D. melanogaster* Spire, figure 3 A, red) was identified to interact with the nucleating factor Cappuccino (fly formin) (Quinlan et al, 2007; Rosales-Nieves et al, 2006). Quinlan, Rosales-Nieves and others revealed that Spire by binding to Cappuccino, inhibits Cappuccino-driven nucleation and actin bundling, but at the same time enhances the WH2 domain driven nucleation of Spire. The four central WH2 domains of Spire, namely A-B-C-D, contain motifs of about 20-21 amino acids and are separated by the following linker sequences: L1 between domains A and B contains 10 amino acids, L2 between domains B and C 11 amino acids, and L3 between domains C and D 12 amino acids. The C-terminus of Spire contains the FYVE zinc finger membrane localization domain (Kerkhoff, 2006; Otto et al, 2000), a domain which is found in many proteins involved in membrane trafficking. The Spir box is a highly conserved region and potential interaction site for Rab-GTPases (Kerkhoff et al, 2001; Ostermeier & Brunger, 1999). At the very C-terminus, the c-Jun N-terminal kinases (JNK) binding domain is localized. In this region the mitogen activated protein (MAP) kinase can bind and phosphorylate the protein (Otto et al, 2000). Spire was extensively discussed recently and until now, it is known that the four WH2 domains ABCD nucleate actin assembly at low Spire/actin ratios and sequester actin at high Spire/actin ratios (Bosch et al, 2007; Campellone & Welch, 2010; Ducka et al, 2010; Quinlan et al, 2005; Quinlan et al, 2007). However, the mechanisms through which Spire nucleates or sequesters actin were a matter of debate.

The cyclase-associated protein (CAP) was first identified in *S. cerevisiae* (Field et al, 1988; Field et al, 1990). It was then further found in various other species like plants, yeast, *D. discoideum, D. melanogaster* and mammals. In higher eukaryotes, two isoforms of this highly conserved and widely distributed protein can be found, namely CAP1 and CAP2, showing about 76 % similarity. CAP in lower eukaryotes and mouse CAP1 were described to be implicated in cell polarity, motility and receptor-mediated endocytosis (Bertling et al, 2004; Noegel et al, 2004; Sultana et al, 2005). In mice, CAP1 is highly abundant and expressed in almost all cells and organs (Bertling et al, 2004) localizing to F-actin-rich regions (Peche et al, 2007). In contrast, CAP2 in mice is only expressed in brain, heart, skeletal muscle and skin (Peche et al, 2007). In these tissues, the less well studied CAP2 localizes in the nucleus or to myofibrillar M-bands (Peche et al, 2007). The ablation of CAP2 in mice leads to a dilated cardiomyopathy (Peche et al, 2013). The multifunctional, actin-associated CAPs have a quadripartite domain structure (figure 3 B). The N-terminal domain mediates nutrition-dependent RAS signaling through binding to the adenylyl cyclase in yeast, but not in other organisms. In *D. discoideum* the amino-terminal domain is important for dimerization and localization of the protein to the cell cortex (Noegel et al, 1999). The N-terminal domain is separated from the C-terminal domain by a proline-rich region which

allows binding of proteins containing SH3 domains (figure 3 B, green). The WH2 domain is followed by the C-terminal domain which binds to G-actin and is responsible for oligomerization (Zelicof et al, 1996). The interaction of CAP1 with G-actin was well investigated, and a role in the regulation of actin dynamics by regulating the ADP/ATP exchange on G-actin could be assigned (Bertling et al, 2004; Makkonen et al, 2013; Moriyama & Yahara, 2002). It is known that CAPs are involved in the organization of the actin cytoskeleton and that WH2 domains bind to G-actin, but the function of the WH2 domain in mouse CAP2 is not clearly known.

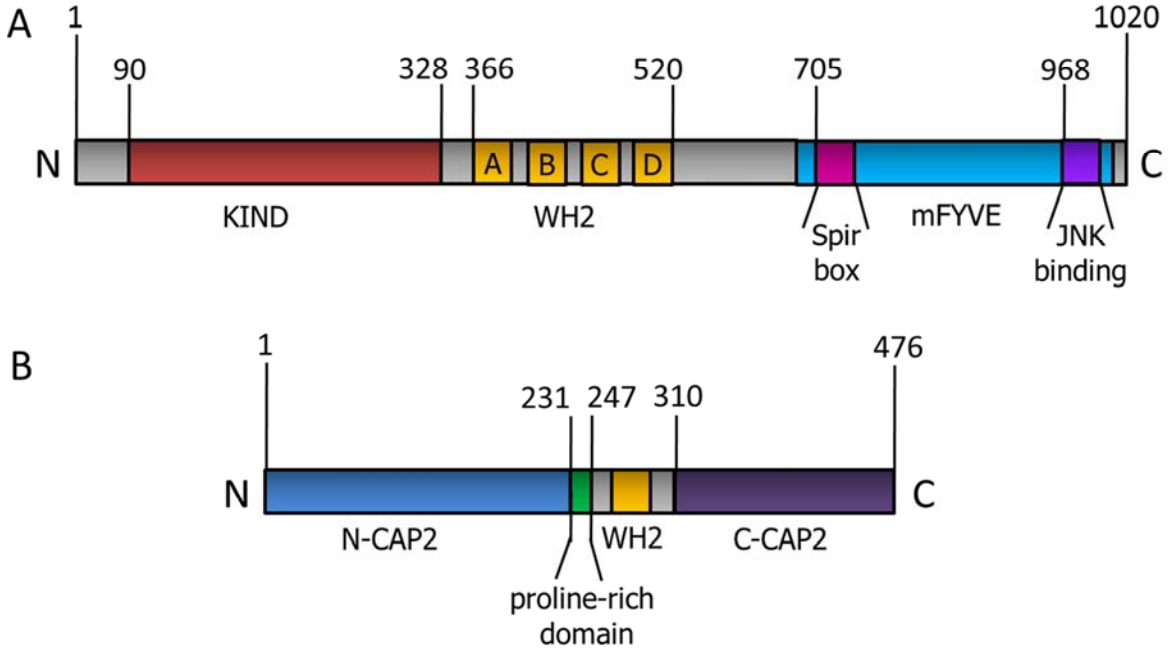

Figure 3: Domain organization of the WH2 domain containing proteins Spire and CAP2. A) *D. melanogaster* Spire consists of 1020 amino acids. The four WH2 domains (yellow) are located in the middle of the protein sequence. B) *M. musculus* CAP2 consists of 476 amino acids. The WH2 domain (yellow) is situated in the C-terminal half of the protein.

1.3 *D. discoideum* as a model system

D. discoideum is a motile soil amoeba which was first isolated and characterized by Kenneth B. Raper (Raper, 1935). The social amoeba belongs to the phylum *Mycetozoa* and shows an extraordinary life cycle that classifies the amoeba as a linker between unicellular and multicellular organisms (figure 4). The professional phagocyte usually lives on forest soil and feeds on bacteria, but upon starvation it undergoes a specific development program leading to the formation of extremely stable spores. The wild type strain AX2 used in this work is derived from the strain NC4 isolated by Raper. AX2 can grow in the simplified axenic medium

AX and HL5 (Schwalb & Roth, 1970; Watts & Ashworth, 1970). In the laboratory, the entire life cycle of *D. discoideum* happens within about 24 hours (Chisholm & Firtel, 2004). The genome of *D. discoideum* is completely sequenced (Eichinger et al, 2005; Glockner et al, 2002) and the haploid chromosome set allows direct analysis of molecular genetic defects (e.g. after specific gene disruption). *D. discoideum* cells share activities with human neutrophils (Devreotes & Zigmond, 1988; Parent, 2004), including cell motility, chemotaxis and phagocytosis. Since *D. discoideum* laboratory culture is easy and inexpensive, highly accessible for biochemical, molecular genetic and cell biological studies, it is a prime organism to analyze the activities of single molecules in their cellular environment.

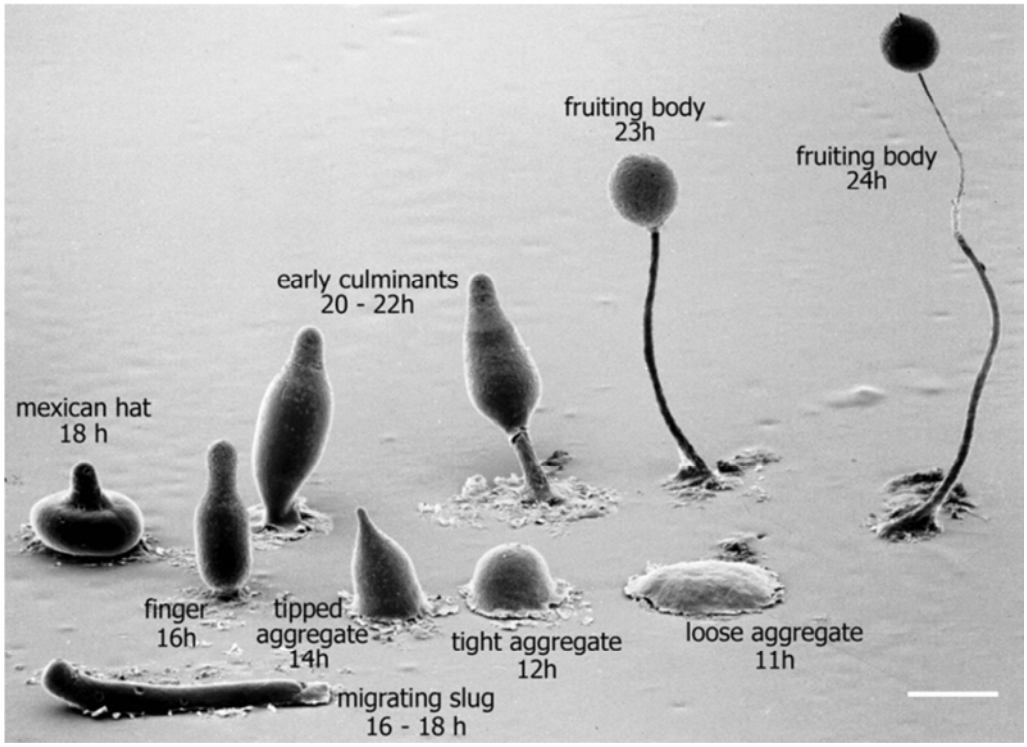

Figure 4: Life cycle of *D. discoideum* (M.J. Grimson & R.L. Blanton, Biological Sciences Electron Microscopy Laboratory, Texas Tech University). The amoebae undergo various developmental stages in response to nutritional stress. The unicellular, vegetative cells start to aggregate when deprived from nutrition until they form a fruiting body with a sorus that contains extremely stable spores. Once favorable conditions are restored, the spores will germinate and the life cycle starts again. The slug phase (16-18h) is sometimes bypassed in native conditions. Nevertheless, all indicated stages can be observed under laboratory conditions within about 24 hours. Scale bar, 500 µm.

D. discoideum is a powerful model organism that has long been used particularly for studying the actomyosin cytoskeleton and chemotactic motility in non-muscle cells. Intriguingly, *Dictyostelium* amoebae comprise a great number of actin variants. *D. discoideum* harbors 33 actins and 8 actin-related proteins (ARPs) (Joseph et al, 2008). The *D. discoideum* 'actinome' comprises the act8-group, which contains 17 distinct genes that

encode identical actin proteins. 95 % of the total actin in a *D. discoideum* cell consists of this isoform (Joseph et al, 2008; Vandekerckhove & Weber, 1980). The functions of the 16 actin variants that differ more or less from the conventional actin remain to be characterized.

1.4 Filactin, an actin variant in *D. discoideum*

Filactin is a novel actin-like protein in *D. discoideum* with a molecular weight of 105,000. Its actin domain is located at the C-terminus and its N-terminus shows a distinct domain organization (figure 5). The filactin actin domain has such a high homology to conventional actin that filactin can be described as an actin variant with extended N-terminus. Interestingly, two short filamin-like sequences in the N-terminal part of the protein lead to filactin's discovery during the *Dictyostelium* Genome Project at the University of Cologne (Eichinger et al, 2005; Glockner et al, 2002) when searching for filamin-like proteins. Due to the homology to filamin and actin the protein was named filactin. Filamins are large, homodimeric flexible actin binding proteins which can stabilize three-dimensional actin webs (Janssen et al, 1996). Furthermore, they can link these cross-linked actin networks to cellular membranes. Filamins combine cellular architectural and signaling functions and are crucial for development and cell movements (Stossel et al, 2001). The homology of filactin to filamin relies not on the actin binding domain of filamin but on the sequence that connects the actin binding domains. This sequence consists of highly homologous repeats of about 96 amino acid residues, which adopt an immunoglobulin (Ig) -like fold (Popowicz et al, 2006). The N-terminal domain of filactin shows a homology to two of these repetitive motifs. Furthermore, at the very N-terminus of filactin, an Ist1-like domain was identified (figure 5, yellow), followed by a PEST-motif (figure 5, orange). The Ist1-like domain shows homology to the N-terminus of human and yeast IST1/Ist1 which is a protein implicated in the ESCRT-pathway (ESCRT, endosomal sorting complexes required for transport).

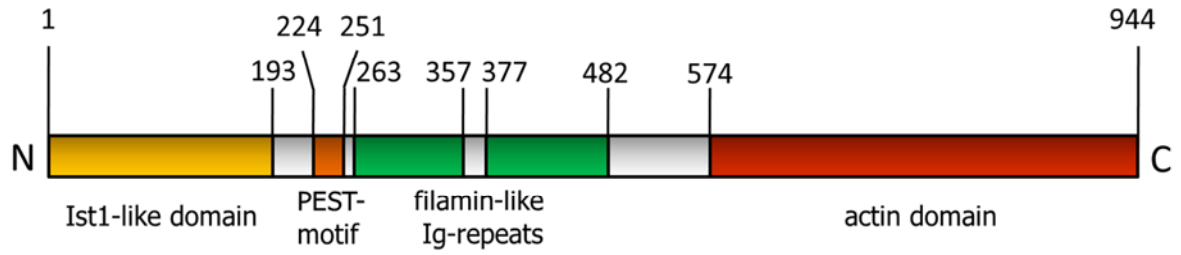

Figure 5: Domain organization of the actin variant filactin. Filactin consists of 944 amino acids, resulting in a molecular mass of about 105,000 Da. The actin domain (red) which shows higher homology to muscle actin than to actin-related proteins is located at the C-terminus. The N-terminus harbors an Ist1-like domain (yellow), a PEST-motif (orange) and two filamin-like Ig-repeats (green).

D. discoideum comprises one copy of the filactin gene, located on chromosome 4. The 3 kb gene contains two introns and the mRNA is present throughout the development. At the protein level the ratio of actin to filactin is approximately 200/1.

Until now, the protein filactin was only found in *Dictyosteliidae* and some *Entamoeba* species, among them the protozoan pathogenic *Entamoeba histolytica*. This parasite causes amoebiasis in humans and is responsible for approximately 100,000 deaths annually, making it, after *Plasmodium*, the second leading cause of death due to a parasite infestation (Ralston & Petri, 2011). The WHO considers amoebiasis as one of the major health problems in developing countries (WHO, 1997). The active stage of *E. histolytica* exists only in the host and in fresh feces, but the more robust cysts survive outside the host in water, soils and on food. The transmission occurs mainly by uptake of contaminated food or water. Even though the presence of filactin is yet only confirmed in *Dictyosteliidae* and certain *Entamoebae*, homologues presumably exist also in higher organisms but have not been identified so far.

1.5 The ESCRT machinery

The endosomal sorting complexes required for transport (ESCRTs) catalyze one of the most peculiar and unusual membrane remodeling events known in cell biology. The protein complexes ESCRT-I and ESCRT-II direct membrane budding away from the cytoplasm by stabilizing the bud neck from the cytosolic face without being consumed in the bud and without coating the cytoplasmic side of the bud. ESCRT-III subsequently cleaves the bud neck. Thus, the topology of scission accomplished by the ESCRT machinery is basically opposite to that of the dynamin family of membrane-scission proteins, which cleave membrane necks by forming a spiral around the membrane neck and constricting it in a GTP-dependent fashion from the outside. The ESCRT machinery consists of five protein

complexes, ESCRT-0, ESCRT-I, ESCRT-II, ESCRT-III, the vps4-vta1 complex and several ESCRT-related proteins (Saksena et al, 2007; Williams & Urbe, 2007). The ESCRT machinery is conserved from archaea to mammals and was first characterized in yeast. ESCRT-III mediated cleavage is essential for many processes, especially for the biogenesis of multivesicular bodies (MVBs), viral budding, cytokinesis and most probably autophagy (figure 6 and review Hurley & Hanson (2010)).

The role of ESCRTs was initially investigated in the formation of MVBs (Babst et al, 2002a; Babst et al, 2002b; Katzmann et al, 2001). MVBs are specialized endosomes containing intraluminal vesicles (Gruenberg & Stenmark, 2004; Piper & Katzmann, 2007). Ubiquitylated cell-surface receptors and other transmembrane proteins that are destined for degradation in the vacuole (yeast) or in the lysosome (mammals) are sorted through the formation of MVBs. In this case, ESCRT-0 clusters ubiquitylated cargo on the early endosome, ESCRT-I and –II induce the bud formation and confine the cargo, and subsequently recruit ESCRT-III which effects the membrane scission away from the cytoplasm into the lumen of the endosome, turning it into a multivesicular body. ESCRT-0, -I and -II are soluble complexes that cycle between cytosolic and membrane-bound states. In contrast, the ESCRT-III subunits stay bound to the membrane of the MVB as tightly bound filaments, tubes and spirals after completed cleavage of the membrane bud (Ghazi-Tabatabai et al, 2008; Hanson et al, 2008; Lata et al, 2008). To recycle the ESCRT-III subunits back into the cytoplasm, the multimeric AAA-type ATPase vps4 and the protein vta1 are needed. In the only energy requiring step of the ESCRT pathway, the ESCRT-III complex is disassembled in the ATP-dependent action of vps4-vta1 (Babst et al, 1997; Babst et al, 1998).

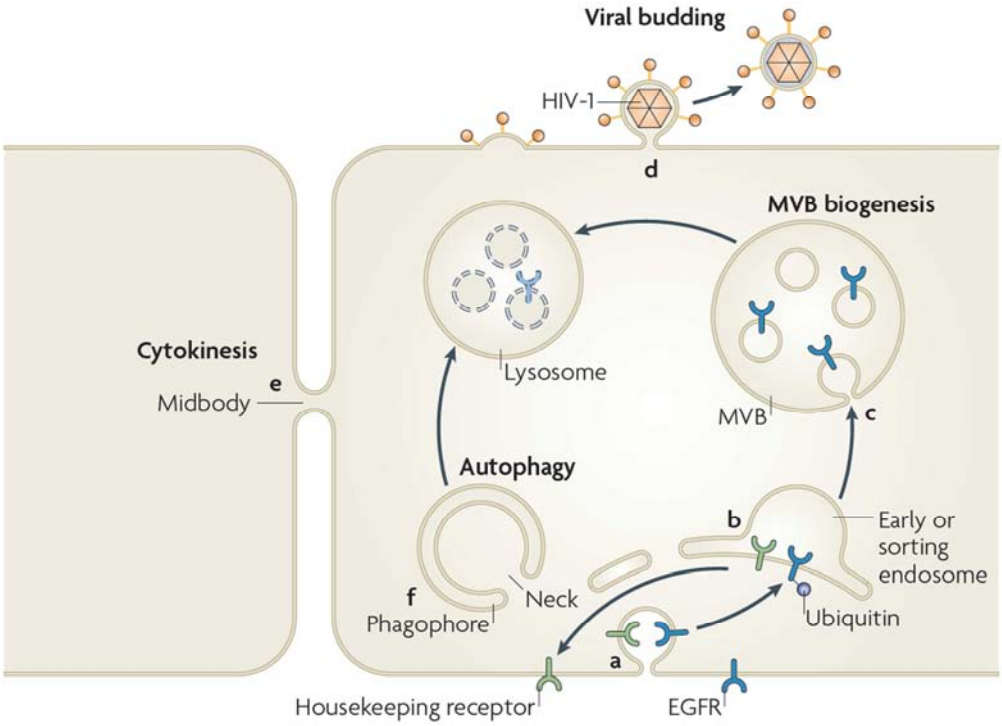

Figure 6: Biological roles of the ESCRTs (Hurley & Hanson, 2010). a) Plasma membrane proteins are endocytosed and ubiquitylated after stimulation. This initial endocytosis is independent of the ESCRT machinery. b) Some receptors and cargos that are not destined for degradation are recycled. c) Multivesicular body (MVB) biogenesis involves clustering of ubiquitylated cargo, the formation of membrane buds and the cleavage of the buds to form intraluminal vesicles (ILVs). For this process all ESCRTs are required. d) All ESCRT-dependent virus budding needs ESCRT-III and vps4. HIV-1 budding additionally needs ESCRT-I. e) Cytokinesis in animal cells needs ESCRT-I, ESCRT-III and vps4. The final cleavage of the membrane neck resulting in the separation of the two daughter cells, is mediated by ESCRT proteins. In Crenarchaeota, ESCRT-III and vps4 are required for cytokinesis. f) Autophagy seems to require all ESCRTs, although it is not clear whether they act directly or indirectly. The presence of ESCRTs during the neck closure has never been confirmed. However, there is an intriguing analogy between the closure of the phagophore neck and the formation of ILVs. An autophagosome has the same topology as a MVB but just with a single ILV, thus it is tempting to speculate about the involvement of the ESCRT machinery in the neck closure process.

The ESCRT pathway was recently investigated in yeast and human, and still new proteins implicated in the machinery continue to be identified. There is a lack of knowledge about the ESCRT machinery in *D. discoideum*. However, the homologous proteins of the ESCRT machinery were identified in *Dictyosteliidae* as well and there are a few studies that support an existence of the ESCRT pathway in *D. discoideum* (Blanc et al, 2009; Mattei et al, 2006). Until now, no protein was found that links the ESCRT pathway to the microfilament system.

1.6 Thesis aims

At the beginning of the experimental part of the thesis, two major questions had to be answered.

(1) Have the well-known and well-studied WH2 domains more activities than just the sequestration of G-actin and how do they influence the dynamics of the actin cytoskeleton?

(2) Do selected actin variants belong to the general pool of conventional actin isoforms or are they specific proteins that just share a sequence homology and are not primary components of the actin cytoskeleton?

Therefore, one aim of this work was to analyze the function of the WH2 domains of *D. melanogaster* Spire and *M. musculus* CAP2 *in vitro*. To that end, recombinant proteins needed to be purified to test their influence on actin dynamics in fluorometric, viscosity, TIRF and spindown assays. In parallel, *in vivo* approaches should shed light on the function of these domains on cell migration and adhesion. A collaborative effort with crystallography groups should, if possible, explain the molecular mechanisms of these additional activities of WH2 domains.

The second aim focused on filactin, a novel actin variant in *D. discoideum*. This protein carries a conserved actin domain, but also an extended N-terminus with a distinct domain organization. Therefore, the experiments had to investigate the influence of filactin on the microfilament system *in vivo* and *in vitro*. Using the example of filactin, the possible roles of actin variants in eukaryotic cells should be examined. Especially immunofluorescence and spindown experiments attempted to clarify whether filactin is part of the microfilament system; additionally, recombinant filactin was to be generated and purified to apply it in fluorometric, viscometric and gel filtration assays. Furthermore, a screen for interaction partners of the N-terminal domains of filactin aimed to identify filactin's role within the cell.

2. Material and Methods

2.1 Material

2.1.1 Instruments

ÄKTA purifier 100	Amersham Biosciences
Balances	Sartorius
BioDocAnalyze	Biometra
Dounce homogenizer	Braun/Wheaton
Fluorescence Spectrometer LS 55	Perkin Elmer
Gene pulse electroporator Xcell	BioRad
Gelsystem MiniPROTEAN	BioRad
PCR-Thermocycler Tpersonal	Biometra
pH-meter pH720	Inolab WTW series
Power supplies	BioRad, Biometra, Consort
Protein Transfer Transblot Semi-Dry	BioRad
Protein Transfer TF 77XP	Serva
Shaker Orbital Incubator SI500	Stuart
Shaking incubator with temperature control	Memmert
Shakers for *Dictyostelium* cultures	Kühner
Sonficator Sonifier250	Banson
Thermomixer	Eppendorf
Tabletop Film Processor Curix 60	Agfa
Vortex Genie 2	Bender & Hobein
Waterbath	GFL, Kühner

Microscopes

Axiovert 25	Carl Zeiss
Axiovert 200M	Carl Zeiss
LSM 510 Meta confocal microscope	Carl Zeiss

Objectives

10x A-Plan 0.25 Ph1	Carl Zeiss
20x LD A-Plan 0.30 Ph1	Carl Zeiss

40x LD A-Plan 0.50 Ph2	Carl Zeiss
63x Neofluar 1.4 oil immersion objective	Carl Zeiss
100x Neofluar 1.3 oil immersion objective	Carl Zeiss

Centrifuges

GS-6KR	Beckman
J2-21M/E	Beckman
J6-HC	Beckman
Microcentrifuge 5415 D, 5417 R	Eppendorf
Optima LE-80K	Beckman
Optima TL ultracentrifuge	Beckman

Rotors

JA-10, JA-14, JA-20	Beckman
Ti35, Ti45, Ti70	Beckman
TLA 100.3	Beckman

2.1.2 Computer Programs

Adobe Creative Suite 2	Adobe Systems
ApE plasmid editor v1.10.4	M. Wayne Davis
AxioVision	Carl Zeiss
BioDoc Analyze	Biometra
BioEdit 7.0.9.0	Tom Hall
EndNote X5	Thomson Reuters
FL WinLab	Perkin Elmer
ImageJ 1.44p	Wayne Rasband
LSM 5, 4.2 SP1	Carl Zeiss
Microsoft Office	Microsoft Corporation
Multalin 5.4.1.	Florence Corpet
SigmaPlot 2000	SPSS Inc.
Unicorn 5.20	GE Healthcare
ZEN	Carl Zeiss

2.1.3 Laboratory consumables

1.5 ml centrifuge tubes	Sarstedt
Amersham Hyperfilm ECL	GE Healthcare
Cell culture plates, 24 wells	Starlab Int.
Cell culture dishes, Ø 100 mm x 20 mm	Greiner bio-one
Dialysis tubings Type 8, 20, 27	Biomol
Gel-blotting paper 3MM Chr	Whatman
GFP-Nano-Trap	Chromotek
High Pure Plasmid Isolation Kit	Roche
High Pure PCR Product Purification Kit	Roche
High precision cuvettes 10mm	Hellma
Nitrocellulose transfer membrane Protran BA85	Whatman
PCR tubes Thermo Tube 0.2 ml	Peqlab
PCR product cloning kit	Qiagen
Phusion High-Fidelity DNA Polymerase	New England Biolabs
Petri dishes Ø 92 mm x 16 mm	Sarstedt
Pipettes 10 ml, 25 ml	Sarstedt
Pipet tips	Biozym, Gilson, Starlab
Plasmid DNA Purification Maxi Kit	Macherey Nagel
Restriction Enzymes	New England Biolabs
RNeasy Mini Kit	Qiagen
Sterile filter, Filtropur S 0.2	Sarstedt
Transcriptor High Fidelity cDNA Synthesis Kit	Roche
Tubes 15 ml, 50 ml	Sarstedt
Ultracentifuge tubes 1.5 ml	Beckman

2.1.4 Reagents

Standard laboratory chemicals were mainly purchased from Biomol, Biorad, Fluka, Invitrogen, Merck, Peqlab, Roche, Roth, Serva or Sigma-Aldrich and had the degree of purity 'p.a.' unless otherwise mentioned. Media and buffers used in this study were prepared with de-ionised water (Millipore), sterilized either by autoclaving or passing through a micro-filter (pore size 0.2 µm).

2.1.5 Antibodies

Monoclonal antibodies used in this study:

Actin, *D. discoideum* (Act-1)	Simpson et al (1984)
Actin, *D. discoideum* (224-236-1)	Westphal et al (1997)
GFP (K3-184-2)	Noegel et al (2004)
GST (268-44-6)	Faix et al (1998)
Filactin N-terminal (3S-55-4)	Daniela Rieger
Filactin C-terminal (4S-59-4)	Daniela Rieger
Interaptin (260-60-10)	Rivero et al (1998)
RFP (K64-372-1)	Angelika Noegel

Secondary antibodies used in this study:

Goat-anti-mouse IgG Cy3-conjugated	Invitrogen
Anti-mouse IgG horseradish peroxidase-linked (ECL)	GE Healthcare

2.1.6 Vectors

Constructs used in this study:

pDEX-GFP(g418)-N1	Meino Rohlfs
pDEX-GFP(g418)-N2	Meino Rohlfs
pDEX-GFP(g418)-C2	Meino Rohlfs
pDRIVE	Qiagen
pFastBac1	Invitrogen
pGEX-6P-1	GE Healthcare
pLPBLP	Faix et al (2004)
pDEXH (g418) mRFP-ATG8	Jan Matthias
pDEXH (g418) mRFP-ATG8-like	Jan Matthias
pDEX (g418) GFP-cofilin (#249-5)	Annette Müller-Taubenberger

Constructs generated in this study:

pDEX-GFP(g418)-N2 filactin full length	BamHI/SalI
pDEX-GFP(g418)-C2 filactin full length	BamHI/XhoI-SalI
pDEX-GFP(g418)-N2 filactin Ist1-like	BamHI/SalI
pDEX-GFP(g418)-N2 filactin filamin-like Ig repeats	BamHI/SalI
pDEX-GFP(g418)-N1 filactin actin-like	BamHI/SacI
pDEX-GFP(g418)-C2 filactin actin-like	BamHI/XhoI-SalI
pDEX-GFP(g418)-N2 vta1	BamHI/SalI
pDEX-GFP(g418)-N2 vps4	BamHI/SalI
pDEX-GFP(g418)-N2 vps46	BamHI/SalI
pGEX-6P-1 filactin full length	BamHI/SalI
pGEX-6P-1 filactin Ist1-like	BamHI/SalI
pGEX-6P-1 filactin filamin-like Ig repeats	BamHI/SalI
pGEX-6P-1 vta1	BamHI/SalI
pGEX-6P-1 vps4	BamHI/SalI
pGEX-6P-1 vps46	BamHI/SalI
pFastBac1 filactin full length	BamHI/SalI
pFastBac1 GFP-filactin full length	SalI/NotI
pFastBac1 filactin actin-like	BamHI/SalI
pFastBac1 GFP-filactin actin-like	SalI/NotI
pLPBLP vps4	SalI/ClaI, PstI/NotI

2.1.7 Bacterial strains

E. coli DH5α	Invitrogen
E. coli DH10Bac	Invitrogen
E. coli BL21 RIL	Stratagene
E. coli ArcticExpress RIL	Stratagene
E. coli DH10Bac FLAG-filactin full length	Present study
E. coli DH10Bac FLAG-GFP-filactin full length	Present study
E. coli DH10Bac FLAG-filactin actin-like	Present study
E. coli DH10Bac FLAG-GFP-filactin actin-like	Present study

2.1.8 *D. discoideum* strains

Strain name	Resistance	Source
AX2 (laboratory wild type strain)		
AX2 GFP	G 10	Meino Rohlfs
AX2 GFP-cofilin	G 10	Annette Müller-Taubenberger
AX2 GFP-actin18	B 5	Annette Müller-Taubenberger
AX2 GFP-actin24	B 5	Annette Müller-Taubenberger
AX2 GFP-actin25	B 5	Annette Müller-Taubenberger
AX2 mRFP-actin	G 10	Annette Müller-Taubenberger
Filactin KO (FiaKO)	B 5	Jan Faix
AX2 GFP-filactin full length	G 10	Present study
AX2 GFP-filactin Ist1-like	G 10	Present study
AX2 GFP-filactin filamin-like Ig repeats	G 10	Present study
AX2 GFP-filactin actin-like	G 10	Present study
AX2 filactin full length-GFP	G 10	Present study
AX2 filactin actin-like-GFP	G 10	Present study
AX2 GFP-vta1	G 10	Present study
AX2 GFP-vps4	G 10	Present study
AX2 GFP-vps46	G 10	Present study
FiaKO GFP-filactin full length	B 5, G 10	Present study
FiaKO GFP-filactin Ist1-like	B 5, G 10	Present study
FiaKO GFP-filactin filamin-like Ig repeats	B 5, G 10	Present study
FiaKO GFP-filactin actin-like	B 5, G 10	Present study
FiaKO filactin full length-GFP	B 5, G 10	Present study
FiaKO filactin actin-like-GFP	B 5, G 10	Present study
FiaKO GFP-vta1	B 5, G 10	Present study
FiaKO GFP-vps4	B 5, G 10	Present study
FiaKO GFP-vps46	B 5, G 10	Present study
FiaKO GFP-cofilin	B 5, G 10	Present study
AX2 mRFP-ATG8	G 10	Present study
AX2 GFP-filactin full length + mRFP-ATG8	G 10	Present study
FiaKO mRFP-ATG8	B 5, G 10	Present study
AX2 mRFP ATG8-like	G 10	Present study
AX2 GFP-filactin full length +mRFP-ATG8-like	G 10	Present study

FiaKO mRFP-ATG8-like	B 5, G 10	Present study
FiaKO GFP-filactin full length + mRFP-ATG8-like	B 5, G 10	Present study

2.2 Methods

2.2.1 Molecular methods

Standard molecular biology protocols were performed essentially as described (Sambrook & Russel, 2001). Genomic DNA from *D. discoideum* strains was isolated using the LyB buffer (10 mM Tris pH 8.0, 50 mM KCl, 2.5 mM $MgCl_2$, 0.45 % NP40, 0.45 % Tween20, 0.5 µg/µl Proteinase K) (Charette & Cosson, 2004). Total RNA from *D. discoideum* strains was purified using the RNeasy Mini Kit (Qiagen), and cDNA was subsequently synthesized using the Transcriptor High Fidelity cDNA Synthesis Kit (Roche). Polymerase chain reactions (PCRs) were performed with either Taq-Polymerase or Phusion High-Fidelity DNA Polymerase (New England Biolabs) according to the manufacturer's manual. PCR products were cloned into expression vectors using standard restriction enzyme mediated cloning or via the PCR product cloning kit (Qiagen). Plasmid DNA was obtained from *E. coli* by using standard alkaline lysis miniprep or by using the silica-based mini- and maxiprep kits (Roche, Macherey Nagel). Chemically competent *E. coli* cells were prepared according to the $CaCl_2$ method (Dagert & Ehrlich, 1979). The accuracy of the DNA sequences inserted into the respective expression vectors was controlled by sequencing using specific primers (Eurofins MWG Operon, Ebersberg).

2.2.2 Biochemical methods

2.2.2.1 SDS-polyacrylamide gel electrophoresis and western blotting

Protein mixtures were separated by standard discontinuous SDS-PAGE (Laemmli, 1970) and either stained with Coomassie Brilliant Blue R 250 or transferred onto a nitrocellulose membrane via semi-dry western blotting using a transfer buffer (25 mM Tris pH 8.5, 190 mM glycine, 20 % methanol, 0.02 % SDS). The membranes were blocked with nonfat milk powder dissolved in NCP buffer (10 mM Tris pH 7.3, 150 mM NaCl, 0.05 % Tween20), incubated with the particular primary and secondary antibodies and developed using the Enhanced Chemiluminescence System (ECL).

2.2.2.2 GST-tagged protein expression, purification and pulldown assays

Constructs in pGEX vectors, inducibly expressing the protein of interest with an N-terminal GST-tag, were transformed into BL21 RIL or ArcticExpress RIL *E. coli* strains. Cultures were inoculated and grown overnight in LB medium containing the particular antibiotics at 37°C, then diluted 1:20 and grown at 37 °C to an OD_{600} of 0.4 – 0.8. Expression was induced by adding 0.5 mM IPTG to the culture and cells were grown at 37°C for 2 hours or at 16°C or 20°C overnight. The bacteria were pelleted and resuspended in PBS (137 mM NaCl, 2.7 mM KCl, 8.1 mM Na_2HPO_4, 1.5 mM KH_2PO_4, pH 7.4) containing 2 mM DTT, 1 mM EDTA, 5 mM benzamidine, 100 µM PMSF and one Complete Protease Inhibitor cocktail tablet (Roche) per 50 ml lysis buffer. The cells were opened by sonification in the presence of 0.5 mg/ml lysosome, the lysates were centrifuged (35,000 g for 20-30 minutes at 4°C) and the supernatant was incubated with the glutathione-sepharose 4B resin (Sigma-Aldrich) at 4°C for 2-3 hours under slight agitation. The matrix was washed with 10-20 column volumes of lysis buffer and either kept on ice for protein interaction pulldown assays with *D. discoideum* cell lysates or eluted with TEDAB buffer pH 7.4 containing 30 mM reduced glutathione. The purity and quality of the protein in the appropriate fractions was analyzed by SDS-PAGE.

In case a pulldown assay was performed, 5 x 10^7 – 1 x 10^8 *D. discoideum* cells were opened in 1 ml homogenization buffer (30 mM Tris pH 8.0, 4 mM EGTA, 2 mM EDTA, 2 mM DTT, 30 % sucrose, 5 mM benzamidine, 100 µM PMSF, 0.2 mM ATP, one Complete Protease Inhibitor cocktail tablet (Roche) per 20 ml buffer) by freezing and thawing them twice or by the addition of 1 % Triton X-100 to the homogenization buffer. The whole cell lysate was centrifuged at 10,000 g and 4°C for 15-30 minutes and the supernatant was used for incubation with the GST-tagged purified protein bound to the sepharose. After an incubation of about 90 minutes, the beads were washed with 10-50 column volumes of homogenization buffer and boiled in SDS sample buffer. The interaction of proteins was subsequently analyzed by SDS-PAGE and western blotting.

2.2.2.3 Immunoprecipitation

For the identification of interacting proteins the GFP-Nano-Trap (Chromotek) was used (Rothbauer et al, 2008). 5 x 10^7 – 1 x 10^8 *D. discoideum* cells overexpressing a recombinant GFP-tagged protein were harvested and opened in lysis buffer (25 mM HEPES pH 7.4, 50 mM NaCl, 1 mM EDTA, 1 mM EGTA, 1 mM DTT, 5 mM benzamidine, 1 µM PMSF, one Complete Protease Inhibitor cocktail tablet (Roche) per 20 ml buffer, 5 % Glycerol, 1 % Triton X-100). The lysate was centrifuged for 15-30 minutes at 10,000 g and 4°C and subsequently the supernatant was incubated with 15 – 20 µl packed GFP-Trap agarose beads equilibrated in

lysis buffer. After about 60 – 90 minutes incubation at 4°C under gentle end-over-end mixing the beads were washed according to the manufacturer's protocol and the GFP-tagged protein and additional bound proteins were eluted by boiling in SDS-sample buffer. Proteins were separated by SDS-PAGE and stained with Coomassie Brilliant Blue R 250 or with silver stain (O'Connell & Stults, 1997). Bands of interest were cut out from the gel and analyzed and identified by MALDI-TOF or Orbitrap mass spectrometry (ZfP, LMU Munich).

2.2.2.4 FLAG-tagged protein expression using the baculovirus system

Since actin and actin-like proteins cannot be properly expressed and folded in prokaryotes, the Bac-To-Bac baculovirus expression system was employed to express recombinant filactin constructs. The desired sequence with an N-terminal FLAG-tag was cloned into the pFastBac1 vector. 300 ng of the vector were transformed into DH10Bac cells which contain the baculovirus shuttle vector (bacmid) with a mini-attTn7 target site and a helper plasmid that encodes certain transposition proteins. These proteins support the transposition of the mini-Tn7 element on the pFastBac1 donor plasmid (containing the sequence of interest) to the mini-attTn7 target site on the bacmid. Successful recombination was identified by the disruption of the lacZ gene on the bacmid which allows a blue/white screening in the presence of X-Gal and IPTG. The bacmid was isolated via miniprep and used for transfection of the immortalized insect cells, namely Sf9 (a clonal isolate of *Spodoptera frugiperda* Sf21 cells) which are cultivated at 28°C. Therefore, 30 – 100 µg bacmid DNA were mixed with 200 µl Sf-900 II SFM medium (Invitrogen) and 10 µl Cellfectin (Invitrogen) and incubated at room temperature for 45 minutes. Subsequently, the mix was added to 2 ml cells (at a density of 5 x 10^5 cells/ml) which were placed in wells of a 6-well-plate and incubated for 5 hours at 28°C. The transfection mixture was removed and Sf-900 II SFM medium supplemented with 5 % fetal bovine serum and gentamycin (0.1 mg/ml) was added. The virus (P_0 virus) is harvested after 72 hours of incubation at 28°C, sterile-filtered and stored at 4°C. The virus was amplified by generating P_1 and P_2 generations. For protein expression, >97 % viable Sf9 cells were infected at a density of 2 x 10^6 cells/ml with P_2 virus at a ratio of about 1/10 (10 ml P_2 virus + 90 ml cells), and incubated as a shaking culture at 110 rpm and 28°C for 48 – 72 hours. Cells were harvested by centrifugation (2,000 g, 15 minutes, 4°C) and pellets of a 100 ml culture were resuspended in 5 ml lysis buffer (15 mM Hepes, pH 7.4, 30 mM NaCl, 1 mM EGTA, 1 mM DTT, 0.1 mM magnesium-ATP, one Complete Protease Inhibitor cocktail tablet (Roche) per 20 ml buffer, 2 % glycerol, 1 % Triton X-100). The lysates were centrifuged at 30,000 g for 10 minutes at 4°C and the supernatant was incubated at 4°C under gentle end-over-end mixing for 90 minutes with 100 µl ANTI-FLAG

M2 Affinity Gel (Sigma) for lysates of a 100 ml culture. The matrix was washed in wash buffer (15 mM Hepes, pH 7.4, 30 mM NaCl, 1 mM DTT, 0.1 mM magnesium-ATP, one Complete Protease Inhibitor cocktail tablet (Roche) per 20 ml buffer, 2 % glycerol,) with 10-30 column volumes in a Poly-Prep Chromatography column (Biorad). For elution, the column outlet was closed and 200 µl elution buffer (wash buffer containing 100 µg FLAG peptide (Sigma)) were used to elute the protein from 100 µl ANTI-FLAG M2 Affinity Gel for 60 minutes. The eluate was collected, the concentration was determined by SDS-PAGE analysis and the purified protein used for further experiments or aliquoted and frozen in liquid nitrogen for storage at -80°C.

2.2.2.5 Actin preparation from rabbit skeletal muscle

Routine actin purification methods were used to obtain actin essentially as described (Spudich & Watt, 1971). The back and upper thigh muscles of a rabbit were chilled, ground twice and, to remove myosin, extracted with high-salt extraction buffer (0.5 M KCl, 0.1 M K_2HPO_4) for 10-15 minutes on a stirrer. The mixture was centrifuged (4,000 g, 4°C, 10 minutes) and re-extracted. The pellet was then stirred in cold distilled water for 10 minutes and subsequently centrifuged as before with repeats until swelling of the sediment was observed. The pellet was incubated with cold acetone for about 30 minutes, filtered and dried overnight. The acetone powder was stored at -20°C for subsequent actin preparations.

Usually, 10 g acetone powder were extracted with 200 ml G-actin buffer (2 mM Tris pH 8.0, 0.2 mM ATP, 0.5 mM DTT, 0.2 mM $CaCl_2$, 0.01 % NaN_3) at 4°C for 30 minutes, filtered through nylon nets and re-extracted for 15 minutes. The filtrate was centrifuged (30,000 g, 30 minutes, 4°C), actin polymerization was promoted by the addition of 50 mM KCl, 2 mM $MgCl_2$ and 1 mM ATP dissolved in 100 mM NaOH and the mixture was incubated at 4°C for two hours or overnight. To remove tropomyosin, solid KCl was slowly added until a final concentration of 0.8 M was reached. Filamentous actin was subsequently pelleted by centrifugation (150,000 g, 3 hours, 4 °C), the supernatant was discarded and the pellet was homogenized in G-buffer with a douncer. For actin depolymerization, the homogenized F-actin pellet was dialyzed against G-buffer for 2-3 days with a total of about 6 buffer changes. The solution was centrifuged at 150,000 g and 4°C for 3 hours, and about 65 % from the top supernatant were further purified using a Sephacryl S300 gel filtration column (2.5 x 45 cm, Pharmacia). Fractions were collected and the actin concentrations determined by measuring the optical density at 290 nm (1 mg/ml pure actin: OD_{290nm} = 0.65) (Wegner, 1976) and their quality tested in a falling ball viscometry assay. The prepared G-actin could

be stored on ice for up to 3 weeks for most applications and was dialyzed against fresh G-buffer before usage.

2.2.2.6 Labeling of actin with pyrene

Actin was labeled for *in vitro* polymerization assays with N-(1-pyrenyl) iodoacetamide (pyrene) essentially as described (Cooper et al, 1983; Kouyama & Mihashi, 1981). After the first ultracentrifugation step during actin preparation the F-actin pellet was dialyzed against P-buffer (1 mM $NaHCO_3$ pH 7.6, 0.1 mM $CaCl_2$, 0.2 mM ATP, 0.1 mM β-mercaptoethanol) for 2-3 days with a total of about 6 buffer changes. After centrifugation (150,000 g, 4°C, 3 hours), about 65 % of the supernatant were collected. Actin polymerization was induced by the addition of 100 mM KCl and 1 mM $MgCl_2$ and a 3-5-fold molar excess of pyrene solved in DMSO was added immediately drop by drop to the vigorously stirred actin solution. In all the following work steps the solution was light protected since pyrene is light sensitive. The solution was incubated under gentle end-over-end mixing overnight in a 50 ml tube at room temperature and subsequently the filamentous actin was pelleted (150,000 g, 4°C, 3 hours). The F-actin pellet was homogenized in G-buffer and dialyzed against G-buffer to promote depolymerization. The dialyzed solution was centrifuged again (150,000 g, 4°C, 3 hours) and the pyrenylated G-actin was purified by gel filtration as described earlier in the actin preparation. The percentage of labeled actin was calculated by measuring actin concentration and pyrene concentration using the respective extinction coefficients (OD_{290nm} = 2.6 → 100 µM actin; OD_{344nm} =2.2 → 100 µM pyrene; micromolar $concentration_{pyrene}$ / micromolar $concentration_{actin}$ = % of pyrene-labeled actin). The percentage of labeled actin should be around 60-90 %. The aliquots were stored at -80°C and dialyzed against G-buffer before use.

2.2.2.7 Actin labeling with amino-reactive dyes

Actin was labeled with the Alexa-fluor carboxylic acid succinimidyl esters Alexa488 and Alexa568 (Invitrogen) to investigate actin dynamics at the TIRF and at the confocal microscope. Actin was prepared as described. Two fractions (2-3 mg actin/ml) were pooled to obtain a solution of about 8 – 10 ml. The G-actin was dialyzed against borate buffer pH 8.00 (50mM boric acid, 0.2 mM $CaCl_2$, 0.2 mM ATP) at 4°C for at least 3 hours with one buffer change each hour. The actin concentration was identified spectroscopically and 10x polymerization buffer (100 mM Imidazole pH 7.2, 30 mM $MgCl_2$, 10 mM ATP, 2 mM $CaCl_2$) was added in a ratio of 1/10 to allow polymerization at room temperature. The dye solved in DMSO was then added drop by drop in a 1–2-fold molar excess to the vigorously stirred actin

solution. From this step onwards, all activities were carried out in the dark since the dyes are light sensitive. The solution was incubated under gentle end-over-end mixing overnight at room temperature and centrifuged (150,000 g, 4°C, 2 hours) to sediment the filamentous actin. The pellet was homogenized in G-buffer to reach a calculated final actin concentration of about 2-3 mg/ml and dialyzed against G-buffer at 4°C for at least 3 hours with one buffer change each hour. After another centrifugation (150,000 g, 4°C, 2 hours) the supernatant was collected and the percentage of labeled actin was determined by spectroscopic methods using the respective extinction coefficients (actin: OD_{290nm} = 2.6 → 100 µM actin; Alexa488: OD_{495nm} =7.1 → 100 µM Alexa488; Alexa568: OD_{578nm} =9.13 → 100 µM Alexa568; micromolar concentration$_{Alexa}$ / micromolar concentration$_{actin}$ = % of Alexa-labeled actin). The percentage of labeled actin should be around 20 %. The aliquots were stored at -80°C and dialyzed against G-buffer before use.

2.2.2.8 *In vitro* actin polymerization assay (fluorometry)

Fluorometric actin polymerization assays were carried out on a Perkin Elmer fluorometer using pyrenylated actin. Upon actin polymerization the environment of the pyrene label changes which results in a 20-fold increase of fluorescence. Only about 10 % of pyrenylated actin are required to produce a convenient signal. Usually 2 µM actin (10 % pyrenylated) in 800 µl volume were used for the measurements. The polymerization-induced fluorescence was captured at 386 nm using an excitation wavelength of 365 nm and 8 nm slit widths. Actin polymerization measurements were carried out in polymerization buffer (10 mM Imidazole pH 7.2, 3 mM $MgCl_2$, 1 mM Na-ATP, 0.2 mM $CaCl_2$). Native WH2 domain constructs, FLAG-filactin or purified SpireWH2-actin complexes and G-actin were mixed and preincubated for about 1-2 minutes prior to addition of polymerization buffer and recording. Filament-disrupting measurements were performed with prepolymerized actin samples. Increasing concentrations of WH2 domain constructs were added and mixed shortly with the F-actin sample prior to starting the measurements approximately five seconds after addition of the respective constructs. The seeded nucleation assay was performed with 20 µl of F-actin seeds. To create actin seeds, 16 µM unlabeled G-actin was polymerized for about 15 hours in 50 mM KCl, the solution was mixed 1:1 with G-buffer, vigorously vortexed to shear the filaments and subsequently kept at room temperature for about 1-2 hours. For the dilution induced depolymerization assay 4 µM 65 % pyrenylated actin was polymerized for at least 4 hours in polymerization buffer and 16 µl of the F-actin solution were subsequently incubated with FLAG-filactin constructs for 1-2 minutes prior to the addition of 780 µl of polymerization buffer and recording.

2.2.2.9 Low shear viscometry

Low shear viscometry assays were carried out in a falling ball viscometer (MacLean-Fletcher & Pollard, 1980). The reaction mixture (160 µl) usually contained 0.5 mg/ml rabbit skeletal muscle actin which was pre-incubated for 1 minute with the respective proteins described in the results. Polymerization was started by the addition of polymerization buffer (10 mM Imidazole pH 7.2, 3 mM $MgCl_2$, 1 mM Na-ATP, 0.2 mM $CaCl_2$). The mixture was briefly vortexed, immediately filled into the capillary and allowed to polymerize for 15 minutes. Then the apparent viscosity of the solution was measured by recording the time a mini steel ball took to pass a certain distance.

Low shear viscometry assays were additionally carried out using an Ostwald viscometer. The reaction mixture (1.6 ml) contained 12 µM polymerized actin. The viscosity of the solution was measured by recording the time required for the solution to flow through a capillary of a known diameter. Then, increasing concentrations of SpireDDD were added. The viscosity of the solution for each SpireDDD concentration was assessed five times.

2.2.2.10 Confocal microscopy

Confocal microscopy data were acquired on an inverted Axiovert LSM 510 Meta confocal microscope (Zeiss) with a 63x or 100x oil immersion objective with a numerical aperture of 1.4 and 1.3, respectively. Excitation of fluorophores was achieved with the 488 nm argon ion laser line, the 543 nm and 633 nm helium neon laser lines, and emission was collected using 510-525 nm band-pass, 585-615 nm band-pass or 650 nm long-pass filters. When imaging fluorescent *D. discoideum* mutants, cells were transferred into an open glass-bottomed chamber and recorded at 10 seconds intervals. To observe actin dynamics *in vitro* at the confocal microscope, coverslips were coated with 0.1 % collodion diluted in isoamylalcohol and dried. An open flow chamber was built up on the coverslip. 5 µM Alexa488-labeled actin (20 % labeled) were prepolymerized for at least one hour in polymerization buffer (10 mM Imidazole pH 7.2, 3 mM $MgCl_2$, 1 mM Na-ATP, 0.2 mM $CaCl_2$). The F-actin solution was subsequently diluted with polymerization buffer to 0.5 – 1 µM and the actin bundling protein fascin was added at a 1/1 molar ratio. The flow chamber was filled with 0.1 mg/ml NEM-HMM diluted in NEM buffer (25 mM Imidazole pH 7.4, 4.4 mM $MgCl_2$, 1 mM EGTA, 0.3 mM KCl, 10 mM DTT; Ali et al (2007)) and incubated for 3 minutes. Subsequently, the flow chamber was washed with polymerization buffer and the F-actin dilution was applied and incubated for 5 minutes before another washing step was carried out to remove unbound filament bundles. WH2 domain constructs were added with a pipet to the inlet of the

chamber by removing the buffer at the outlet with a filter paper while recording at two frames per second.

2.2.2.11 Total internal reflection fluorescence microscopy

Total internal reflection fluorescence (TIRF) microscopy was performed at the Bausch laboratory (Technische Universität München) with the help of Michael Wohlhöfler. Microscopy data were acquired on an Axiovert 200 inverted microscope (Zeiss) with a 100x oil immersion objective with a numerical aperture of 1.4. Alexa555-actin (20 % labeled) was prepolymerized for at least 30 minutes in TEGA polymerization buffer (2 mM Tris pH 8.0, 2 mM $MgCl_2$, 0.2 mM DTT, 0.5 mM ATP, 1 mM EGTA). The samples were observed in a flow chamber which was prepared with nitrocellulose-coated coverslips. After the incubation with α-actinin (0.3 µM), surfaces were first passivated using 1 mg/ml BSA and then the prepared F-actin was applied. SpireWH2 domain constructs were added by a syringe pump attached to the flow chamber. The disintegration of actin filaments and bundles after addition of SpireDDD was recorded at two frames per second.

2.2.2.12 Transmission electron microscopy (negative stain)

Transmission electron microscopy was performed at the Baumeister laboratory (Max-Planck-Institut für Biochemie, Martinsried) with the help of Oana Mihalache. Electron microscopy grids were first cleaned in a plasma cleaner (Diener, Ebhausen). About 5 µl of the protein samples (1-5 µg/ml) were pipetted on a parafilm and the grids were placed on the sample drops with their carbon coated side and incubated for 1-2 minutes, after washing in two drops of buffer the protein was solved in for 1 second each. Superfluous buffer was removed with a filter paper and the grid was placed in a 2 % uranylacetate solution, incubated for 2 minutes and dried. Data were acquired on a CM20 electron microscope at 160kV and 58,000-fold magnification.

2.2.2.13 Gel filtration using the ÄKTA 100 system

For protein size analysis and protein purification, the gel filtration columns Superose 6 10/300 GL and Superose 12 10/300 GL (GE Healthcare) were used. The columns were equilibrated with a modified G-buffer (5 mM Tris pH 8.0, 50 mM NaCl, 0.2 mM ATP, 0.5 mM DTT, 0.2 mM $CaCl_2$, 0.01 % NaN_3). The flow rate was set between 0.1–0.5 ml/min for Superose 6 and 0.5–1 ml/min for Superose 12. The columns were calibrated using protein molecular weight standards range 12.4 – 450 kDa (Serva). The void volume was identified

with Dextran blue 2000 (GE Healthcare). Usually 0.1-3 mg purified protein were injected, and 500 µl-fractions were collected and analyzed by SDS-PAGE.

2.2.3 Cell biological methods

2.2.3.1 *D. discoideum* cell culture and transformation

D. discoideum AX2 (laboratory wild type strain) and mutant cells derived from AX2 were cultivated axenically in sterile HL5 medium (Formedium), either in cell culture dishes, in shaking culture at 150 rpm or on lawns of *Klebsiella aerogenes*. For long term storage, cells were frozen in *D. discoideum* storage medium (82 % AX-medium, 9 % horse serum, 9 % DMSO) or spores were obtained from phosphate agar plates and frozen in Soerensen buffer pH 6.0 (14.6 mM KH_2PO_4, 2 mM Na_2HPO_4).

D. discoideum wild type or mutant cells were transformed with the appropriate plasmids by electroporation. 2 x 10^7 cells were extensively washed in cold Soerensen buffer and electroporation buffer pH 6.1 (50 mM sucrose, 10 mM KH_2PO_4), resuspended in 1 ml cold electroporation buffer, and then electroporated in the presence of about 25 µg DNA in a 4 mm electroporation cuvette using a Gene Pulser XCell (Biorad) and the standard settings (square wave, V= 1.0 kV, 1 ms pulse length, two pulses, 5 seconds pulse interval). Subsequently the cells were transferred to a cell culture dish and after gentle shaking (50 rpm, room temperature, 15 minutes) 2 µM $CaCl_2$ and 2 µM $MgCl_2$ were added. After another 15 minute incubation, HL5 medium was added and the cells were allowed to recover for about 24 hours before the respective antibiotic (either 10 µg/ml G418 or 5 µg/ml blasticidin) was added to select the transformants. Single clones were obtained by spreader dilution on *K. aerogenes* lawns. Cloned transformants were checked by microscopy and western blot analysis using the appropriate antibodies.

To obtain overexpression mutants, constructs for the expression of fluorescently labeled proteins (with C- or N-terminal GFP or mRFP tags) were transformed into *D. discoideum* cell lines. All GFP- and mRFP-constructs were expressed under the actin15 promoter. To generate knock out (KO) mutants, gene replacement constructs with a blasticidin resistance cassette were transformed and successful transformants were checked by PCR analysis.

The filactin KO strain was generated by Jan Faix (Medizinische Hochschule Hannover) by replacement approach with a blasticidin resistance cassette. The filactin gene targeting vector was constructed by cloning the genomic PCR products BamHI/PstI at the 5' end (nucleotides 126 – 885 of filactin genomic DNA) and HindIII/SalI at the 3' ends (nucleotides

1623 – 2192 of filactin genomic DNA) into the corresponding sites of pLPBLP (Faix et al, 2004). The target vector was then digested with BamHI/SalI and used to disrupt the filactin gene in wild type cells. Null mutants were initially screened by PCR using two sets of primers as shown in the scheme (figure 7).

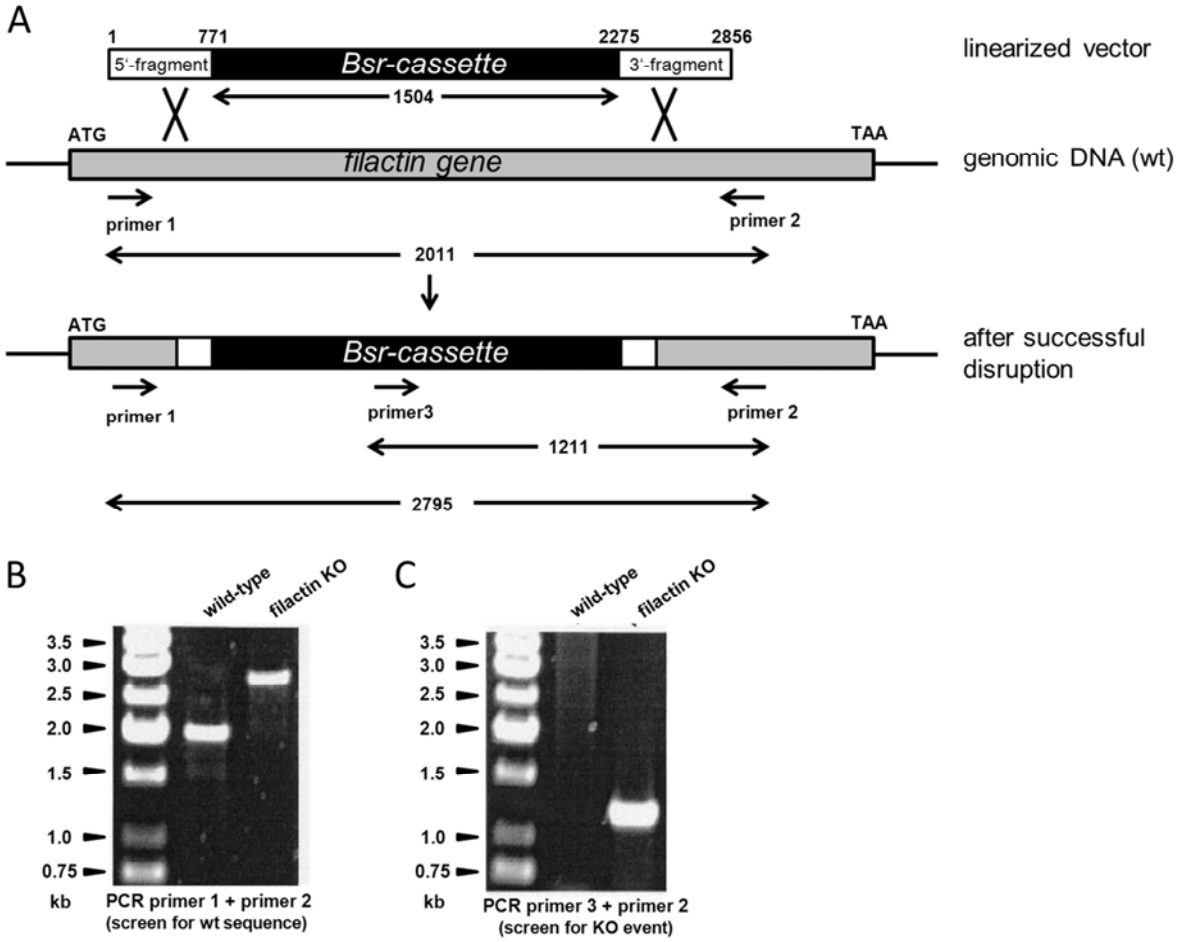

Figure 7: Filactin gene disruption strategy, courtesy of Jan Faix. A) The schematic diagram represents the strategy for knocking out filactin in the AX2 wild type strain. B) The insertion of the blasticidin resistance cassette was confirmed by PCR analysis with primer 1 and primer 2 indicated in A). The insertion of the blasticidin resistance cassette increases the size of the PCR fragment compared to the wild type. C) The insertion of the blasticidin resistance cassette was further confirmed by PCR analysis with primer 2 and primer 3 that binds within the blasticidin sequence. Only in clones with successful filactin gene disruption a PCR product can be generated.

2.2.3.2 Immunofluorescence

To study subcellular localization of proteins, indirect immunofluorescence was performed. Exponentially growing t0 cells were seeded on coverslips which were previously washed with 3.6 % HCl and rinsed with H_2O. After allowing the cells to settle on the coverslips the medium was removed and the cells were fixed with -20°C methanol unless otherwise noted. After a 10-15 minute incubation at -20°C, the coverslips were washed several times with PBS

(137 mM NaCl, 2.7 mM KCl, 8.1 mM Na_2HPO_4, 1.5 mM KH_2PO_4, pH 7.4) supplemented with 100 mM glycine. Subsequently, the fixed samples were washed with PBG (PBS + 0.5 % BSA, 0.045 % fish gelatin) and incubated with the primary antibody overnight at 4°C. The fixed preparations were washed with PBG and incubated for 60 minutes with the secondary fluorescence-dye coupled adequate antibody (goat-anti-mouse IgG Cy3-conjugated, unless otherwise mentioned). DNA was stained with either TO-PRO-3 iodide or DAPI (Invitrogen). The stained samples were quickly rinsed with ddH_2O, embedded in gelvatol and stored in the dark at 4°C.

3. Results I: WH2 domain containing proteins

3.1 Analysis of Spire and CAP2 protein sequences

In this part of the study the focus was exclusively put on the G-actin binding WH2 motifs of the proteins Spire and CAP2. As mentioned above, the Spire protein contains the four WH2 domains A-B-C-D in tandem. They contain motifs of about 20-21 amino acids and are separated by the following linker sequences: L1 between domains A and B, L2 between domains B and C, and L3 between domains C and D. CAP2 comprises only one WH2 domain. Figure 8 displays an alignment of the WH2 domains of Spire and CAP2. The regions forming the amphipathic helices during actin binding and the C-terminal extension with the L++V/T motif ('+' representing basic amino acids) are conserved.

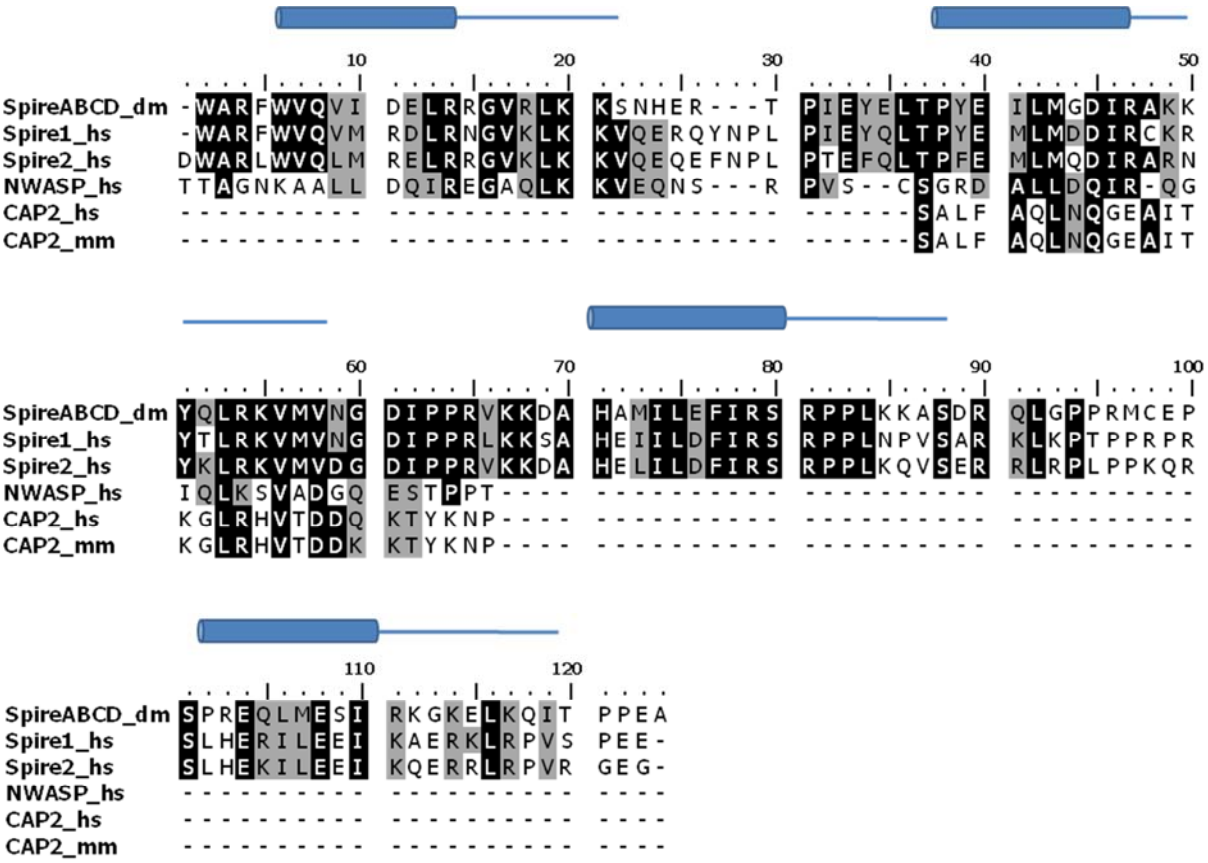

Figure 8: Alignment of the WH2 domains of Spire, CAP2 and N-WASP from different organisms. Spire contains four WH2 domains, CAP2 only one and the reference N-WASP comprises two WH2 domains. SpireABCD_dm (*D. melanogaster,* Q9U1K1) aa 366-485, Spire1_hs (*Homo sapiens*, Q08AE8) aa 269-390, Spire2_hs (*H. sapiens*, Q8WWL2) aa 241-363, NWASP_hs (*H. sapiens*, O00401) aa 401-460, CAP2_hs (*H. sapiens*, P40123) aa 261-290 and CAP2_mm (*M. musculus*, Q9CYT6) aa 261-290 were used. Identical residues are shown on a black background; similar residues are displayed on a grey background. Blosum 62-12-2 was used as alignment parameter and the threshold for shading was set to 50 %. The secondary structure during actin binding of *Drosophila* Spire is schematically depicted above the sequence, with a tube representing an amphipathic helix followed by a straight line that highlights the location of the conserved L++V/T motif.

3.2 The different WH2 constructs used in this study

Table 1: The different WH2 domain constructs used in this study

No.	Designation (amino acids)	Molecular mass (Da)
1	SpireNT (1-520)	58,977
2	SpireABCD (371-480)	12,920
3	SpireBCD (396-480)	9,900
4	SpireBC (396-450)	6,380
5	SpireCD (432-480)	5,590
6	SpireD (463–485)	2,370
7	SpireC-L3 (428-460)	3,820
8	SpireL3-D (448-485)	3,810
9	SpireL3 (448-462)	1,460
10	SpireDDD	9,611
11	CAP2-WH2 (247-310)	8,000

Table 1 shows the different WH2 domain constructs used in this work. The CAP2-WH2 construct (table 1, construct no. 11) was cloned and purified by Vivek Peche from the Angelika Noegel laboratory (Universität zu Köln). The sequence was cloned into the pGEX 4T-3 vector, the GST-CAP2-WH2 fusion protein was purified and the GST-moiety was cleaved by thrombin. All Spire constructs (table 1, construct no. 1-10) were cloned and purified by Tomek Sitar and Anna Ducka from the Tad Holak laboratory (Max-Planck-Institut für Biochemie, Martinsried) as described (Ducka, 2011). The proteins were expressed as GST-fusion proteins (pGEX-6P-1 vector), except for the SpireNT construct, which was cloned in the pET16b vector and isolated by His-tag purification. After cleavage of the tags the proteins were further purified on a gel filtration column using Superdex 200, Superdex 75, or Superdex 30 resins, depending on the molecular weight of the protein.

The influence of 1–4 WH2 domains on actin dynamics was investigated by different means. SpireNT (table 1, construct no. 1) contains all four WH2 domains and additionally the KIND domain at the N-terminus. Also the effect of linker 3 between WH2 domain C and D (L3, table 1, construct no. 9) was tested, since it was previously described as an actin monomer binding protein with weak nucleating activity (Zuchero et al, 2009). The artificial construct SpireDDD (table 1, construct no. 10) which carries three identical WH2 domains separated by L3 was used to avoid more complex Spire-actin interactions that might complicate the interpretation of the data, e.g. cooperative binding of actin to the WH2

domains. The WH2 domain D was used to generate the artificial construct since it was reported in previous studies that it is the most important domain for nucleation of actin filaments (Quinlan et al, 2005). Furthermore, WH2 domain D and B exhibit the strongest actin binding, with a K_d = 0.17 µM as investigated by Isothermal Titration Calorimetry (Sitar et al, 2011). Figure 9 shows some of the constructs as they will be displayed in the following results in this part of the thesis.

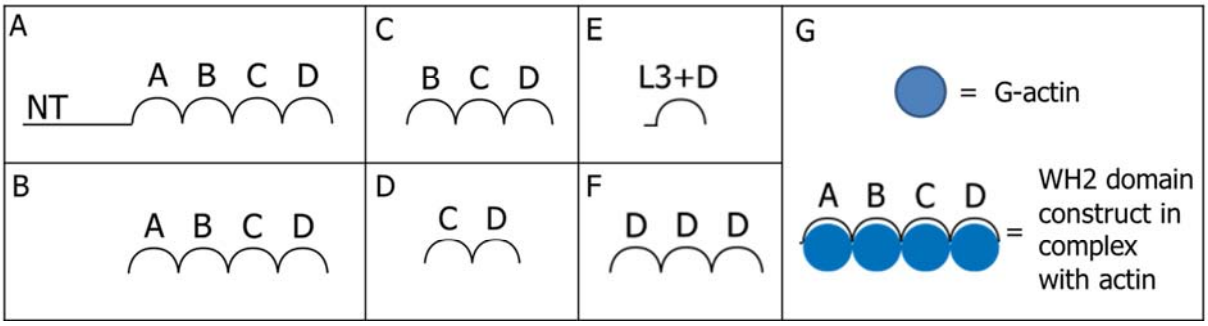

Figure 9: Representation of selected constructs used in this study. A) Spire NT (aa 1-520) comprising the N-terminal KIND-domain. B) SpireABCD (aa 371-480). C) SpireBCD (aa 396-480). D) SpireCD (aa 432-480). E) SpireL3+D (aa 448-480). F) The artificial construct SpireDDD with three identical WH2 domains D separated by linker L3. G) Depiction of schematical G-actin and the WH2 domain construct SpireABCD in complex with actin.

3.3 CAP2 exhibits a G-actin sequestering activity and can disrupt actin filaments

A single WH2 domain was identified in CAP (cyclase-associated protein) (Ksiazek et al, 2003). Here, the function of the WH2 domain of mouse CAP2 was investigated. The purified CAP2-WH2 protein usually ran at ca. 15 kDa even though its calculated size is 8 kDa (figure 10 A). Furthermore, it appeared in a cloudy shape on the gel and was often difficult to stain at all. To test whether the WH2 domain was able to disrupt existing filaments, 2 µM actin (10 % pyrenylated) were polymerized. Then, increasing concentrations of CAP2-WH2 were added to the filaments. Upon addition of the WH2 domain, the pyrene-fluorescence decreased immediately in a dose-dependent manner (figure 10 C). The complete disappearance of filaments (and hence of the pyrene-fluorescence) was set to 100 %. In a spindown experiment the disruption of the filaments was investigated as well (figure 10 B). F-actin can be separated from G-actin and other soluble proteins by ultracentrifugation at 120,000 g. In the control with polymerized actin only, most of the actin is in the pellet. When the CAP2-WH2 protein was added, most of the actin shifted to the supernatant fraction together with the CAP2-WH2. When the actin filaments were stabilized with phalloidin, the

WH2 domain could not disrupt these filaments and most of the actin was found in the pellet. Since CAP2-WH2 stayed in the supernatant, it is clear that it did not decorate the filaments.

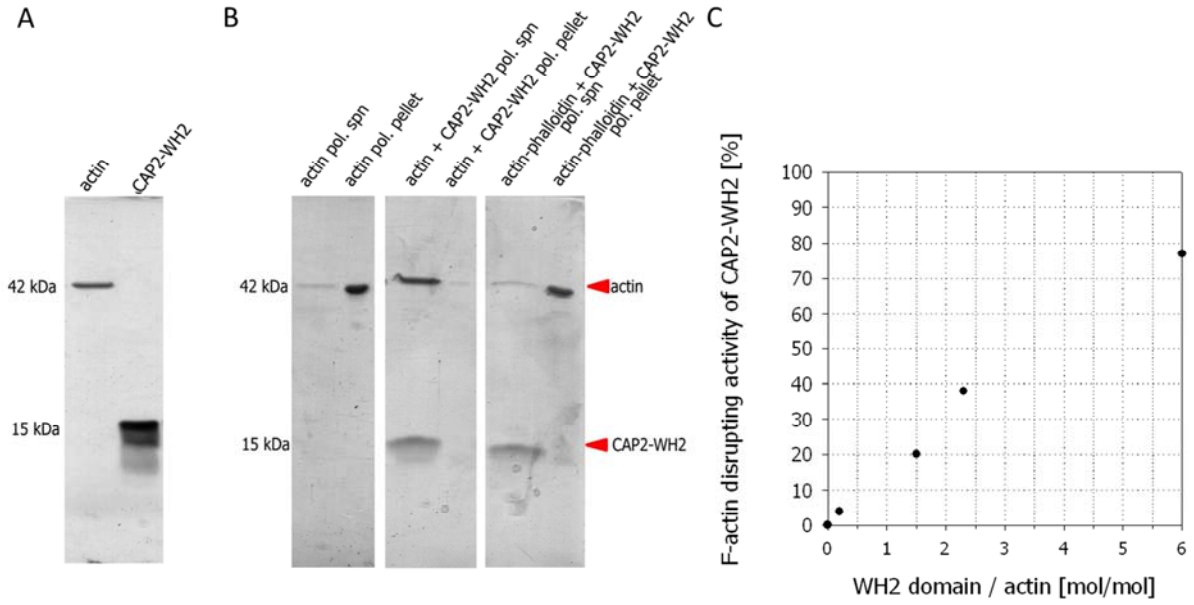

Figure 10: Purified CAP2-WH2 disrupts preformed actin filaments. A) Purified rabbit skeletal muscle actin and CAP2-WH2 on a Coomassie Blue stained SDS-gel. The CAP2-WH2 has a molecular weight of ca. 8,000 but runs at ca. 15,000. The band usually appears in a cloudy shape. B) Coomassie Blue stained gel of the fractions of a F-actin spindown after addition of CAP2-WH2 to actin and phalloidin-stabilized actin filaments. The first gel piece shows the actin control. 2 µM actin were polymerized, then ultracentrifuged, and supernatant and pellet fractions were analyzed on the SDS-gel. In the control, most of the actin is found in the pellet. On the second gel piece, 2 µM prepolymerized actin was incubated with 12 µM CAP2-WH2 and the sample was ultracentrifuged. In contrast to the control, most of the actin is now found in the soluble fraction together with the CAP2-WH2 protein. In the third gel piece 2 µM prepolymerized actin was stabilized with 1.3 µM phalloidin. Then, 12 µM CAP2-WH2 was added. Most of the actin is found in the pellet, whereas the CAP2-WH2 remains in the supernatant. C) F-actin disrupting activity of CAP2-WH2. The ability of CAP2-WH2 to disintegrate actin filaments was measured in fluorometric assays, where the complete disappearance of actin filaments was set to 100 %.

The disruption of filaments and filament bundles was also investigated at the confocal microscope (figure 11). Alexa488-actin was polymerized and bundled with fascin. 6 µM CAP2-WH2 diluted in polymerization buffer was added and the disappearance of the filaments was recorded. Several filament bundles depolymerized apparently from their ends, but the bundles were also disintegrated by removal of actin from their middle, resulting in randomly distributed gaps along the bundles (figure 11, arrowheads indicate gaps at e.g. 01:22 minutes). After about 5 minutes, the bundles completely disappeared.

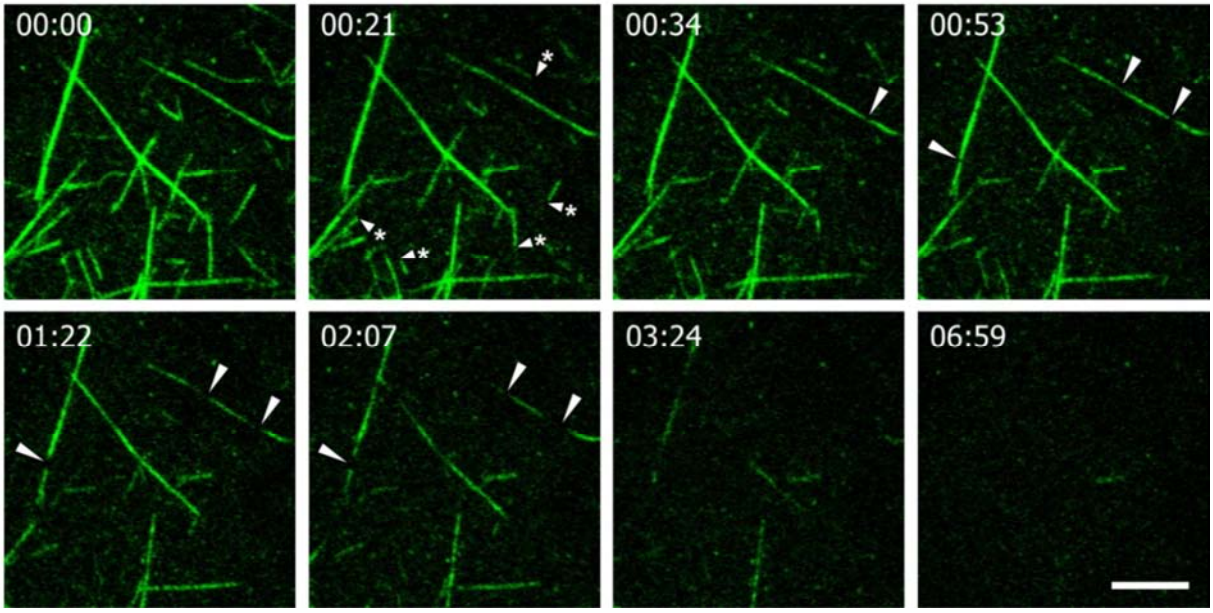

Figure 11: Disruption of F-actin-fascin bundles by the CAP2-WH2 domain imaged with a confocal microscope. 1 µM Alexa488-actin bundled with 0.3 µM fascin was bound onto the coverslip via NEM-HMM. At 00:00 minutes 6 µM CAP2-WH2 in polymerization buffer was added to the F-actin sample. In the beginning the bundles depolymerize mainly from their ends (compare areas marked by arrowheads and asterisks at 00:21 minutes with the first panel). The filaments also disintegrate, especially along the bundles, in randomly distributed gaps (see areas marked by arrowheads at 00:34, 00:53, 01:22 and 02:07 minutes). Scale bar, 5µm.

3.4 Functional analysis of Spire

Here, the effect of SpireWH2 domains on actin dynamics was investigated. Under certain conditions, they can (1) nucleate actin polymerization, (2) disintegrate actin filaments and (3) sequester actin monomers.

3.4.1 Nucleating activities of SpireWH2 domains

Concerning actin dynamics, the Spire protein was initially described as an actin nucleator (Quinlan et al., 2005). Here, the nucleating activity could be confirmed, however only at substoichiometric concentrations of WH2 domains over actin and it required at least two WH2 domains in tandem.

3.4.1.1 Free SpireWH2 domains nucleate actin polymerization only at substoichiometric concentrations

Free SpireWH2 domains in tandem nucleate actin polymerization at substoichiometric concentrations. This finding which was already described previously for SpireNT, -ABCD, -BCD and –CD (Bosch et al, 2007; Campellone & Welch, 2010; Ducka et al, 2010; Quinlan et al, 2005; Quinlan et al, 2007) could be confirmed in this study. Even the artificial construct

SpireDDD exhibits this activity (figure 12 C). The nucleating activities of SpireNT, SpireBCD and SpireDDD are displayed in representative polymerization assays (figure 12). When the SpireWH2 domains are present at substoichiometric ratios in the polymerization assay (1 WH2 domain over 10 actin monomers), actin polymerization and thereby the increase of fluorescence occurs faster than in the control. This observation accounts for all measured SpireWH2 constructs (table 1) that comprise at least two WH2 domains in tandem. At higher ratios, the sequestering activity takes over which will be presented in more detail below (see 3.4.2.1). The decrease of pyrene-fluorescence at the steady state compared to the control will also be discussed in the following (see 3.4.2.2).

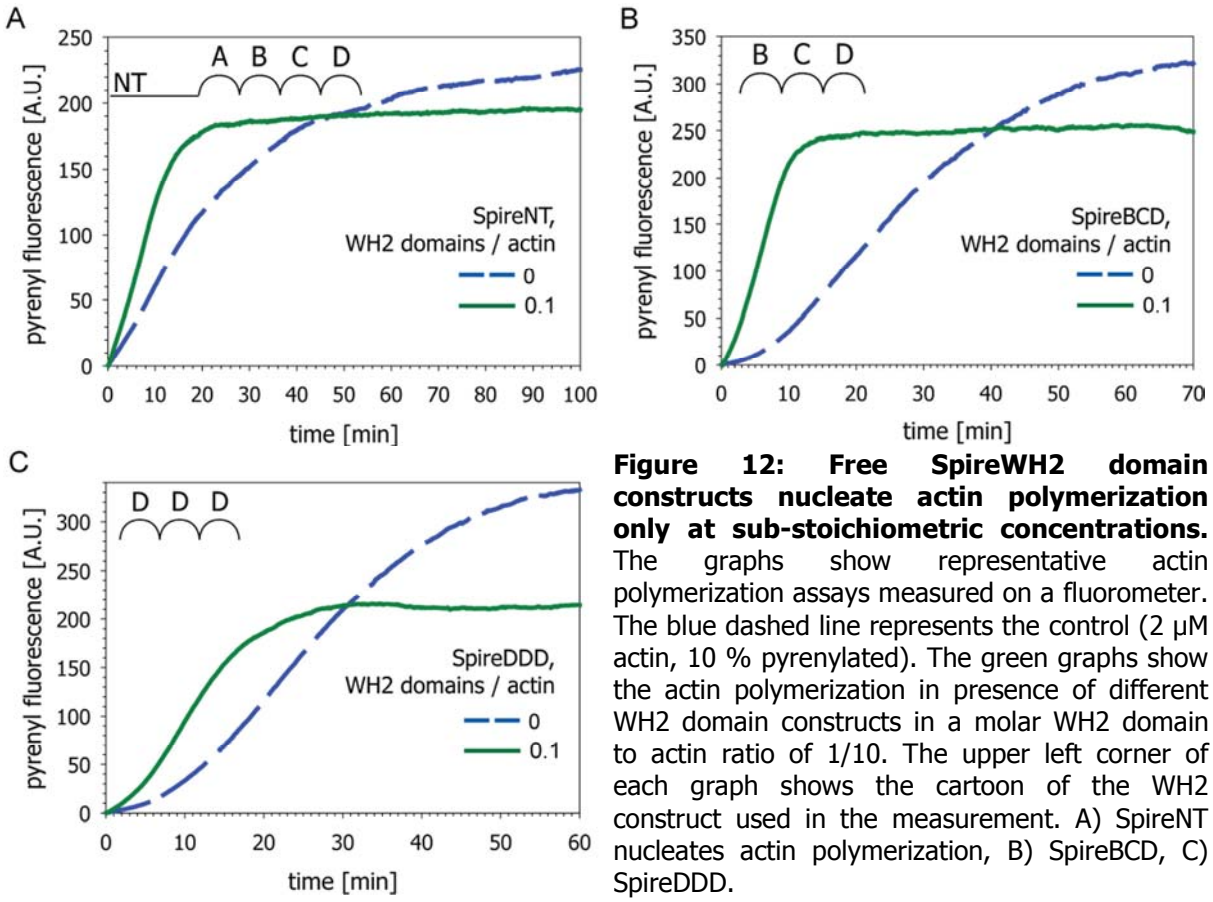

Figure 12: Free SpireWH2 domain constructs nucleate actin polymerization only at sub-stoichiometric concentrations. The graphs show representative actin polymerization assays measured on a fluorometer. The blue dashed line represents the control (2 µM actin, 10 % pyrenylated). The green graphs show the actin polymerization in presence of different WH2 domain constructs in a molar WH2 domain to actin ratio of 1/10. The upper left corner of each graph shows the cartoon of the WH2 construct used in the measurement. A) SpireNT nucleates actin polymerization, B) SpireBCD, C) SpireDDD.

3.4.1.2 Preformed SpireWH2-actin complexes act as perfect nuclei for actin polymerization

To prepare the SpireWH2-actin complexes, the purified SpireWH2 domain constructs SpireNT, SpireBCD and SpireCD were mixed with an abundant amount of actin (molar ratio WH2 domain/actin, 1/2-4) and the formed complexes were separated by gel filtration (Sitar et al, 2011). These actin-loaded WH2 domains perfectly nucleate polymerization in a transient fashion in polymerization assays. Both substoichiometric and stoichiometric concentrations of these complexes form efficient F-actin nuclei (figures 13 A-C). Free WH2 domains would sequester under these conditions (compare figure 14). In contrast, the purified SpireWH2-actin complexes completely saturated with unlabeled actin cannot remove G-actin molecules from the solution and the nucleating activity is not obscured by G-actin sequestering. However, the decrease of fluorescence at steady state can be observed under these conditions as well as for uncomplexed SpireWH2 constructs (compare figures 12 and 14). Moreover, SpireWH2-actin complexes cannot disrupt preformed actin filaments like uncomplexed SpireWH2 domains (see 3.4.2.3). When adding increasing concentrations of SpireBCD-actin to preformed actin filaments (10 % pyrenylated) at steady state, the level of fluorescence remained unchanged and thus no F-actin disrupting activity could be observed (figure 13 D). Only when the mixture of SpireBCD-actin and F-actin was incubated for a longer period of time and measured again, a drop of the pyrene-fluorescence could be detected (figure 13 D, red dot at WH2/actin ratio 1.0).

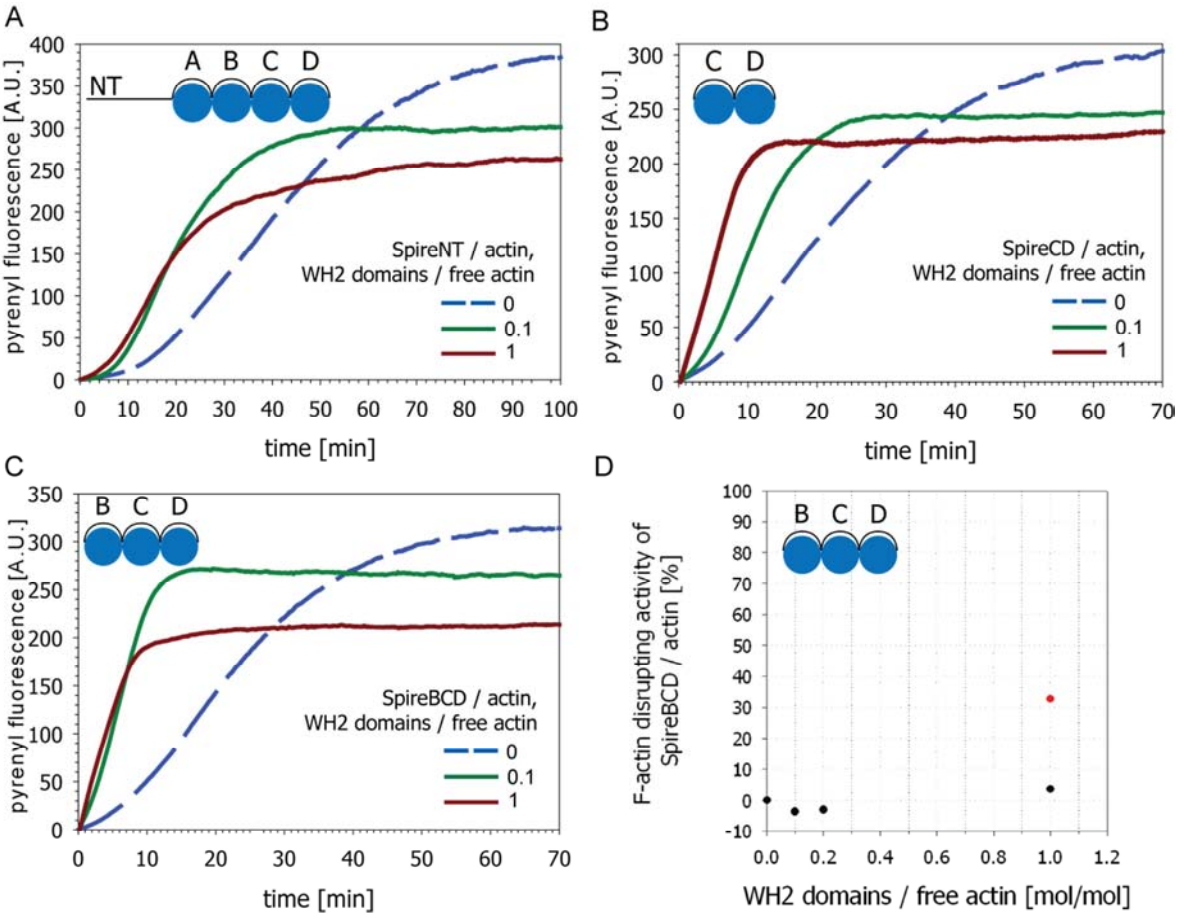

Figure 13: Preformed SpireWH2-actin complexes act as perfect nuclei for actin polymerization and cannot disrupt filaments like free WH2 domains. The graphs A-C show representative actin polymerization assays measured at the fluorometer. The blue dashed lines represent the polymerization of 2 µM actin (10 % pyrenylated) alone. The green and red graphs show the actin polymerization in the presence of SpireWH2-actin complexes in a molar ratio of 1/10 (WH2 domain/actin monomers) and 1/1, respectively. The upper left corner of each graph shows the cartoon of the WH2 construct used in the measurement. All complexes nucleate actin polymerization at sub- and even at stoichiometric concentrations. D) SpireBCD-actin complexes cannot disrupt preformed actin filaments as uncomplexed SpireBCD does. Adding increasing concentrations of these complexes to F-actin does not decrease the pyrene-fluorescence immediately. However, the pyrene-fluorescence decreases over time. When measuring the sample two hours after addition of the SpireBCD-actin complexes to F-actin at a 1/1 molar ratio, a decrease of fluorescence of about 30 % is observed (red dot at WH2/actin ratio 1/1) which suggests that actin is released from the SpireBCD-actin complex and pyrenylated actin is removed by the now unoccupied SpireWH2 construct (figure modified after Sitar et al (2011)).

3.4.2 Actin sequestering and filament-disrupting activities of SpireWH2 domains

3.4.2.1 WH2 domains sequester actin at stoichiometric concentrations

As already mentioned above, SpireWH2 domains sequester actin at stochiometric concentrations. Figure 14 shows that Spire constructs with at least two WH2 domains in tandem nucleate filaments at substoichiometric concentrations (eg. WH2/actin ratio=0.1) but

sequester actin at higher concentrations (WH2/actin ratio=1). The same constructs in complex with actin would still nucleate actin polymerization at these high concentrations (compare figures 13 A-C). SpireWH2 constructs possessing only a single WH2 domain cannot nucleate filaments, but exhibit the expected sequestering activity, e.g. SpireL3+D, and the smallest possible construct SpireD without the linker, consisting of 24 amino acids only (aa 463–485). The dose dependent decrease of fluorescence at steady state after polymerization can be observed for all constructs.

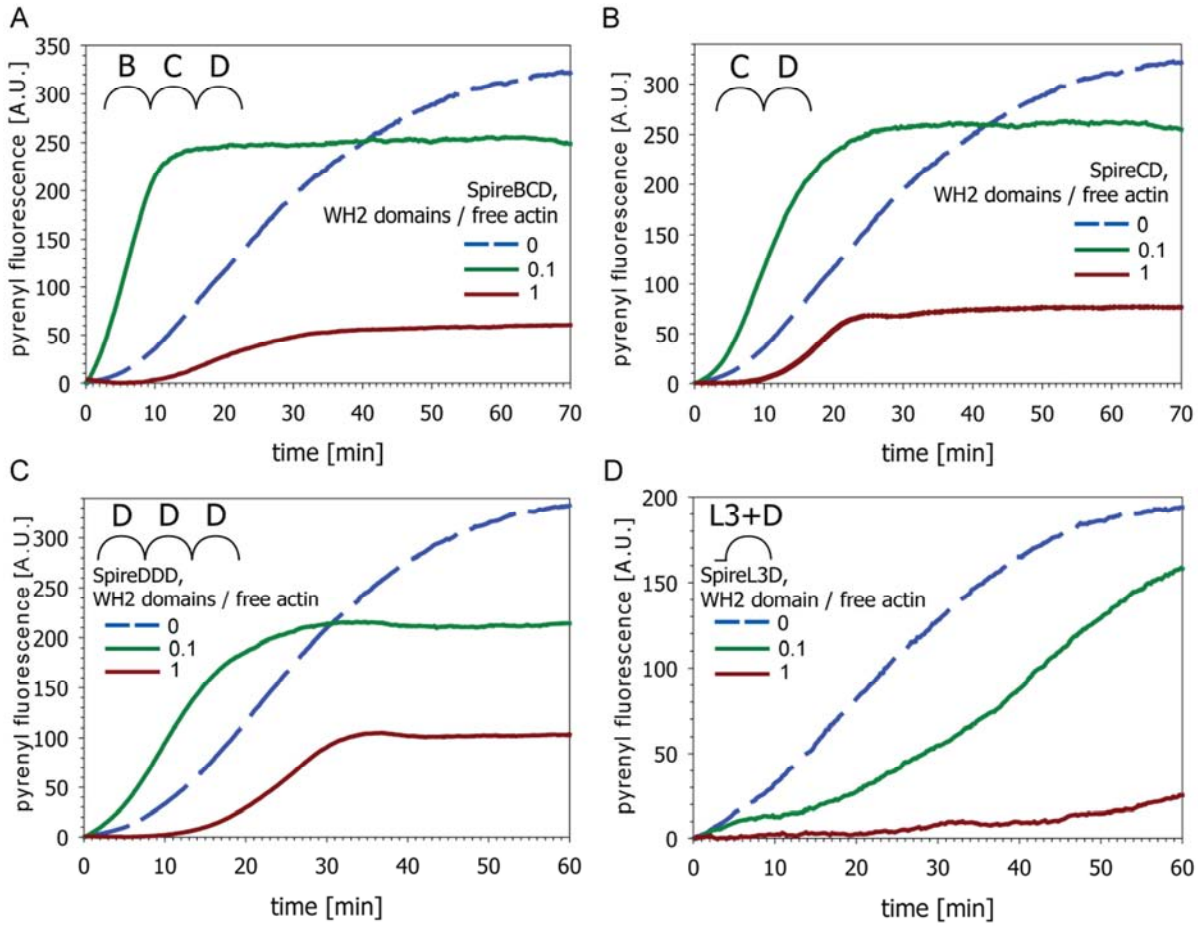

Figure 14: SpireWH2 domains in tandem show nucleation only at substoichiometric ratios and sequester actin at increasing concentrations. The graphs show representative actin polymerization assays measured at the fluorometer. The blue dashed line represents the control (2 µM actin, 10 % pyrenylated). A) - C): The green and the red graphs show the actin polymerization in the presence of WH2 domain constructs at the molar ratios indicated. D) SpireL3+D cannot nucleate actin polymerization since it comprises only one single WH2 domain, but it shows the expected sequestering activity (figure modified after Sitar et al (2011)).

3.4.2.2 Dose-dependent decrease of polymerization-induced fluorescence signal at steady state

As compared to control levels (actin alone), the lower steady state fluorescence appears with all SpireWH2 constructs (figures 12, 13, 14). This is puzzling because all samples contained the same amounts of pyrenylated actin. Figure 15 shows a comparison of the decrease of fluorescence at steady state for selected SpireWH2 constructs with and without bound actin. This suggests that Spire is released from the emerging filament after nucleation, can then sequester free G-actin molecules and thus reduce the free labeled or unlabeled G-actin concentration.

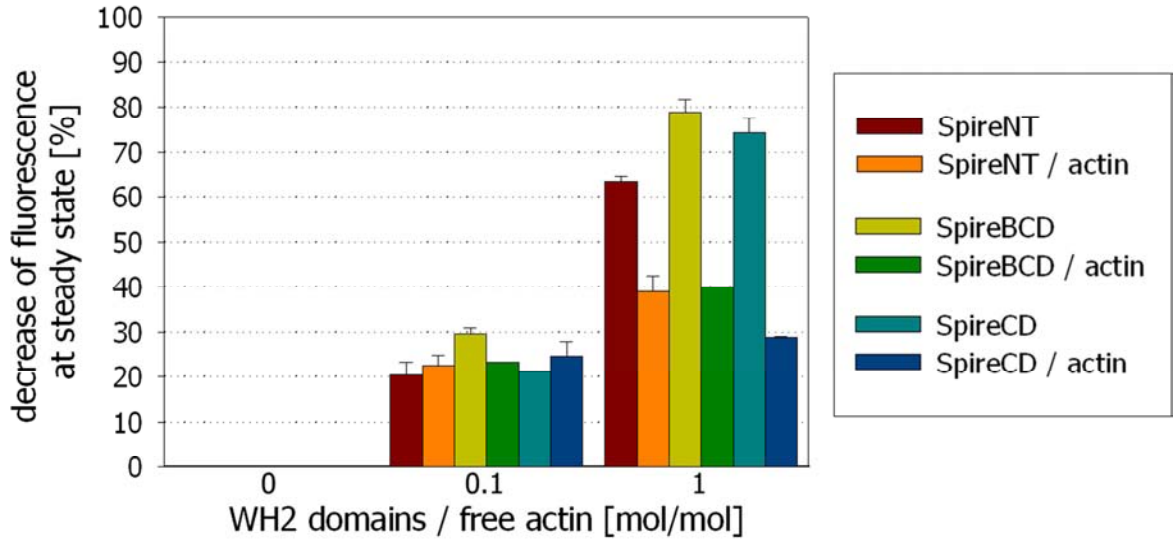

Figure 15: Decrease of pyrene-fluorescence at steady state after actin nucleation or sequestration by SpireWH2 constructs. The decrease of fluorescence compared to control levels (actin alone) after the polymerization assays as shown in figures 13 and 14 was analyzed and plotted. No decrease of fluorescence occurs in the absence of SpireWH2 constructs, but occurs when SpireWH2 constructs are added in a WH2 domain/actin ratio of 0.1 and 1.0. The error bars represent the standard error of the mean.

3.4.2.3 SpireWH2 domains disintegrate actin filaments extremely fast

It was very surprising that SpireWH2 constructs efficiently disrupt preformed actin filaments, because that implicates that the WH2 domains, being G-actin binding motifs, had bound to F-actin as well. The WH2 domains seem to have such a high affinity for actin that they can forcefully sequester monomers from filaments, thus breaking the whole structures. Figure 16 A shows a representative fluorometric assay. First, actin (2 µM, 10 % pyrenylated) was completely polymerized for about 80 minutes (blue graph). Then, increasing concentrations of SpireDDD were added, starting with a molar WH2/actin ratio of 1/30 (red graph). Surprisingly, the pyrene-fluorescence drops in only a few seconds to a much lower and

stable plateau. No slow decline of the fluorescence could be observed as, for example, the well-known dilution-induced actin depolymerization from the barbed ends. Adding higher concentrations to the F-actin sample resulted in subsequent rapid fluorescence drops until no fluorescence could be measured anymore. In the graphs of figures 16 B-D the complete disappearance of fluorescence and thus of actin filaments was set to 100 % 'F-actin disrupting activity'. This activity could be observed for all SpireWH2 constructs, including the constructs with only one WH2 domain (SpireL3+D, SpireD, SpireC+L3). Addition of the linker construct L3 (linker between WH2 domain C and D) to polymerized labeled F-actin did not decrease the fluorescence, thus the linker alone could not disrupt preformed filaments (data not shown). The F-actin disrupting activity of SpireDDD, SpireABCD and SpireL3+D is depicted in figures 16 B, C and D, respectively. When F-actin is stabilized by phalloidin, filament disruption was inhibited. However, phalloidin treated F-actin could co-sediment the WH2 domains (compare figure 20).

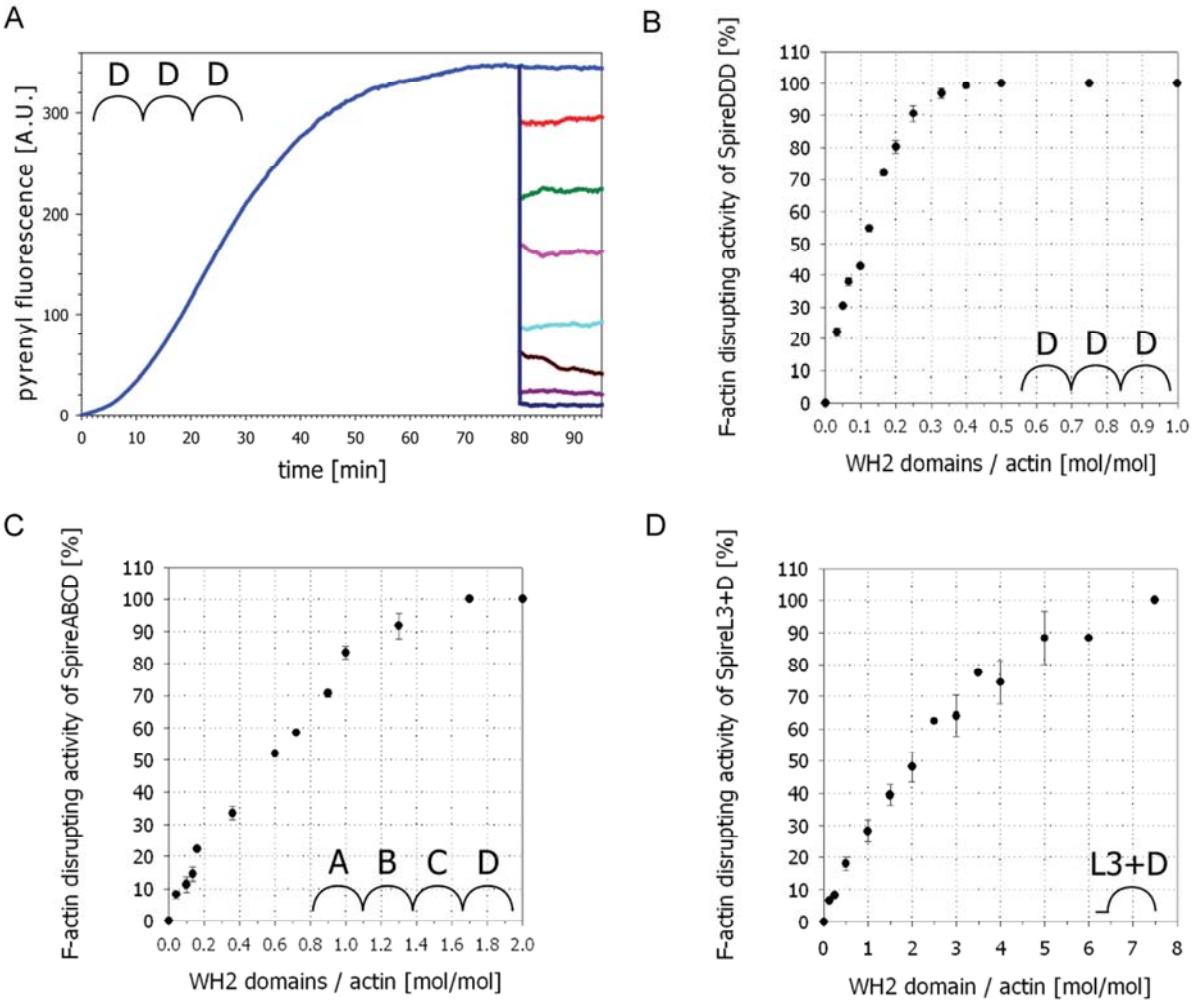

Figure 16: SpireWH2 constructs disrupt preformed actin filaments extremely fast. A) 2 µM actin (10 % pyrenylated) was polymerized until the steady state was reached. Addition of increasing concentrations of SpireDDD reduced the fluorescence signal in a dose-dependent manner: molar WH2/actin ratios 1/30 (red), 1/10 (green), 1/8 (pink), 1/5 (cyan), 1/3 (brown), 1/2 (violet), 1/1 (dark blue). The pyrene-fluorescence drops immediately to a stable plateau without any slow decline of the fluorescence. B-D) Relative activity of different SpireWH2 constructs, the error bars represent the standard error of the mean (figure modified after Sitar et al (2011)).

To exclude the possibility that SpireWH2 constructs quench pyrene-fluorescence, viscometry measurements were carried out as well. Any possible fluorescence quenching effect could be excluded, since addition of SpireWH2 domains to actin reduced the viscosity of the actin gel, both when co-polymerized with SpireWH2 constructs (figures 17 A and B) and when the SpireWH2 domains were added to completely polymerized actin (figure 17 C). Falling ball viscometry experiments confirmed the strong sequestering activity of SpireWH2 domains (figures 17 A and B). The F-actin disrupting activity of SpireWH2 domains was confirmed by low shear Ostwald viscometry measurements (figure 17 C). Hence, the sequestering and F-actin disrupting activities of SpireWH2 domains are independent from the nucleating activity since the rapid decrease of pyrene-fluorescence and the dose-dependent loss of viscosity in an F-actin solution can be detected with single WH2 domains as well.

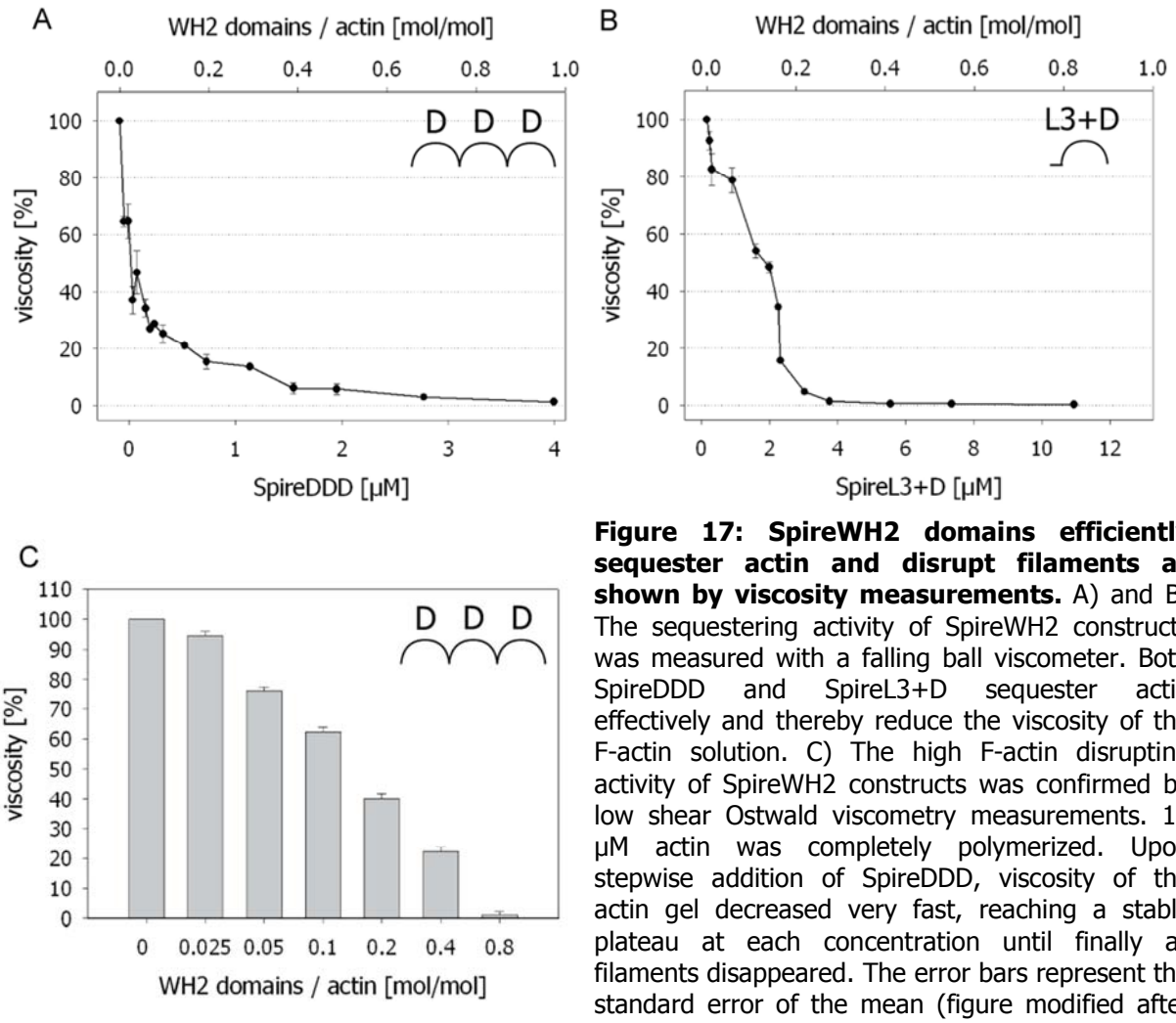

Figure 17: SpireWH2 domains efficiently sequester actin and disrupt filaments as shown by viscosity measurements. A) and B) The sequestering activity of SpireWH2 constructs was measured with a falling ball viscometer. Both SpireDDD and SpireL3+D sequester actin effectively and thereby reduce the viscosity of the F-actin solution. C) The high F-actin disrupting activity of SpireWH2 constructs was confirmed by low shear Ostwald viscometry measurements. 12 µM actin was completely polymerized. Upon stepwise addition of SpireDDD, viscosity of the actin gel decreased very fast, reaching a stable plateau at each concentration until finally all filaments disappeared. The error bars represent the standard error of the mean (figure modified after Sitar et al (2011)).

The breakage of the filaments by SpireWH2 domains was also shown by total internal reflection fluorescence (TIRF) microscopy (figure 18 and movie S1 http://www.pnas.org/content/suppl/2011/11/17/1115465108.DCSupplemental/SM01.mov). The SpireWH2 constructs attack the filaments at multiple places, resulting in initially randomly distributed gaps which then increase at both ends. Figure 18 B shows a kymograph of a filament which was disrupted by SpireDDD. It is clear that the filament was disintegrated from its ends but especially from its middle where the gaps in the filament become visible after about 20 seconds.

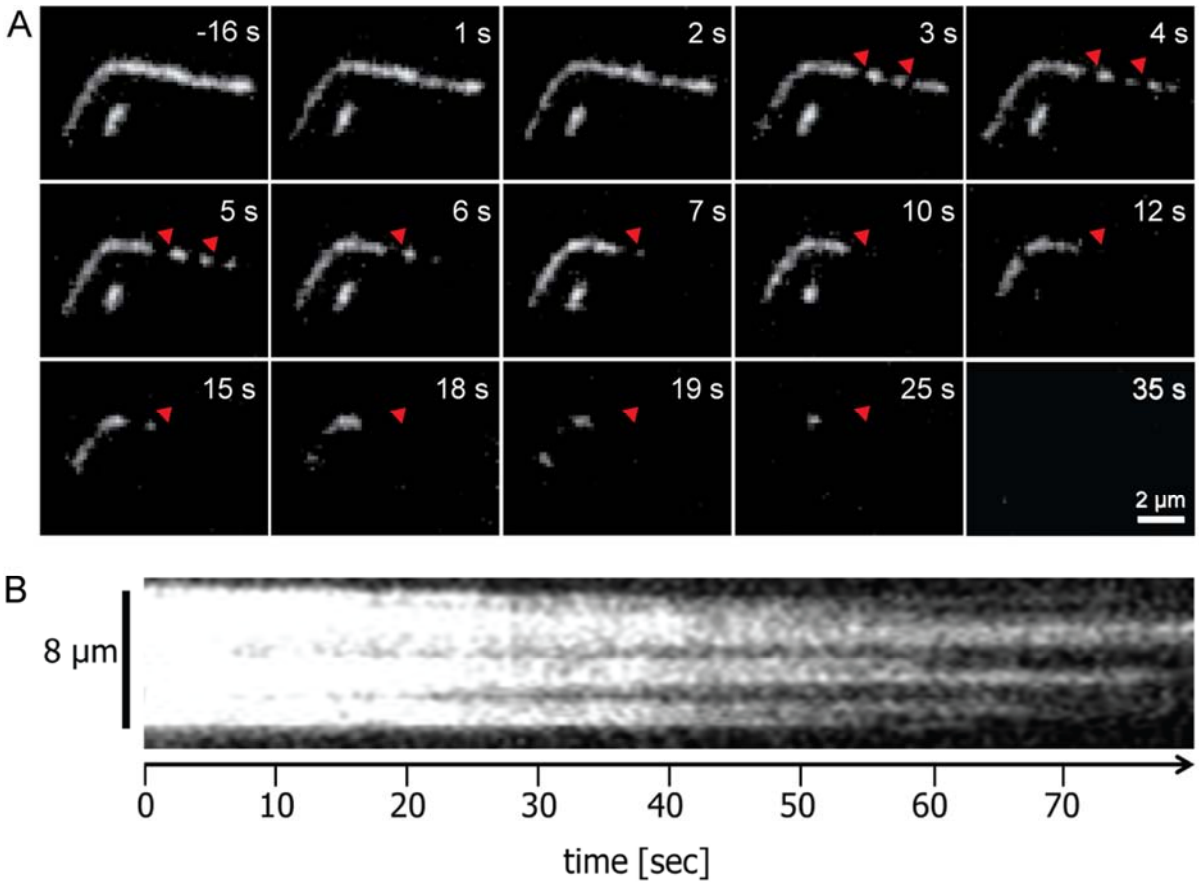

Figure 18: SpireWH2 constructs disrupt preformed actin filaments extremely fast as shown by TIRF microscopy. The kinetics of filament disruption (see also movies S1 and S2) have been visualized on a TIRF microscope. A) Alexa555-actin was polymerized and the filaments were treated with SpireDDD (time t0). Red arrowheads indicate areas of initial filament disruption. Note that the F-actin is disrupted in a matter of seconds and does not follow the well-known depolymerization kinetics from barbed ends only. B) Kymograph depiction of filament disruption by SpireDDD (generated by Michael Wohlhöfler, Bausch laboratory, TU München). The 8 µm filament is displayed in the vertical, and its disruption over time is shown in the x-axis. The filament consists of 20 % Alexa555-actin. Upon addition of SpireDDD, the filament was disrupted from its ends but also pieces were ripped out from its middle. The filament almost completely disappeared within 80 seconds (figure modified after Sitar et al (2011)).

Most intriguingly, SpireDDD can even disrupt actin-fascin bundles very quickly. These bundles usually consist of about 20 actin filaments (Claessens et al, 2008). Recent studies revealed that actin-fascin bundles are extremely stable and resistant against disruption by cofilin over days (Schmoller et al, 2011). Alexa555-actin was bundled with fascin in a 1/1 ratio and the bundles were seeded onto a coverslip. In a TIRF assay, 3 µM SpireDDD were added to the bundles. SpireDDD can forcefully sequester actin monomers even from these filament bundles. Like observed for the the filaments, also the bundles showed initially randomly distributed gaps when treated with SpireWH2 constructs. The bundles completely disappeared within about 80 seconds (movie S2 http://www.pnas.org/content/suppl/2011/11/17/1115465108.DCSupplemental/SM02.mov).

3.4.3 SpireWH2 domains bind G-actin but are not stably associated with actin filaments

SpireWH2 tandem constructs nucleate actin polymerization at substoichiometric concentrations, at higher concentrations G-actin sequestration is the most prominent activity, the decrease of pyrene-fluorescence at steady state is present both after nucleation and sequestration. These observations clearly suggest that SpireWH2 domains interact with G- as well as F-actin. To investigate whether the SpireWH2 tandem constructs remain bound along filaments over a prolonged time, spindown assays were performed. First, a standard polymerization assay was carried out with 15 % tetramethylrhodamine (TMR)-labeled SpireDDD (figure 19 A). The sample to which Spire was added in a WH2/actin ratio of 1/30 (figure 19 A, green graph) was ultracentrifuged to separate F-actin from the soluble fraction. Subsequently, a scan between 550 and 590 nm was performed at the fluorometer with supernatant and pellet fractions (figure 19 B). The emission maximum of TMR is at about 575 nm. Clearly, TMR-SpireDDD could only be detected in the soluble fraction (figure 19 B, red graph), whereas no TMR-signal could be measured in the F-actin pellet fraction (figure 19 B, green graph) and thus TMR-SpireDDD could not be co-sedimented with filamentous actin. These data suggest that SpireWH2 constructs are released from the emerging filament after effected nucleation.

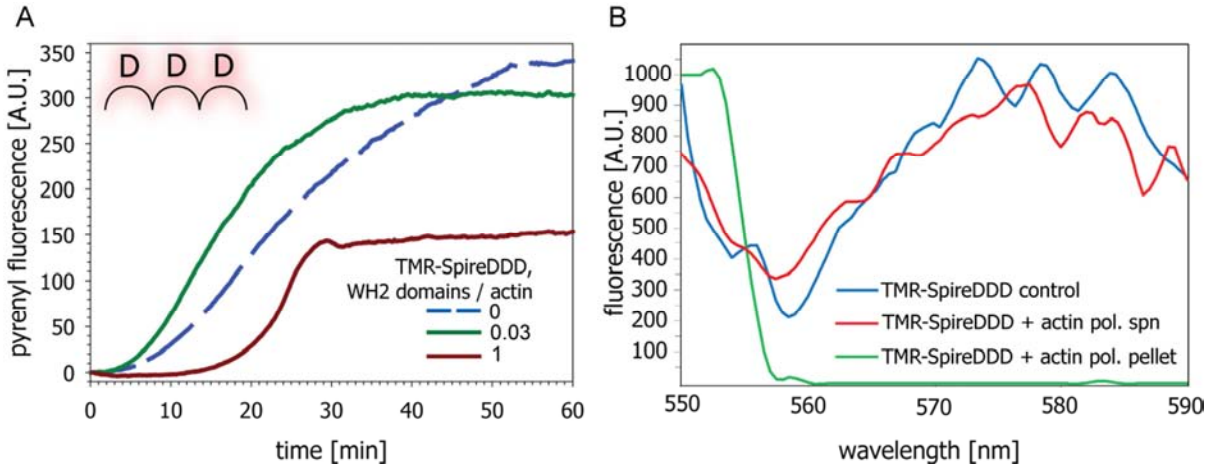

Figure 19: SpireWH2 domains are not associated with actin filaments after effected nucleation as shown by a spindown assay with TMR-labeled SpireDDD. A) 2 µM actin (10 % pyrenylated) were polymerized in presence of the indicated ratios of 15 % TMR-labeled SpireDDD. SpireDDD shows nucleation of actin polymerization when added at substoichiometric concentrations and sequesters actin when added in higher concentrations. B) The nucleation sample (green graph from A) was ultracentrifuged and supernatant and pellet were scanned at the fluorometer. The emission maximum of TMR is at around 575 nm (compare TMR-SpireDDD control, blue graph). TMR-SpireDDD could only be detected in the supernatant (red graph) but not in the F-actin pellet fraction (green graph).

Another F-actin spindown assay was conducted in which the centrifugation was performed after the addition of SpireDDD to preformed filaments. In one sample, the actin filaments were stabilized with phalloidin, then SpireDDD was added and the sample was subsequently centrifuged and analyzed on a Coomassie Blue stained SDS-gel (figure 20). After effected disruption of preformed actin filaments, SpireWH2 constructs were found in the supernatant (figure 20, SpireDDD in lane 7), where now also most of the actin was located (at ca. 42 kDa). Thus, SpireWH2 constructs disrupt the F-actin, sequester the actin molecules and take them into the soluble fraction. However, when the filaments were stabilized with phalloidin, SpireWH2 constructs could not disrupt these filaments. Nevertheless, the affinity to actin seems to be so high that they can bind to the filaments and even can be co-sedimented together with the phalloidin-F-actin (figure 20, SpireDDD in last lane) although WH2 domains are G-actin binding motifs in principle. This accounts for single SpireWH2 domains as well; an assay with SpireL3+D leads to the same result. These data suggest that phalloidin connects F-actin subunits so tightly that SpireWH2 domains can bind but not break the filaments by removing monomers and that the affinity of SpireWH2 domains is so high that they even bind to actin in the filament conformation. Concluding, SpireWH2 domains are not associated with F-actin unless the filaments are stabilized with phalloidin. Usually, after effected nucleation, sequestration or disruption of actin filaments they are always found in the soluble fraction.

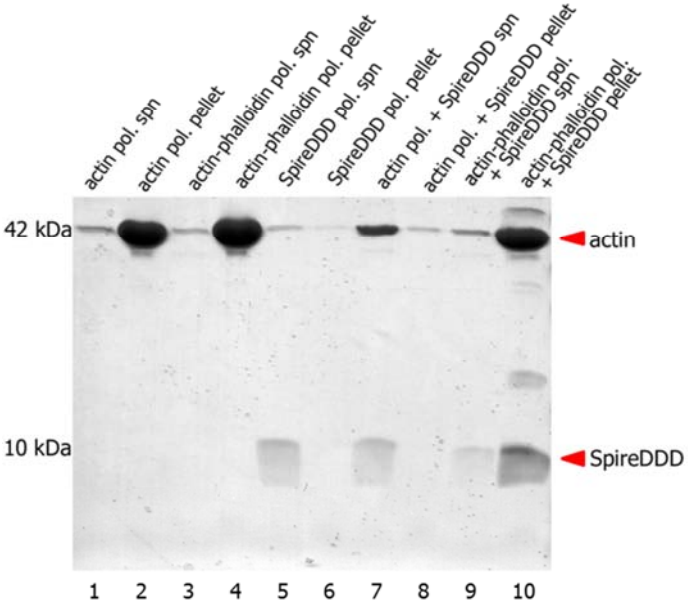

Figure 20: SpireWH2 domains only efficiently disrupt F-actin if not phalloidin-stabilized. Coomassie Blue stained SDS-gel showing an F-actin spindown. SpireWH2 domains chop up actin filaments, thereby shifting the actin into the soluble fraction in an F-actin spindown. However, SpireWH2 domains cannot disrupt phalloidin-stabilized filaments, but decorate them. In the assay, 2 µM actin was polymerized, then stabilized with phalloidin where noted. SpireDDD was added in a ratio of 2 WH2 domains / 1 actin molecule. The samples were ultracentrifuged and the pellet and soluble fractions were analyzed on a SDS-gel as indicated. Pellet fractions are concentrated 10-fold.

The binding of SpireDDD to actin was investigated in a preliminary fluorescence resonance energy transfer (FRET) experiment. TMR-labeled SpireDDD was used as a donor, and QSY 7-labeled actin as an acceptor. QSY 7 is an essentially non-fluorescent quencher, having its absorption maximum at about 560 nm. The emission maximum of TMR is at about 575 nm, while its excitation maximum is at around 540 nm. The fluorescence of TMR-SpireDDD was monitored in a scan from 550 to 585 nm (figure 21). When TMR-SpireDDD in water was measured, a fluorescence peak at around 575 nm could be captured (figure 21, blue graph). QSY 7-labeled actin or water alone did not show any emission of fluorescence in this spectrum (figure 21, green graph). When QSY 7-labeled actin was incubated together with TMR-SpireDDD, the fluorescence was decreased and a quenching efficiency of about 60 % could be detected, indicating that QSY 7-actin and TMR-SpireDDD were binding to each other under non-polymerizing conditions.

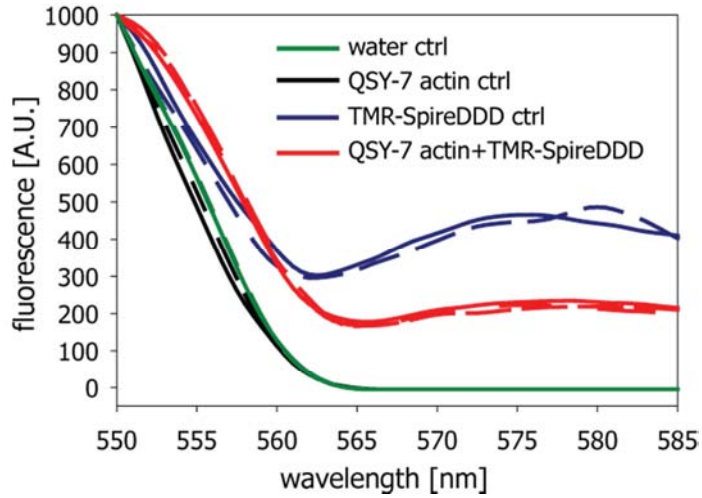

Figure 21: SpireWH2 constructs bind to G-actin as shown by FRET. The emission spectrum of TMR-SpireDDD was measured. TMR-SpireDDD alone shows a peak of fluorescence at about 575 nm (blue graph). Water and QSY 7-labeled actin alone do not show any peak in this emission spectrum (green and black graph). When QSY 7-actin and TMR-SpireDDD were incubated together, the fluorescence intensity was decreased by about 60 %, indicating a binding of actin and SpireDDD, which resulted in fluorescence quenching.

3.5 *D. discoideum* amoebae respond to treatment with SpireWH2 constructs

Most surprisingly, *D. discoideum* amoebae respond to the treatment with SpireWH2 constructs. This is an unexpected behavior since proteins usually cannot simply enter cells to trigger intracellular processes. However, starting from a concentration of 3 µM SpireDDD either diluted in HL5 medium or Soerensen buffer, the cells stop migrating and round up (figure 22 A). The cells perfectly recover if SpireDDD is removed by washing the cells. The amoebae did not respond to heat-inactivated SpireDDD. Adding SpireDDD to migrating fluorescent GFP-cofilin and RFP-actin expressing cells seems to affect their actin cytoskeleton (figure 22 B). Upon addition of SpireDDD the cells look like as if they would have been treated with the toxin Latrunculin A which inhibits actin polymerization by sequestering monomeric actin.

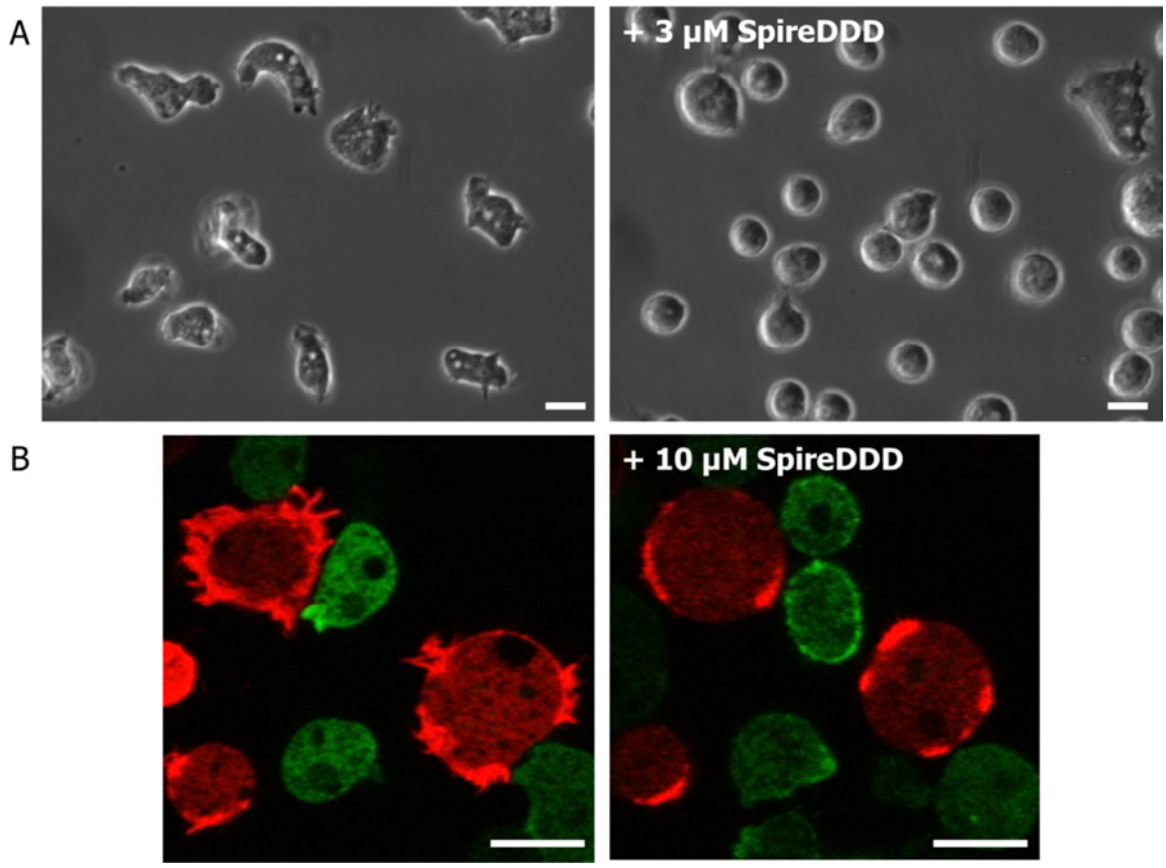

Figure 22: *D. discoideum* amoebae respond to treatment with SpireWH2 domains. . A) *D. discoideum* amoebae respond to treatment with SpireDDD starting from a concentration of 3 µM diluted in Soerensen buffer. B) GFP-cofilin and RFP-actin expressing cells were treated with 10 µM SpireDDD diluted in HL5 medium. Scale bar, 10 µm.

Even more intriguingly, the addition of increasing concentration of SpireWH2 domains induced the formation of cytoplasmatic rods in *Dictyostelium* amoebae. When incubating GFP-cofilin expressing cells with 30 µM SpireDDD for one hour, the cells form cytoplasmic rods and look clearly different to untreated cells (figure 23). The addition of SpireWH2 domains seems to exert a certain stress on the cells. Possibly, the SpireWH2 constructs might pass the membrane of *D. discoideum* cells and disrupt the filamentous actin network. To further investigate whether SpireWH2 domain constructs would enter a *D. discoideum* cell, the addition of 5 µM TMR-labeled SpireBCD to GFP-cofilin expressing *D. discoideum* cells was recorded at the confocal microscope. During this experiment, the cells responded to the treatment, rounded up and even formed GFP-cofilin rods. However, no TMR-SpireBCD could be detected within the cells (data not shown).

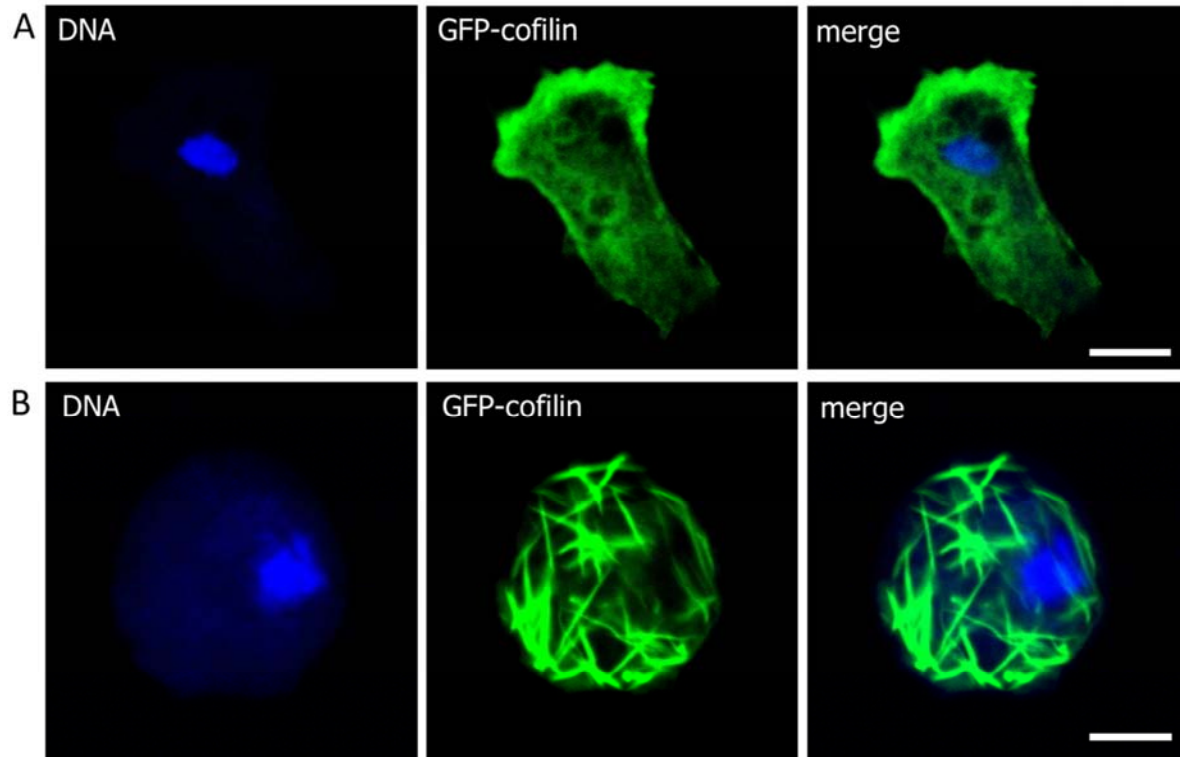

Figure 23: *D. discoideum* cells round up and form cytoplasmic cofilin rods upon addition of high concentrations of SpireDDD. Fixed AX2 GFP-cofilin cells. The DNA was stained by ToPro (blue). Scale bar, 5 µm. A) Untreated AX2 GFP-cofilin control cell. The GFP-cofilin localizes at the cell cortex, in this cell especially in the leading edge. B) The AX2 GFP-cofilin cells were incubated with 30 µM of SpireDDD diluted in HL5 medium for 60 minutes. The cells rounded up and formed cytoplasmic cofilin-rods.

4. Results II: Actin variants in *Dictyostelium* amoebae

In this part of the thesis, *D. discoideum* actin variants and in particular filactin were analyzed. The identity of actin variants with conventional *D. discoideum* actin ranges from 37 % - 97 %. Act3 differs from conventional actin by only 8 amino acids, whereas act31 is highly divergent with only 143 identical residues out of 365 amino acids. Act24 and act25 are 82 % and 78 % identical with conventional actin, respectively. Filactin is the most extraordinary actin variant in *D. discoideum*, since it comprises besides its actin domain a large extended N-terminus. Previous studies confirmed that the genes encoding these actin variants are transcribed in vegetative and developing *D. discoideum* NC4 cells (Romans et al, 1985). For filactin, act24 and act25 more than 15 expressed sequence tags (ESTs) were found. For act3, act18 and act31 one to 5 ESTs were documented (Joseph et al, 2008; Urushihara et al, 2004). Hypothetically, act3, act24, act25 and filactin could be part of the cytoskeleton, whereas other more divergent actin variants, e.g. act18 or act31 might have rather regulatory than structural functions. Table 2 shows a summary of information available about the actin variants investigated in more detail in this study.

Table 2: Actin variants analyzed in this study. (Sources: Dictybase.org, NCBI Blast)

	act24	**act25**	**filactin actin domain (aa 574-944)**
Dictybase Gene ID	DDB_G0289505	DDB_G0289507	DDB_G0284389
Identity with *D. discoideum* conventional actin (P07830)	82 %	78 %	64 %
Identity with human beta-actin (P60709)	80 %	74 %	67 %
Identity with rabbit muscle actin (P68135)	78 %	72 %	65 %
location of the gene	Chromosome 5	Chromosome 5	Chromosome 4
number of amino acids	377 aa	385 aa	370 aa
Number of identified ESTs	>15	>15	>15
predicted molecular function	nucleotide binding; structural molecule activity; structural constituent of the cytoskeleton; protein binding; ATP binding; myosin binding	nucleotide binding; structural molecule activity; structural constituent of the cytoskeleton; protein binding; ATP binding; myosin binding	nucleotide binding; structural molecule activity; protein binding; ATP binding
predicted cellular component	cytoskeleton; actin cytoskeleton	cytoskeleton; actin cytoskeleton	cytoskeleton

The protein sequences of the actin variants show high similarity to *D. discoideum* conventional actin and rabbit muscle actin (figure 24).

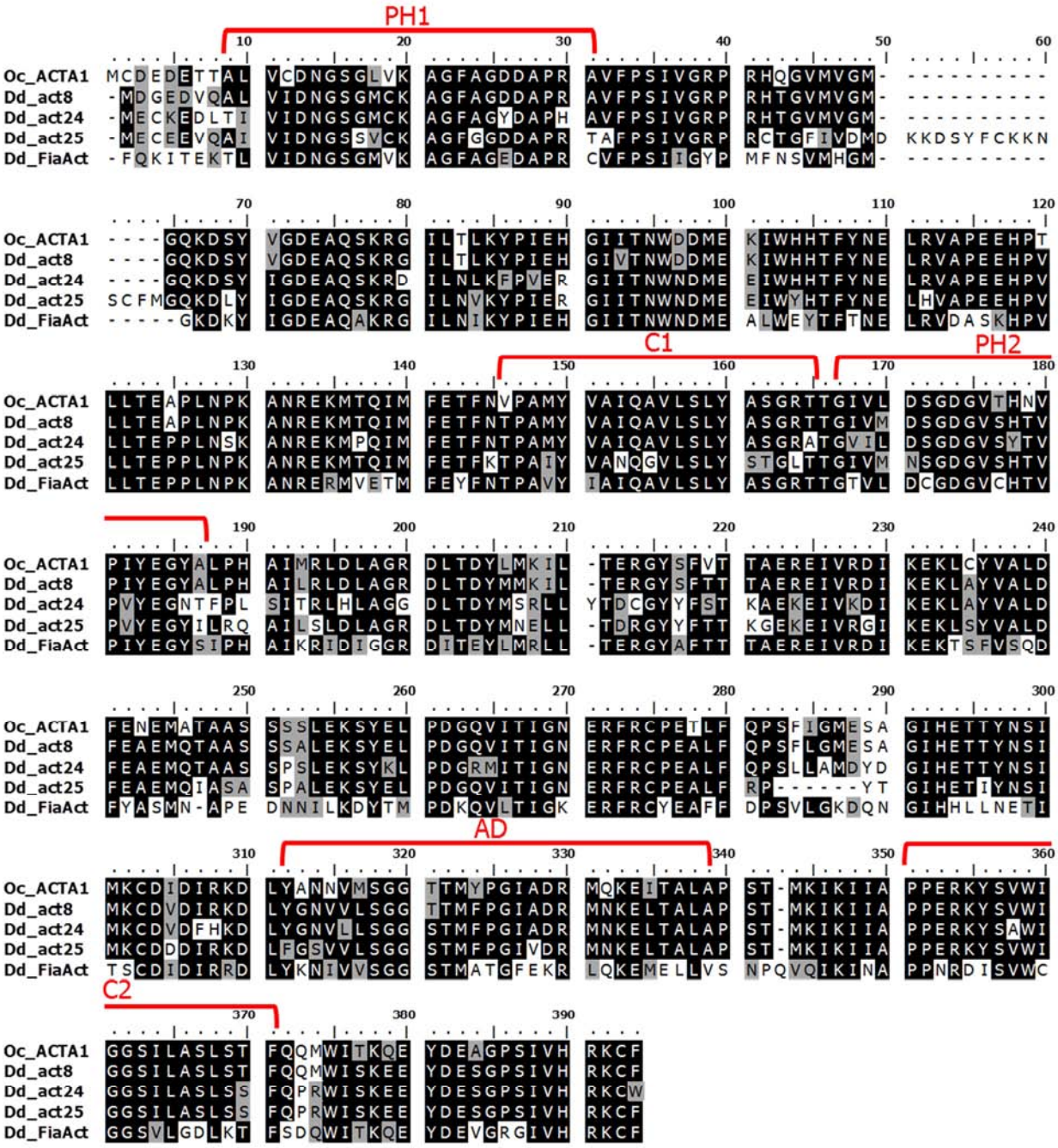

Figure 24: Alignment of selected *D. discoideum* actin variants. Rabbit muscle actin (Oc_ACTA1, P68135) and Dd_act8 as the conventional actin in *D. discoideum* (P07830) were set as a reference. The filactin actin domain is defined as aa 574-944 of the filactin protein. Identical residues are shown on a black background, similar residues are displayed on a grey background. Blosum 62-12-2 was used as alignment parameter and the threshold for shading was set to 56 %. The five conserved actin sequence motifs of rabbit muscle actin and the *D. discoideum* act8 group are highlighted by red brackets: PH1, phosphate binding loop 1; C1, connecting motif 1; PH2, phosphate binding loop 2; AD, adenosine binding loop; C2, connecting motif 2.

4.1 Analysis of the actin variant filactin, a potential new player in the ESCRT pathway

The protein filactin belongs to the actin variants of *D. discoideum*. It distinguishes itself from the other 15 known actin variants by its long N-terminal extension with a distinct domain organization (figures 5 and 25). The actin domain which shows 64 % identity to the conventional *D. discoideum* actin (act8-group, figure 24) and 67 % identity to human β-actin, is located at the very C-terminus (aa 574-944). The N-terminus shows homology to three different sequence motifs: (1) an Ist1-like domain at the very N-terminus, (2) a PEST-motif and (3) two filamin-like Ig repeats.

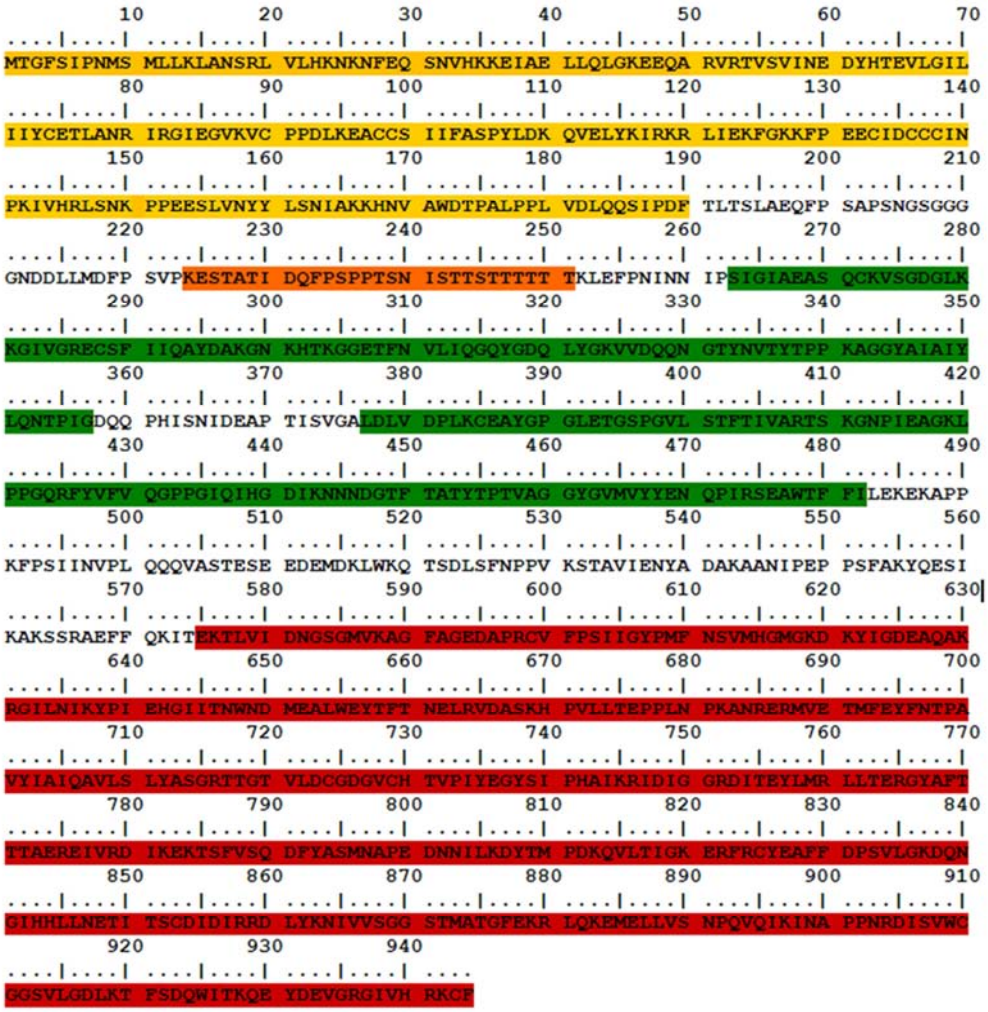

Figure 25: Amino acid sequence and domain organization of filactin. Filactin is composed of 944 amino acids, resulting in a molecular weight of about 105,000. The actin domain (red) showing higher homology to muscle actin than to actin-related proteins (ARPs) is located at the C-terminus. The N-terminus exhibits a distinct domain organization, including an Ist1-like domain (yellow), a PEST-motif (orange) and two filamin-like Ig repeats (green).

Homologs of filactin were identified via BLASTp sequence analysis in *D. fasciculatum*, *D. purpureum*, *Polysphondylium pallidum* as well as in *E. histolytica*, *E. nuttalli*, *E. invadens* and *E. dispar* (figure 26).

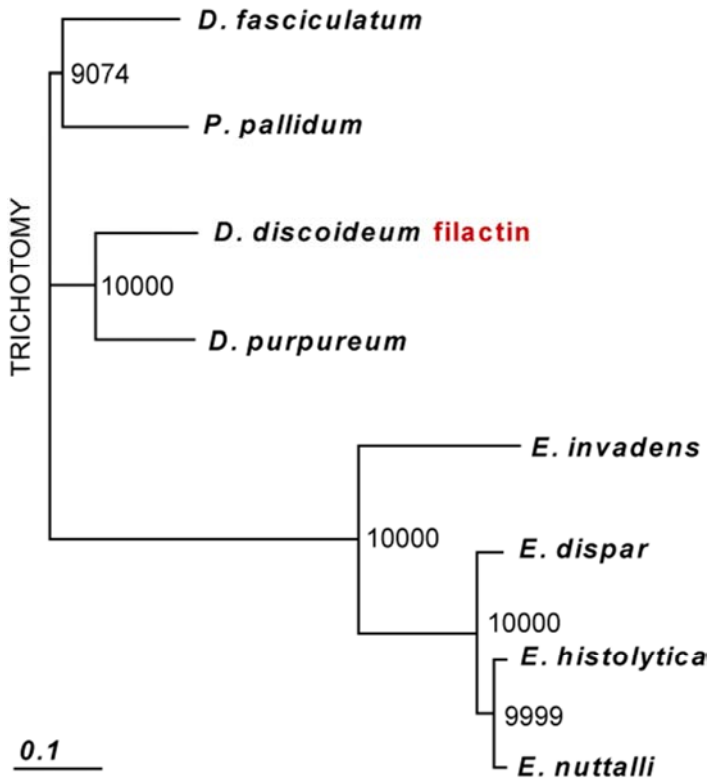

Figure 26: Evolutionary tree for the filactin protein family. MUSCLE alignments of *D. discoideum* filactin (XP_638602.1) and its homologs in *D. fasciculatum* (XP_004357688.1), *D. purpureum* (XP_003289904.1), *P. pallidum* (EFA82454.1), *E. invadens* (XP_004261427.1), *E. dispar* (XP_001734710.1), *E. histolytica* (XP_652978.1) and *E. nuttalli* (EKE41601.1) were used to create dendrograms with the CLUSTALX Tree View program. Bootstrap values are provided at the node of each branch. The scale bar indicates amino acid substitutions per site.

The filactin-like protein in *D. purpureum* is 74 % identical to filactin and shows high similarity even at the nucleic acid sequence level. In the other *Dictyosteliidae* shown in figure 26, the filactin homologs are about 63 – 65 % identical to filactin. In *Entamoebae*, the PEST-motif is missing as well as the 'unstructured' region between the filaminlike Ig repeats and the actin domain. Apart from the harmless *E. dispar*, the *Entamoebae* species shown in the tree are pathogens of either reptiles (*E. invadens*), macaques (*E. nuttalli*) or humans (*E. histolytica*).

4.1.1 Analysis of the filactin protein sequence

In this study, an Ist1-like domain (Ist1 = Increased sodium tolerance 1) was identified at the very N-terminus of filactin. Until now, the N-terminal domain was described as 'DUF292' (domain of unknown function 292) in dictybase.org. Via sequence analysis, the homology to the N-terminal part of yeast and human Ist1/IST1 was assigned (figure 27 and 28). Ist1 was first identified in *S. cerevisiae* and shown to be implicated in the ESCRT pathway, especially in the regulation of membrane scission and ESCRT-III disassembly (Dimaano et al, 2008; Entian et al, 1999).

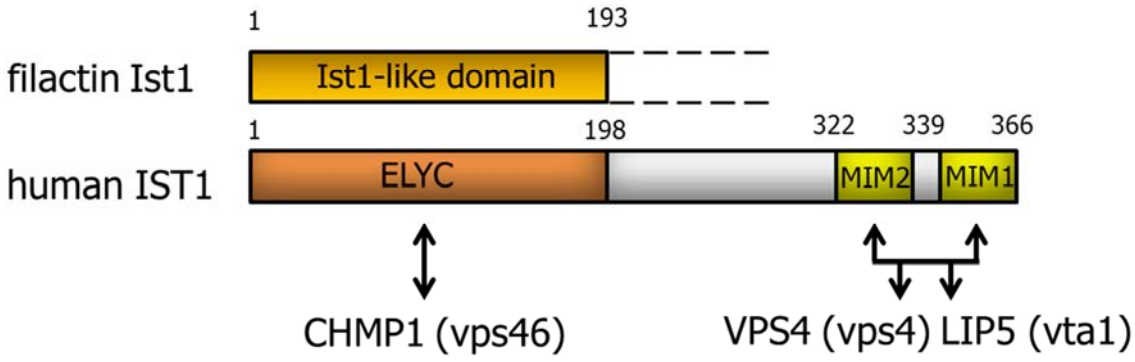

Figure 27: Homology of the filactin Ist1-like domain to the N-terminal part of human IST1. The filactin Ist1-like domain shows 35 % identity to the N-terminal domain of human IST1. In difference to filactin, the human IST1 harbors an ELYC-motif, responsible for protein interactions. The C-terminal part of human IST1 contains two MIMs (MIM, MIT-interacting motif; MIT, microtubule-interacting and transport) which seem to be specific for distinct targets. The interaction partners of human IST1 are indicated in capital letters below the both-way arrows, the corresponding homologs in *D. discoideum* follow in brackets. CHMP1, charged multivesicular body protein 1; vps46, vacuolar protein sorting 46; vps4, vacuolar protein sorting 4; LIP5, lysosomal trafficking regulator-interacting protein 5; vta1, vps twenty associated 1.

The *D. discoideum* genome encodes an Ist1-like protein (gene ID DDB_G0289029), which contains the domains present in human IST1. Filactin, however, only shares homology to IST1 only in its N-terminal Ist1-like domain and lacks the MIM domains (MIM, MIT-interacting motif; MIT, microtubule-interacting and transport). MIM domains are sequence motifs of ESCRT-III proteins that were found to interact with MIT domains (MIT, microtubule-interacting and transport). MIT domains were first identified in endosomal trafficking proteins (Ciccarelli et al, 2003) and the ESCRT proteins vta1 and vps4 contain these motifs as well.

The Ist1-like domain of filactin shows 35 % identity to the N-terminal part of human IST1 (figure 27). A ribbon model of the filactin Ist1-like domain was generated using human IST1 (Bajorek et al, 2009b) as a template (figure 28). Proteins belonging to the ESCRT-III complex vary significantly in primary sequence, but share a common secondary structure of

N-terminal core domains (ca. 150 residues), containing various α-helices (figure 28 A). In ESCRT-III proteins, the C-terminal α5 helix seems to be responsible for autoinhibiting the N-terminal core domains, especially hydrophobic residues near the tip of the helical hairpin of the α1 and α2 helices (Bajorek et al, 2009b; Muziol et al, 2006; Xiao et al, 2009). In the 'closed' and monomeric conformation, residues along the hairpin surface responsible for membrane binding and polymer assembly remain hidden and prevent premature membrane binding and oligomerization, consequently the protein remains in the cytoplasm. In the 'open' conformation, autoinhibitory interactions are released and the subunits can bind to each other and to the membrane during their assembly into functional ESCRT-III polymers. ESCRT-III proteins can assemble into filamentous polymers on membranes. These filaments have an intrinsic tendency to curve and form ring-like spiral filaments on the membrane (Ghazi-Tabatabai et al, 2008; Hanson et al, 2008; Saksena et al, 2009).

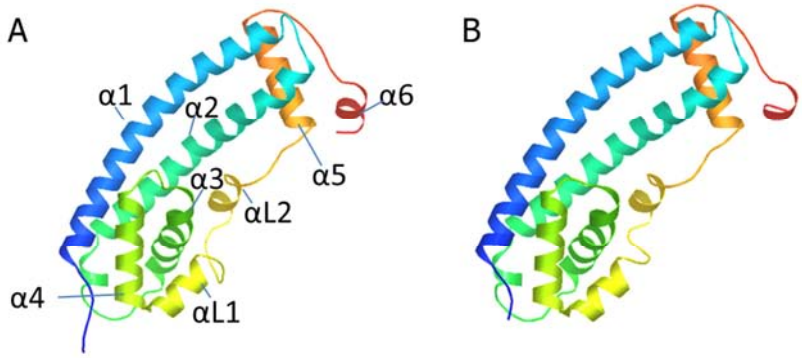

Figure 28: Ribbon model of the N-terminal part of human IST1 used as template and the modeled filactin Ist1-like domain. Swiss Model Expasy was used (Arnold et al, 2006). The color code is a rainbow gradient starting at the N-terminus in blue and ending at the C-terminus in red. A) Human IST1 (PDB 3FRRA, residues 1-189) was used as a template (Bajorek et al, 2009b). The N-terminal domain of human IST1 shares the common secondary structure of ESCRT-III proteins and contains 8 α-helices. B) Filactin Ist-like domain (aa 1- 240) modeled to the N-terminal part of human IST1.

In humans and yeast, the Ist1 protein was shown to interact with other proteins of the ESCRT machinery, namely CHMP1/Did2, VPS4/vps4 and LIP5/vta1 via its different domains, (Bajorek et al, 2009a; Dimaano et al, 2008; Rue et al, 2008). The filactin Ist1-like domain shows only a homology to the N-terminal part of IST1/Ist1 which binds to CHMP1/Did2 in human or yeast. The N-terminal ELYC motif of yeast Ist1 was described to be involved in the binding to the yeast CHMP1-like protein Did2 (Dimaano et al, 2008), corresponding to *D. discoideum* vps46. However, another study specifies different residues to be responsible for CHMP1/Did2 binding. On a structural basis, Xiao and others (2009)

identified residues forming a conserved binding groove for Ist1-Did2 interaction, highlighted by red arrows in figure 29. In human IST1, different residues mostly in the same regions were described to be important for CHMP1B binding (figure 29, blue arrows, Bajorek et al, 2009b). Both in filactin and *D. discoideum* Ist1-like protein, the ELYC motif is not conserved as in human and yeast. However, about 60 % of the residues predicted to be responsible for protein-interaction are conserved in the filactin Ist1-like domain. Compared to the residues described to be essential in human IST1 to bind to CHMP1B, four out of five residues are conserved in the filactin Ist1-like domain, and all of them are conserved in *D. discoideum* Ist1-like. To test a possible interaction of *D. discoideum* vps46 with the Ist1-like domain of filactin, a GFP-vps46 overexpressing *D. discoideum* strain was generated in this study, as well as a GST-vps46 fusion protein. The data of these experiments are presented below (see 4.2.4.).

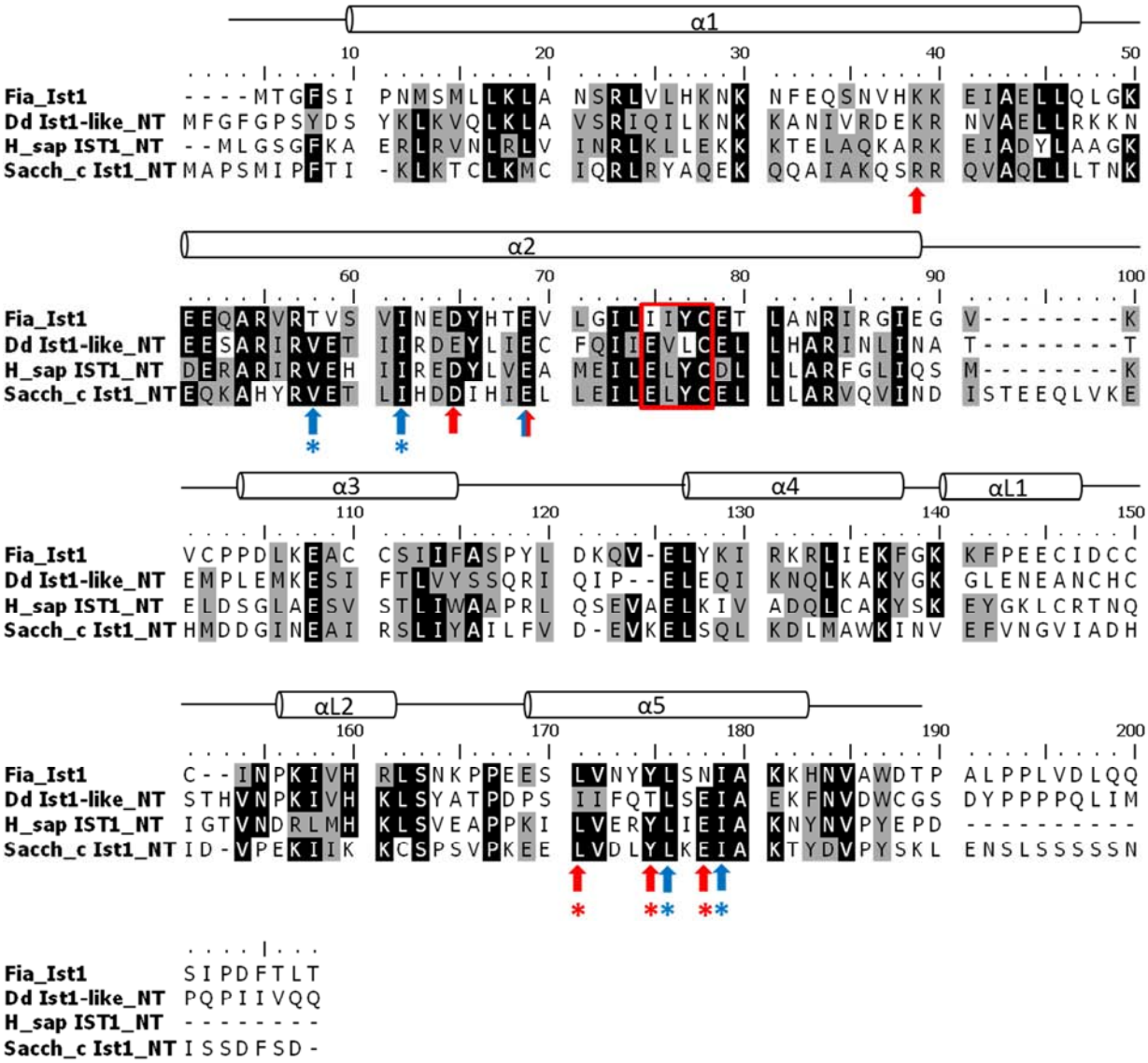

Figure 29: Alignment of the filactin Ist1-like domain (aa 1-190) to the N-terminal part of human IST1, yeast Ist1 and *D. discoideum* Ist1-like. Amino acid 1-198 of *H. sapiens* IST1 (Swiss Prot P53990), aa 1-204 of *S. cerevisiae* Ist1 (Swiss Prot P53843) and aa 1-198 of *D. discoideum* Ist1-like (DDB_G0289029) were used. The yeast and human Ist1/IST1 proteins harbor an ELYC-motif (red box, alignment aa 75-78,) responsible for protein interactions. This ELYC-motif is not completely conserved in the filactin Ist1-like domain and also not in the *D. discoideum* Ist1-like protein. Residues described to be involved in forming the conserved binding groove for the human CHMP1B and yeast CHMP1-like protein Did2 are marked with blue and red arrows, respectively. Residues essential for that binding (Bajorek et al, 2009b; Xiao et al, 2009) are additionally highlighted by stars. The secondary structure of human IST1 is depicted above the sequence.

A putative PEST-motif can be found downstream from the Ist1-like domain (figure 25, orange). A PEST motif is a peptide sequence with relatively high local concentrations of the amino acids proline (P), glutamic acid (E), serine (S), threonine (T) and to a lesser extent aspartic acid (D) (Rechsteiner & Rogers, 1996; Rogers et al, 1986). These internal sequences are recognized by protein degrading enzymes, e.g. the proteasome or calpain, reducing the

half-life of the protein drastically. This could explain why filactin is so sensitive to proteolytic cleavage.

Filactin contains two central domains which are homologous to typical filamin-like Ig repeats. Filamins are homodimeric F-actin-crosslinking proteins. Each monomer consists of an actin binding domain and a rod segment containing 6 (*D. discoideum*) to 24 (*H. sapiens*) highly homologous repeats of about 96 residues which are arranged in an Ig-like fold (Popowicz et al, 2006). The filactin filamin repeats are 32 % and 37 % identical to *D. discoideum* filamin Ig repeat #5 and 31 % and 33 % identical to human filamin B Ig repeat #13, respectively. Figure 30 shows a model of *D. discoideum* filamin and a ribbon model of the predicted structure of filactin's filamin-like Ig repeats.

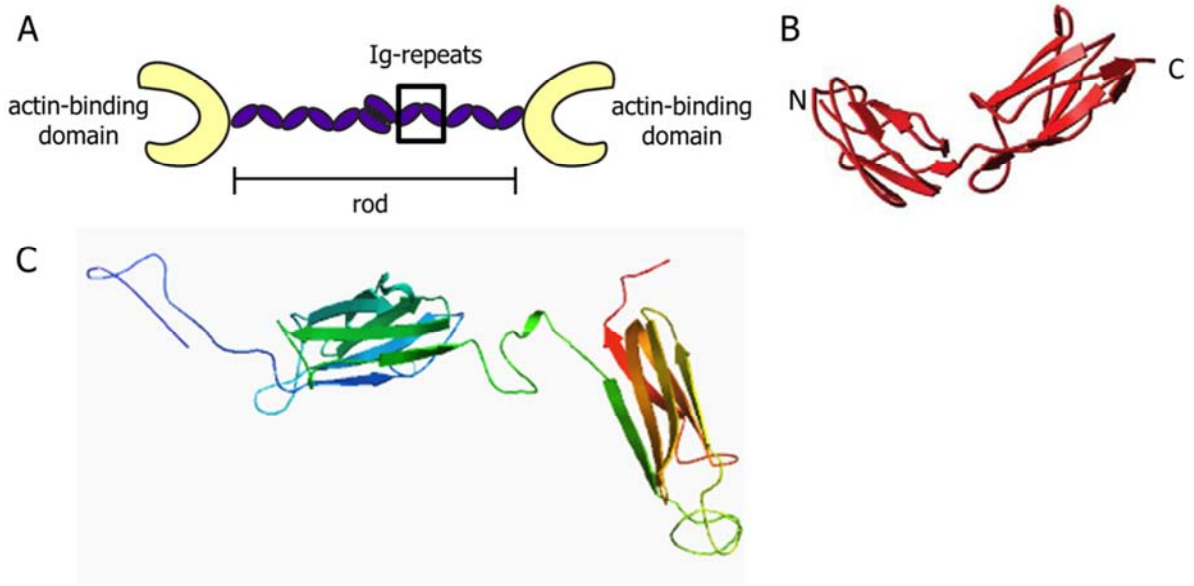

Figure 30: Filamin-like Ig folds in *D. discoideum* filactin. A) Model of *D. discoideum* filamin (modified after Popowicz et al, 2004). Each subunit in the dimer contains an N-terminal F-actin binding domain, a rod with 6 Ig repeats, and the dimerization is based on a direct interaction of the domains #6 (McCoy et al, 1999; Popowicz et al, 2004). The filactin filamin repeats are homologous to these repeats. B) Ribbon model of *D. discoideum* filamin Ig repeats #4 and #5 of the filamin rod segment (modified after Popowicz et al, 2004). C) Ribbon model of filactin filamin-like Ig repeats (aa 241- 490) modeled to the crystal structure of *D. discoideum* filamin rod repeats (PDB 1wlh1A, Swiss Model Expasy).

The actin domain of filactin is located at the C-terminus of the protein (aa 574-944). The alignment displayed in figure 24 demonstrates that it is highly similar to other actins. It shares 67 % identity with human β-actin and has higher homology to muscle actin than to actin-related proteins. Filactin thus belongs to the *bona fide* actins and can be classified as an actin with elongated N-terminus. The putative structure of the filactin actin domain (figure 31 B) shows that it fits very well into the 3D structure of rabbit muscle actin.

Consequently, the putative structure is organized like conventional actins with a large left side and a small right side which both can be subdivided further into a total of four subdomains (SD 1 - SD 4, figure 31 C; Joseph et al (2008)). The five conserved sequence motifs which are present in actins seem to be conserved in the filactin actin domain as well: the adenosine binding loop (AD), two phosphate binding loops (PH1 and PH2) and two connecting domains (C1 and C2) (figure 31 C). Most likely the filactin actin domain can bind ATP in its cleft between the main-domains one and two.

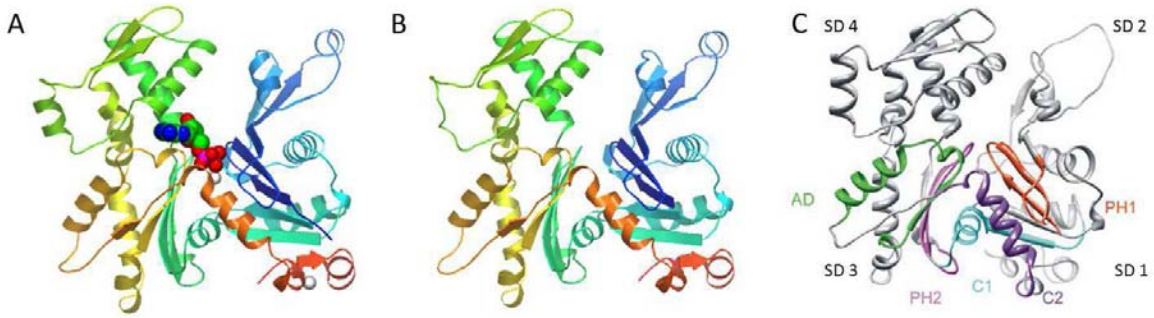

Figure 31: Ribbon model of rabbit muscle actin and the modeled filactin actin domain (aa 574-944). A) Ribbon model of the crystal structure of uncomplexed Oryctolagus cuniculus actin in the ADP state (PDB 1J6ZA; Otterbein et al, 2001) which was used as a template to model the putative structure of the filactin actin domain shown in B. C) Model of *D. discoideum* act8 organized in 4 subdomains (SD 1-SD 4) (modified after Joseph et al, 2008). Five extremely conserved sequence motifs line the nucleotide binding pocket: the adenosine binding loop AD (green), the two phosphate binding loops PH1 and PH2 (red and purple, respectively) and the subdomain connecting motifs C1 and C2 (blue and violet, respectively).

4.1.2 Filactin antibodies

In this thesis, two monoclonal filactin antibodies were used, namely 3S-55-4 and 4S-59-4. The hybridoma cell lines were generated by Daniela Rieger. To generate the 4S-59-4 antibody, a mouse was immunized with the C-terminal part of filactin containing the actin domain. This antibody recognizes the actin domain of filactin and exhibits a weak cross-reaction with conventional actin (blue cross, 42 kDa, figure 32 C). The 3S-55-4 antibody recognizes the N-terminus of filactin and is even more specific than the 4S-59-4 since it does not cross-react with other actin proteins (figure 32 B). The specificity of both antibodies was tested using the filactin knock out (KO) cell line (generously provided by Jan Faix, Medizinische Hochschule Hannover). The 105 kDa filactin band present in the wild type AX2 cell line (figures 32 B and C, lane 1) is clearly missing for the filactin KO cell line (figures 32 B and C, lane 2).

In this study, the binding epitope of the 3S-55-4 antibody could be narrowed down to the filactin filamin repeats. Cell lines overexpressing the following different GFP-tagged

filactin domain constructs were used for western blot analysis: GFP-filactin (GFP-FiaFL, aa 1–944), GFP-filactin Ist1-like (GFP-FiaIst1, aa 1-196), GFP-filactin filamin repeats (GFP-FiaFilR, aa 259-488) and GFP-filactin actin (GFP-FiaAct, aa 570 – 944). The anti-GFP antibody K3-184-2 was used as a control (figure 32 A). As displayed in figure 32 B, the antibody 3S-55-4 binds to endogenous full length filactin (red arrow head, 105 kDa) and to the overexpressed GFP-filactin filamin repeats (red star, 52 kDa). The antibody 4S-59-4 (figure 32 C) recognizes endogenous full length filactin (blue arrow head, 105 kDa) as well as GFP-tagged full length filactin (data not shown), the GFP-filactin actin domain (blue star, 70 kDa) and it cross-reacts with another actin at around 42 kDa (blue cross).

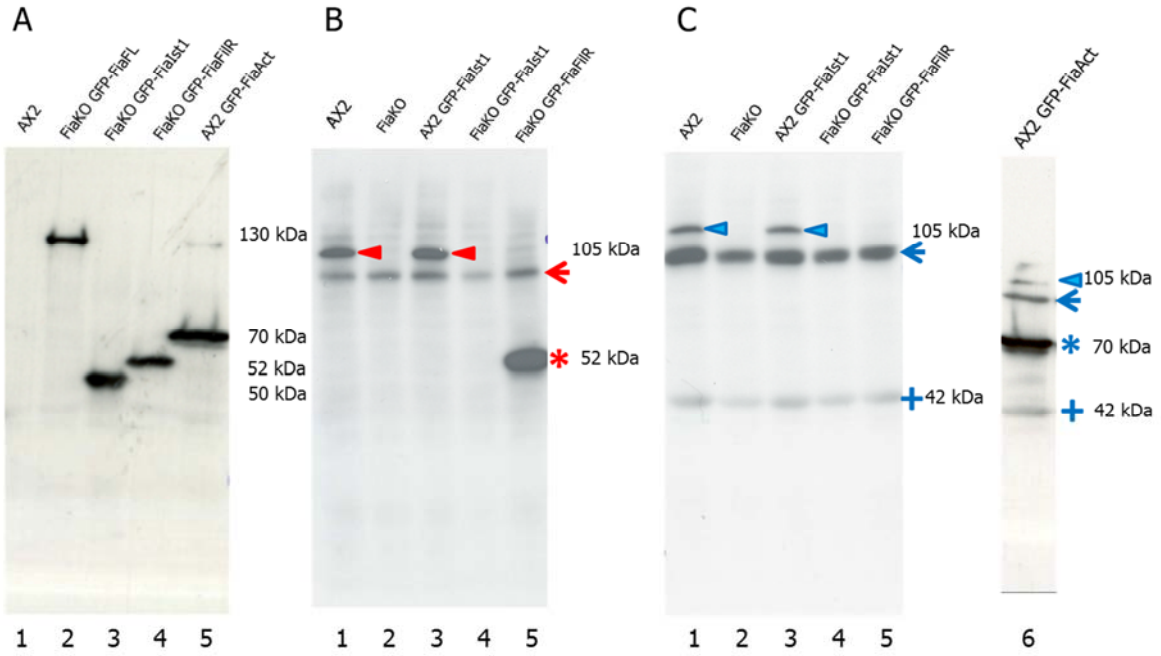

Figure 32: Defining the binding epitopes of the monoclonal filactin antibodies 3S-55-4 and 4S-59-4. A) Western blot using the monoclonal GFP antibody K3-184-2 to test the overexpression of the GFP-tagged filactin constructs. B) Western blot using the monoclonal antibody 3S-55-4. The antibody recognizes the endogenous filactin at around 105 kDa (lane 1 and 3, red arrow head) and the overexpressed GFP-tagged filamin repeats in lane 5 (red star). The antibody shows a reaction with an unknown protein at around 90 kDa (red arrow). C) Western blot using the monoclonal antibody 4S-59-4. The antibody binds to the endogenous filactin at around 105 kDa (lane 1, 3 and separate lane 6, blue arrow head) and to the GFP-tagged filactin actin domain (separate lane 6, blue star). Moreover, it shows a cross-reaction with an actin at around 42 kDa (blue cross) and with an unknown protein at around 90 kDa (blue arrow).

It is noteworthy that the filactin C-terminal antibody 4S-59-4 shows a cross reaction with another actin (probably conventional actin), whereas the actin antibody act-1 recognizing *D. discoideum* conventional actin (Simpson et al, 1984) cannot bind to the filactin actin domain (data not shown). In addition, the actin antibody 224-236-1 (Westphal et al, 1997) is also not binding to filactin (data not shown).

4.1.3 Filactin is associated with the actin cytoskeleton

4.1.3.1 Localization studies of filactin in *D. discoideum* using fluorescence microscopy

GFP-filactin (GFP-tag at the N-terminal side) co-localizes with conventional actin at the cell cortex (figure 33 C) and is also found in the cytoplasm where it localizes at vesicle-like structures. Filactin full length with the GFP-tag at the C-terminus (filactin-GFP) shows the same localization (data not shown). Immunofluorescence studies using the filactin antibodies 3S-55-4 and 4S-59-4 confirm the cortical and cytoplasmic localization (figures 33 A and B).

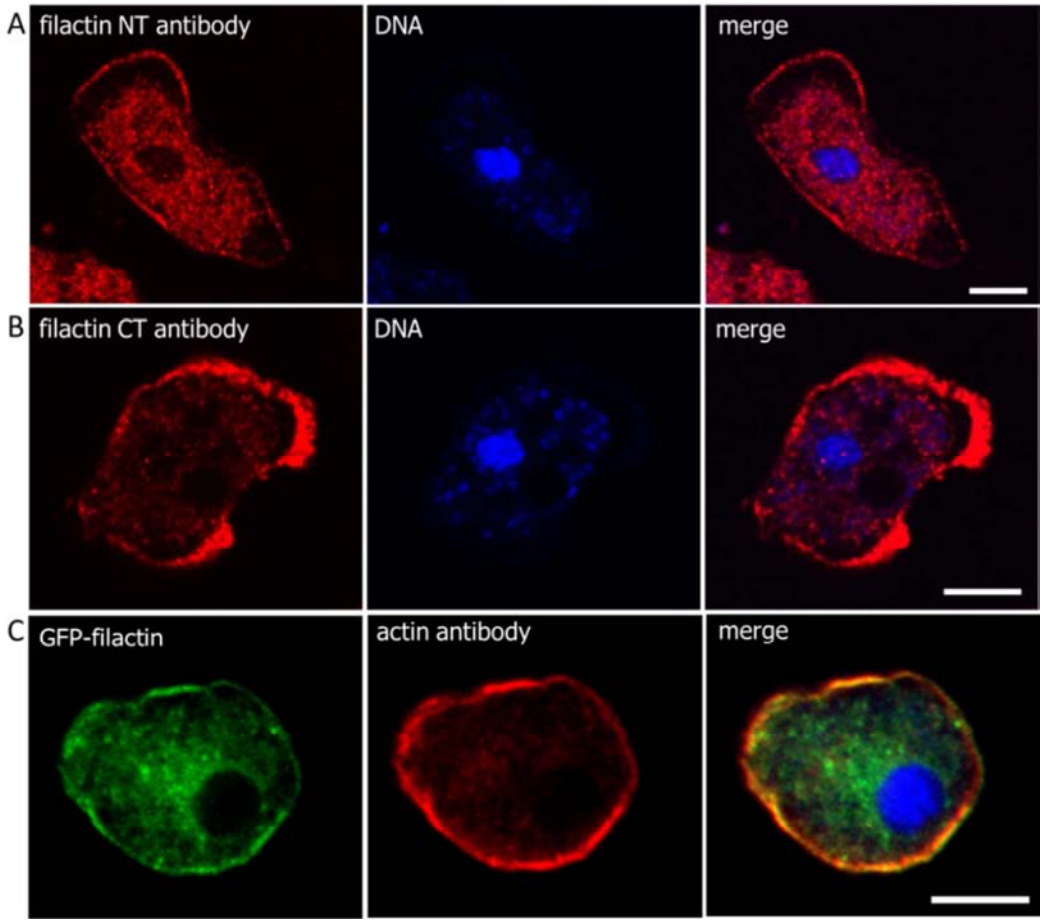

Figure 33: Localization of filactin in *D. discoideum* cells. The cells were fixed and incubated with the respective primary antibody. Scale bar, 5 µm. A) AX2 cell treated with the filactin antibody 3S-55-4, recognizing the N-terminal part of filactin. The antibody clearly marks the cortex of the cell and vesicle-like structures in the cytoplasm. B) AX2 cell treated with the filactin antibody 4S-59-4 which binds to the actin domain of filactin and shows a minor cross-reaction with actin. The cortical stain is more pronounced than in A. Also vesicle-like structures are visible. C) AX2 GFP-filactin cell incubated with act-1 antibody. GFP-filactin localizes to the cell cortex, thus co-localizes with conventional actin. GFP-filactin also localizes in the cytoplasm in vesicle-like structures. In the merge panel, the DNA is displayed in blue (stained with ToPro).

In addition to the full length filactin the localization of the different filactin domains was investigated. The GFP-tagged filactin actin domain (aa 574-944) co-localizes with actin in the cell and is additionally present in the cytoplasm (figure 34).

Figure 34: Localization of the GFP-tagged filactin actin domain in *D. discoideum* cells. The fixed cells were incubated with the act-1 antibody. GFP-filactin actin co-localizes with actin. Furthermore, it is also present in the cytoplasm. Scale bar, 5 µm.

GFP-filactin Ist1-like (aa 1-196) and the GFP-filactin filamin repeats (aa 259-488) localize predominantly in the nucleus and in the cytoplasm (figure 35) in vegetative *D. discoideum* cells. This is a surprising finding since the sequences do neither contain a nuclear localization signal nor does filactin full length localize in the nucleus in vegetative cells. The constructs do not show a co-localization with conventional actin.

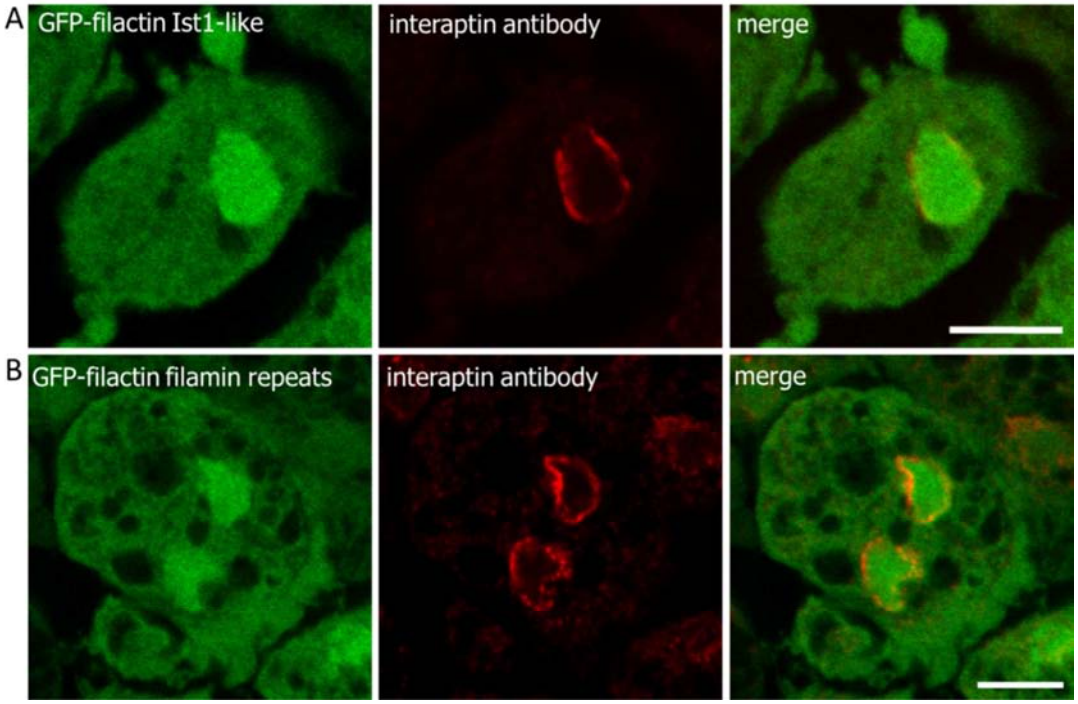

Figure 35: Localization of GFP-tagged N-terminal filactin domains in *D. discoideum* cells. The cells were fixed under agar with picric acid and incubated with the interaptin antibody (260-60-10). Interaptin marks the nuclear envelope. The N-terminal filactin domains localize in the cytoplasm and in the nucleus. Scale bar, 5 µm. A) Filactin KO cells expressing the GFP-Ist1-like domain stained with interaptin antibody. B) Filactin KO cells expressing GFP-filamin repeats stained with interaptin antibody.

4.1.3.2 Filactin is part of the Triton-insoluble cytoskeleton and is present in soluble and membrane fractions

To investigate biochemically whether filactin co-localizes with F-actin in *D. discoideum* cells, two different assays were carried out: (1) analysis of the Triton-insoluble cytoskeleton and (2) analysis of a differential centrifugation.

The Triton-insoluble cytoskeleton assay was performed according to McRobbie and Newell (1983). Filactin, both the GFP-tagged and the endogenous one, could be detected in the Triton-insoluble cytoskeleton (figure 36 A, last lane). Furthermore, it was present in soluble fractions but also pellets together with membranes in the differential centrifugation assays (figure 36 A-C). However, the differential centrifugation assays suggest that filactin might be more soluble than associated with F-actin since neither GFP-tagged nor endogenous filactin could be detected in the 100,000 g pellets (figures 36 B and C). These data indicate that filactin is primarily soluble but also associates with membranes and F-actin.

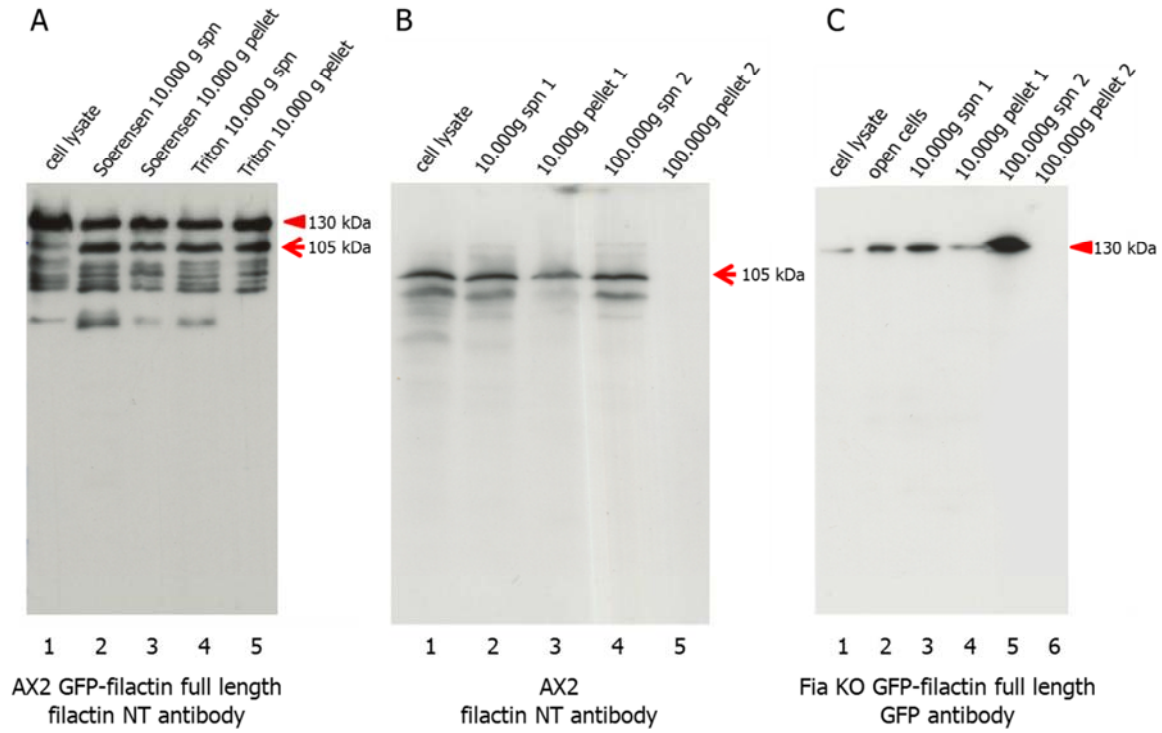

Figure 36: Filactin is part of the Triton-insoluble cytoskeleton and is present both in soluble and membrane fractions. A) Triton-insoluble cytoskeleton of AX2 cells expressing GFP-filactin full length (7.5 x 10^5 cells/lane). The western blot was incubated with filactin antibody 3S-55-4. GFP-filactin is detected at about 130 kDa (arrow head), endogenous filactin at 105 kDa (arrow). Filactin is present both in supernatant (spn) and pellet fractions. The bands below 100 kDa most probably result from protein degradation. B) Differential centrifugation of AX2 cell lysates (5 x 10^5 cells/lane for cell lysates and spn fractions, pellet fractions were concentrated 3-fold). The western blot was incubated with filactin antibody 3S-55-4. Endogenous filactin was found both in soluble and membrane fractions (arrow head), but could not be detected in the 100,000 g pellet. C) Differential centrifugation of filactin KO cells expressing GFP-filactin full length (6.5 x 10^5 cells/lane for cell lysate and spn fractions, the pellet fractions were concentrated 4-fold). The western blot was incubated with the GFP antibody K3-184-2. GFP-tagged filactin in a filactin KO background is found both in soluble and membrane fractions (arrow), but could not be detected in the 100,000 g pellet. The seemingly increased concentration of GFP-filactin in the 100,000 g supernatant most probably is an artifact.

4.1.3.3 Filactin is part of stress-induced nuclear actin rods

Nuclear actin rods are protein bundles that are present in the nucleus of *D. discoideum* spores (Sameshima et al, 2000) and can be induced in vegetative cells under stress conditions. In all organisms tested so far, actin can migrate into the nucleus upon treatment with dimethyl sulfoxide (DMSO) or increased temperatures and form rod-shaped paracrystals (Fukui, 1978; Osborn & Weber, 1984). These rods consist of actin and a set of actin binding proteins, including cofilin, actin-interacting protein 1 (Aip1) and coronin (Minamide et al, 2010; Nishida et al, 1987; Vandebrouck et al, 2010). In our experiments AX2 GFP-cofilin cells were used as a reference. In vegetative cells, cofilin co-localizes with actin (figure 37 A). Upon treatment with DMSO, not only actin but also cofilin migrates into the nucleus to form bundles (figure 37 B).

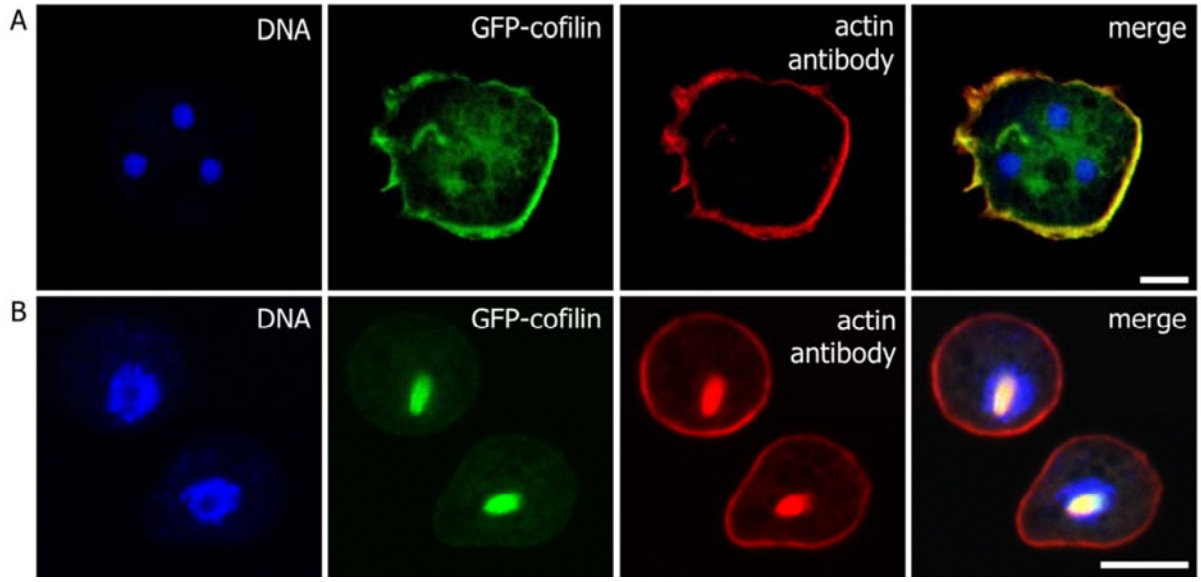

Figure 37: Actin and GFP-cofilin are present in nuclear actin rods. AX2 GFP-cofilin cells were fixed and incubated with the act-1 antibody. Scale bar, 5 µm. A) GFP-cofilin co-localizes with actin in the cell. B) Cells were incubated with 5 % DMSO for 60 minutes and then fixed. Upon incubation with DMSO, both actin and GFP-cofilin migrate into the nucleus and form bundles.

To find out whether filactin was also part of the actin-cofilin bundles, AX2 GFP-cofilin cells were incubated with DMSO, fixed and then stained with the filactin antibody 3S-55-4. Figure 38 A shows the cells before incubation with DMSO, figure 38 B depicts DMSO-treated cells. Filactin is clearly co-localizing with the actin-cofilin rods.

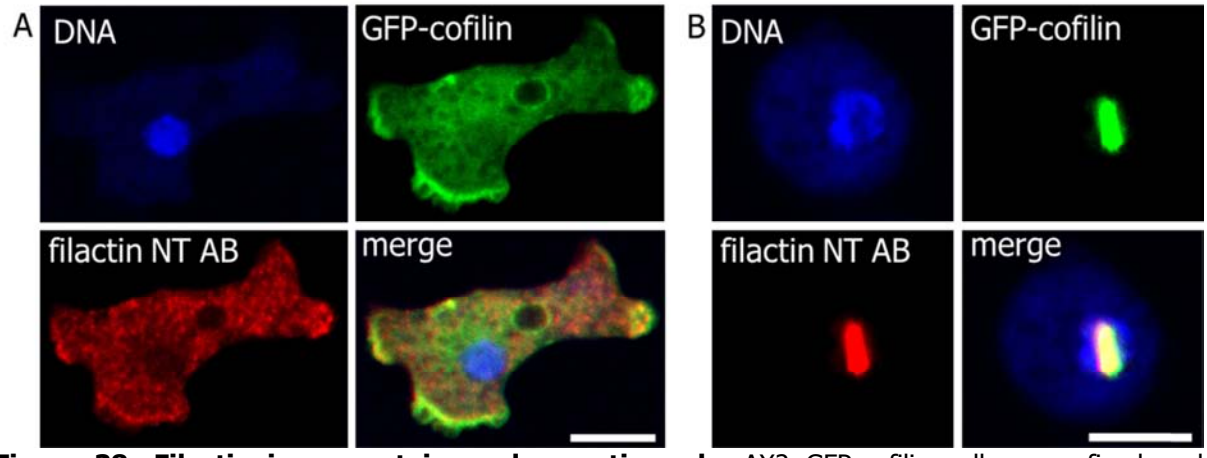

Figure 38: Filactin is present in nuclear actin rods. AX2 GFP-cofilin cells were fixed and incubated with the filactin N-terminal antibody 3S-55-4. Scale bar, 5 µm. A) Filactin co-localizes with GFP-cofilin at the cell cortex and is also present in the cytoplasm. B) Cells were incubated with 5 % DMSO for 60 minutes and then fixed. Upon incubation with DMSO, the nuclear rods are formed; both GFP-cofilin and filactin are part of the bundles in the nucleus.

However, when incubating AX2 GFP-filactin cells with DMSO, the GFP-tagged filactin cannot be found in the rods (figure 39), it stays in the cytoplasm. The endogenous filactin is

still present in the rods (data not shown). Also in a filactin KO background, GFP-filactin is not able to enter the nucleus. Additionally, when imaging *D. discoideum* spores, GFP-cofilin is found in the rods in spores, but GFP-filactin is not, both in a wild type and a filactin KO background (data not shown).

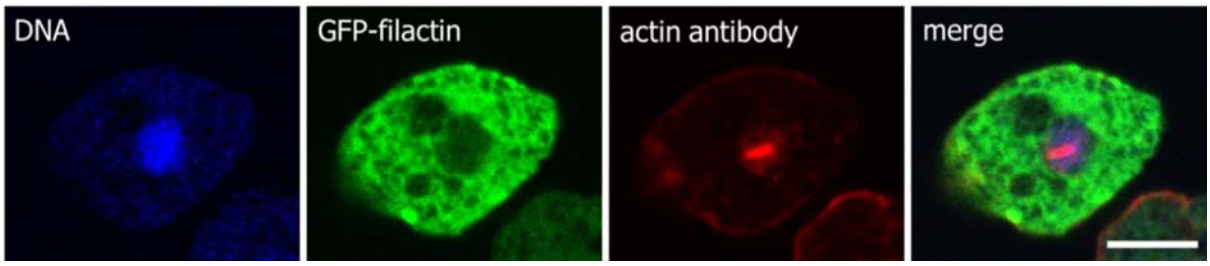

Figure 39: GFP-filactin is not present in nuclear rods. AX2 GFP-filactin full length cells were incubated with 5 % DMSO for 60 minutes, fixed and incubated with the act-1 antibody. Note that the GFP-filactin is present in the cytoplasm but not in the nucleus. Scale bar, 5 µm.

Since the GFP-filactin protein has a mass of ca. 130 kDa it might be just too big to cross the nuclear membrane. To analyze whether the GFP-tagged actin domain of filactin is able to go into the nucleus and to co-localize with the rods, AX2 cells expressing this fusion construct were incubated with DMSO. The GFP-fusion protein is able to cross the nuclear membrane and could be found enriched in the nucleus. However, it is not part of the protein rods, but localizes around them (figure 40 A). Also immunofluorescence experiments confirmed this result. Furthermore, the localization under stress conditions of the filactin N-terminal domains was analyzed. Upon treatment with DMSO, both GFP-filactin Ist1-like and GFP-filactin filamin repeats are found in the nucleus, but not in the rods (figures 40 B and C). Since none of the GFP-tagged filactin constructs was found in the rods – neither in the wild type nor in the filactin KO background - the GFP-tag probably might hinder an integration of filactin into the rods and/or inhibit transport into the nucleus.

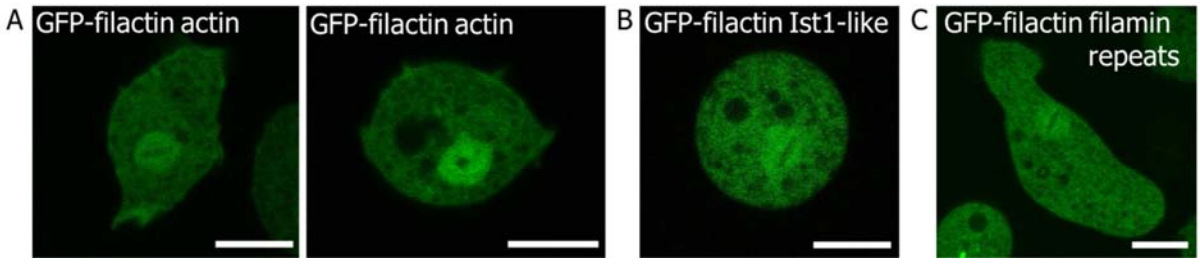

Figure 40: GFP-tagged filactin domains are not present in the nuclear rods. The cells were incubated with 5 % DMSO for 60 minutes and then imaged live with a confocal microscope. Upon incubation with DMSO, the GFP-fusion proteins are enriched in the nucleus, but are not present in the rods. Note the dark rod-shaped shadow where the GFP-proteins are not present. Scale bar, 5 µm. A) AX2 GFP-filactin actin cells. The first picture shows the rod in a side view, the second picture shows a top view. B) AX2 GFP-filactin Ist1 cell. C) AX2 GFP-filactin filamin repeats cells.

Even though endogenous filactin is part of the nuclear actin rods, it might not be essential for their formation. Time series experiments were carried out with filactin KO cells, filactin KO cells expressing GFP-cofilin and AX2 GFP-cofilin cells. The cells were incubated in parallel with 5 % DMSO for 0, 5, 15, 30, 60 and 90 minutes. The cells were fixed at the respective timepoints and actin was visualized using the act-1 antibody. The rod formation in the KO background already started in certain cells already after 15 minutes of incubation with DMSO, just as in the control cells. Proper rods were formed after approximately 60 minutes (data not shown).

4.1.3.4 The purified filactin actin domain acts as an actin sequestering protein in *in vitro* assays

Filactin is notoriously difficult to purify. Since former approaches to purify it from *D. discoideum* cells were not successful, a new purification assay was established in this study. The FLAG-tagged filactin full length protein and the filactin actin domain with and without N-terminal GFP were expressed using the baculovirus system in Sf9 insect cells. Figure 41 shows the purified and eluted protein constructs. The filactin actin domain could constantly be purified in higher amounts than the full length protein. The full length filactin also was much more sensitive to degradation, probably due to its PEST-motif.

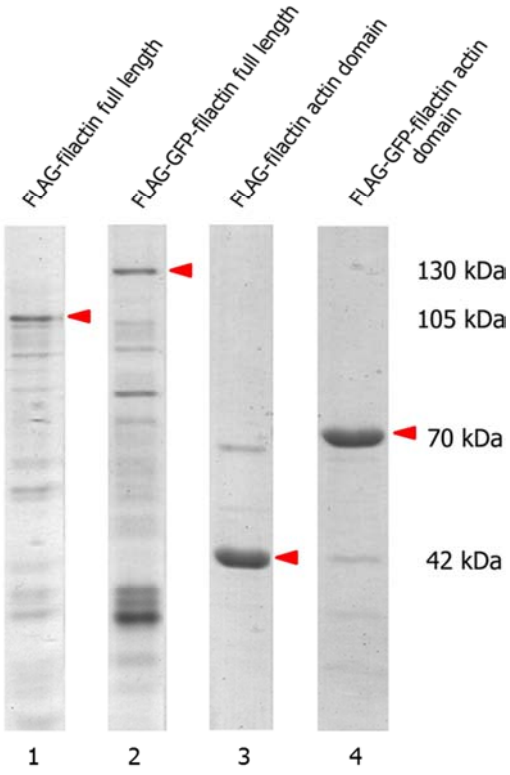

Figure 41: FLAG-filactin constructs purified from Sf9 cells. Filactin and GFP-filactin could not be obtained in high concentrations and were also very sensitive to proteolytic degradation (lane 1 and 2, 105 and 130 kDa). The purified filactin actin domain with and without GFP-tag was very stable (lane 3 and 4, 42 and 70 kDa, respectively) and could be obtained in higher concentration than the full length constructs.

The purified proteins were used in fluorometric studies to investigate their impact on actin polymerization. The filactin actin domain acts as an actin sequestering protein *in vitro* as shown in figures 42 A and 43 A. The filactin full length protein was usually limiting since the concentration was too low. However, it was obvious that the full length protein did not exhibit the same effect as the actin domain only. No significant sequestering activity could be observed, neither in the fluorometric nor in the viscometric assays (figures 42 B and 43 B). In contrast, the filactin actin domain had an effect on actin polymerization. Besides the sequestering activity shown in figure 42 A, it further revealed its sequestering abilities in the capping assay depicted in figure 42 C. When the preformed actin seeds were incubated with the filactin actin domain and then added to actin and polymerization buffer, the nucleation of actin polymerization was inhibited, and the fluorescence signal was even decreased below the control's signal after ca. 30 minutes of polymerization. In addition, the filactin actin domain accelerated dilution-induced depolymerization (figure 42 D). The activity observed of the filactin actin domain and the filactin full length did not change in presence/absence of calcium or EGTA and was not altered by different salt concentrations (up to 100 mM NaCl).

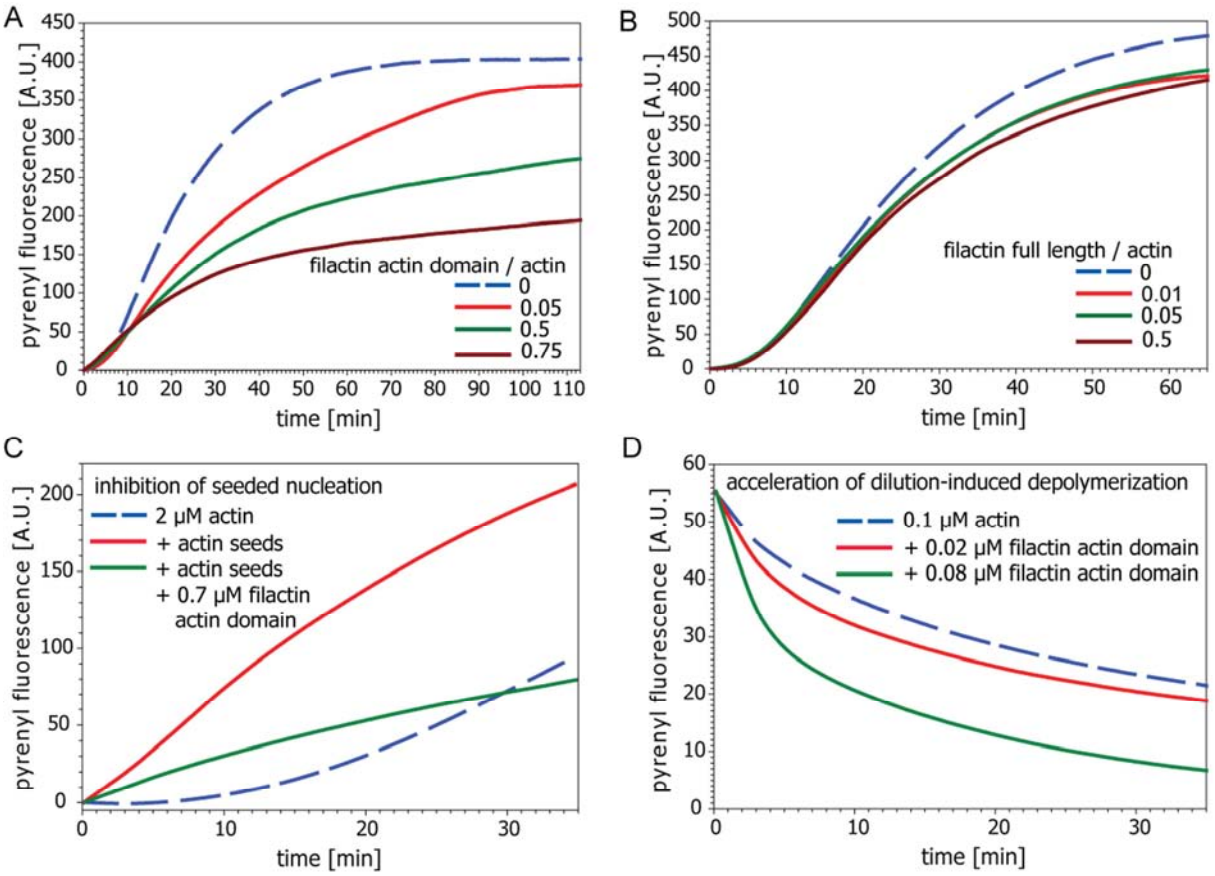

Figure 42: Influence of filactin constructs on actin polymerization as measured by fluorometric methods. The polymerization and depolymerization of actin (10 % pyrenylated actin) was measured in the presence of purified FLAG-filactin full length or FLAG-filactin actin domain. A) Filactin actin acts as actin sequestering protein. The fluorescence signal decreases with the increase of the filactin actin concentration. B) Filactin full length does not act as actin sequestering protein. The fluorescence signal did not decrease significantly with the increase of the filactin concentration. C) Filactin actin inhibits seeded nucleation of actin polymerization. The addition of preformed actin seeds lead to a quicker actin polymerization (red graph) compared to the control (blue dashed graph). Pre-incubation of filactin actin with the actin seeds resulted in inhibition of the nucleation (green graph) and a decrease of fluorescence signal even below the control on the long term. D) Filactin actin accelerates dilution-induced depolymerization. The depolymerization of actin just below the critical concentration of the barbed end was monitored with the addition of increasing amounts of filactin actin which accelerated depolymerization.

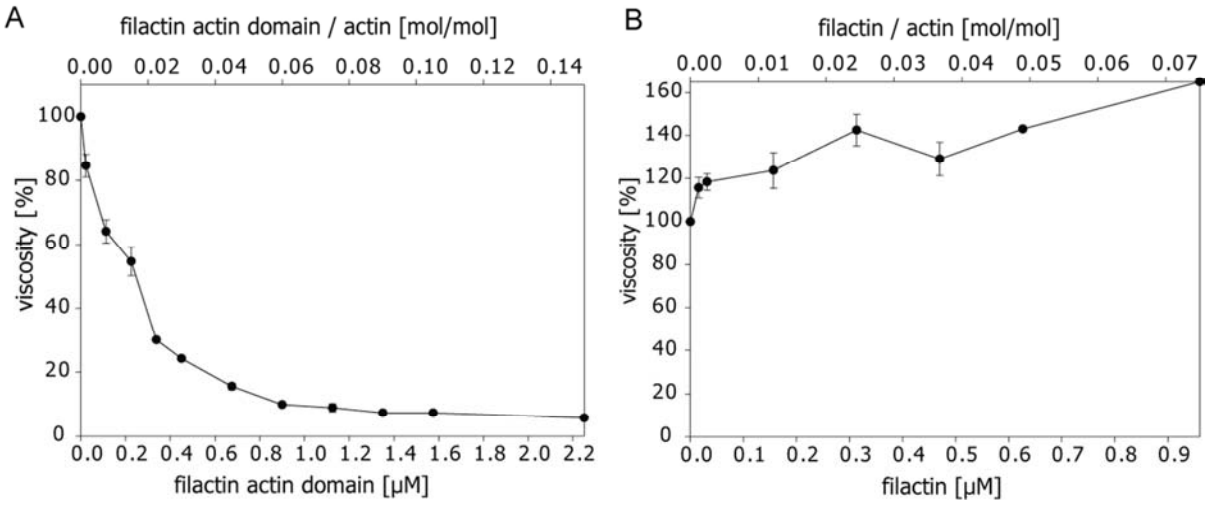

Figure 43: Influence of filactin constructs on actin polymerization as measured by low shear viscometry. 15 µM actin was incubated with the indicated, increasing amounts of purified FLAG-filactin full length or FLAG-filactin actin domain and the viscosity of the solution was measured with a falling ball viscometer. The error bars indicate the standard error. A) The filactin actin domain reduces the viscosity of the actin solution. Already when added in a molar ratio of 1/20 (filactin actin domain/actin), the viscosity was reduced by ca. 85 %. B) Filactin full length slightly increases the viscosity of the actin solution. When filactin was added to actin in a molar ratio of 1/20 (filactin/actin) the viscosity was increased by about 40 %.

Since it was still unclear from the conducted fluorometric and viscometric experiments whether the filactin actin domain acts as G-actin sequestering or probably as F-actin capping protein, a spindown experiment was carried out. F-actin and G-actin can be separated by centrifugation at 120,000 g. The F-actin is pelletable whereas the soluble G-actin stays in the supernatant. After co-polymerization of actin with the GFP-tagged filactin actin domain which was monitored on the fluorometer (figure 44 A), the F-actin fraction and soluble fraction were separated by centrifugation of the sample. The GFP-filactin actin domain was mostly found in the supernatant (figure 44 B, lane 3, 70 kDa), but also to a lesser extent in the pellet fraction (figure 44 B, lane 4, 70 kDa). It is remarkable that in the sample in which the filactin actin domain was added to the actin polymerization, the amount of soluble actin increased (figure 44 B, lane 1 and lane 3 at 42 kDa). These data indicate that filactin by sequestering actin monomers increased the concentration of actin in the supernatant, which is in accordance with the fluorometer data. Thus, the filactin actin domain is most probably a sequestering protein but might still be able to bind to filamentous actin.

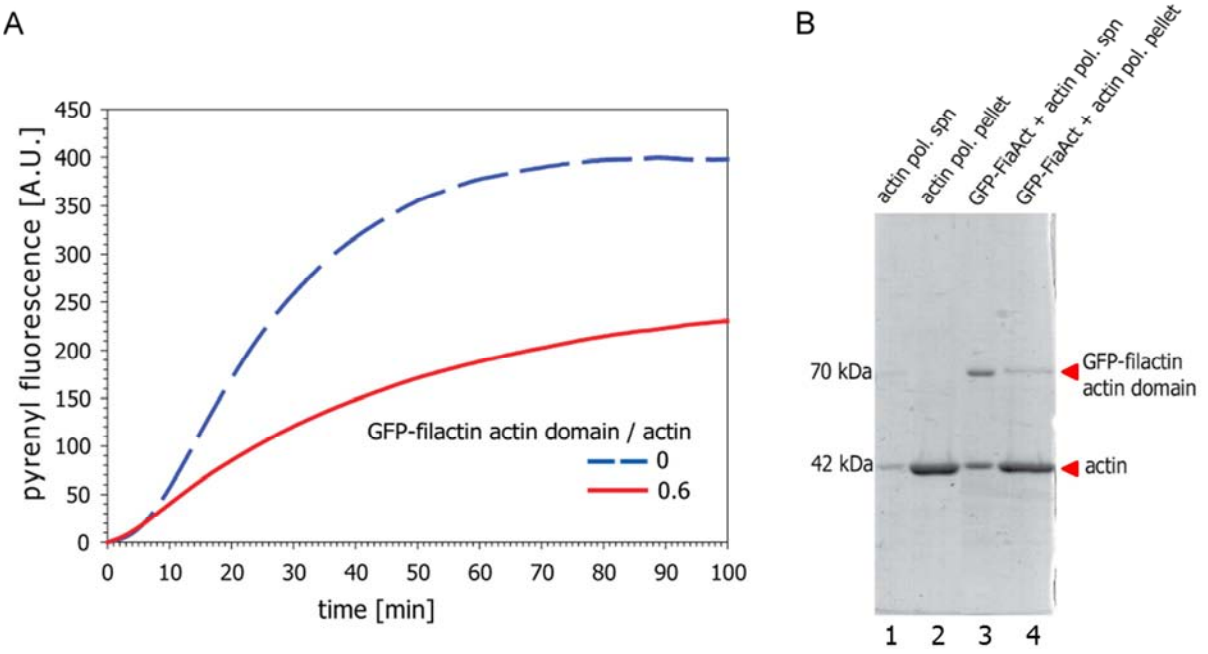

Figure 44: The filactin actin domain acts as an actin sequestering protein but can be detected together with F-actin as well. A) 2 µM actin (10 % pyrenylated) was polymerized in the presence and the absence of 1.2 µM FLAG-GFP-filactin actin. B) The samples from (A) were ultracentrifuged, pellet and soluble fraction were separated and analyzed on a SDS-gel. Pellet fractions are concentrated 2-fold. In the actin control (lane 1 and 2), most of the actin is found in the pellet. In the sample with filactin actin most of the added protein is detected in the supernatant, and along with it also the concentration of soluble actin increased (lane 3). However, the FLAG-GFP-filactin actin domain can also be centrifuged together with F-actin (lane 4).

4.1.4 Filactin might be associated with the ESCRT pathway

4.1.4.1 Filactin interacts with ESCRT-related proteins vta1, vps4 and vps46

To identify potential interaction partners of filactin, GFP-Traps (Chromotek) were performed with cell lines expressing the GFP-tagged full length filactin, the Ist1-like domain, filamin repeats and the actin domain. The GFP-fusion proteins bind to the beads coated with GFP antibody and can be pulled down together with their interaction partners. Figure 45 A shows a Coomassie Blue stained SDS-gel of a GFP-Trap with GFP-filactin and GFP-filactin filamin repeats. In mass spectrometry analyses, the protein vta1 (vacuolar protein sorting twenty-associated 1) was reproducibly detected to interact with filactin, in particular with the filamin repeats. Hence, a GST-vta1 construct was created as well as a GFP-vta1 overexpressing *D. discoideum* cell line. GST-vta1 could pull down endogenous filactin from a AX2 cell lysate (figure 45 B) and GFP-vta1 could pull down endogenous and additional purified FLAG-filactin (figure 45 C). Thus, vta1 is associated with filactin in *D. discoideum*.

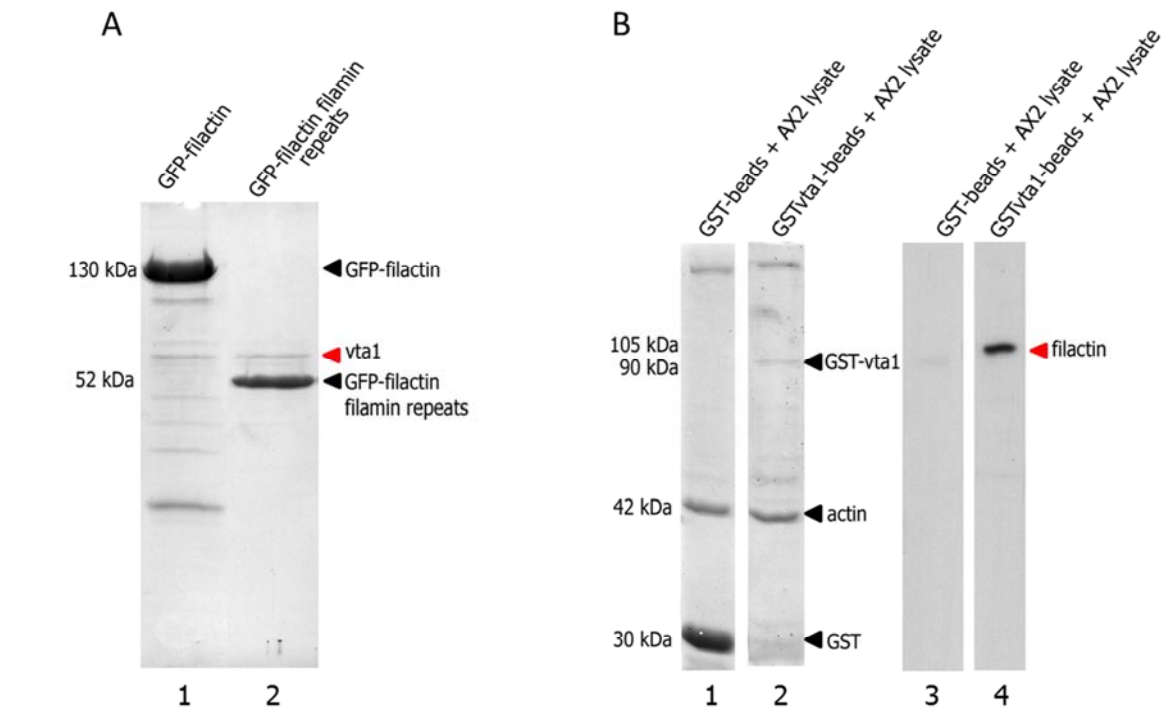

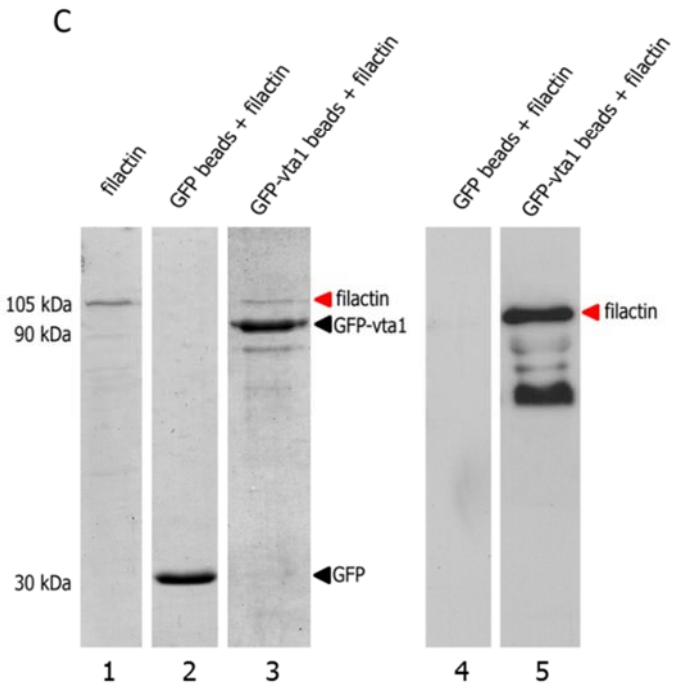

Figure 45: Filactin interacts with the ESCRT-related protein vta1. A) Coomassie Blue stained SDS-gel. Vta1 (indicated by red arrow head) was reproducibly identified in GFP-Traps to be associated with filactin, in particular with its filamin repeats (lane 2). B) GST-vta1 pulls down endogenous filactin. GST only and GST-vta1 were incubated with AX2 lysate, centrifuged, washed and analyzed on a SDS-gel. The left side shows a Coomassie Blue stained gel, the right side shows a western blot incubated with the filactin antibody 3S-55-4. C) GFP-vta1 pulls down purified FLAG-filactin. The left side shows a Coomassie Blue stained gel, the right side shows a western blot incubated with the filactin antibody 3S-55-4. Purified FLAG-filactin (lane 1) was incubated with GFP beads and GFP-vta1 beads obtained in a GFP-Trap. The beads were subsequently centrifuged, washed and boiled in SDS-sample buffer. The FLAG-filactin pulled down by GFP-vta1 is already visible on the Coomassie Blue stained gel (lane 3, red arrow head).

Since the identified filactin interacting protein vta1 interacts with the AAA ATPase vps4 (vacuolar protein sorting 4) in the context of the ESCRT machinery in yeast and humans, a GST-vps4 construct and a GFP-vps4 overexpressing *D. discoideum* cell line were generated. Furthermore, in yeast Ist1 interacts with Did2, namely vps46 (vacuolar protein sorting 46) in *D. discoideum*. Therefore, constructs were also generated for the Did2 homolog vps46. The interaction of vta1 and vps4 described in yeast and humans could be confirmed to be also conserved in *D. discoideum* (figure 46 C). In addition, vps4 and vps46 seem to interact with filactin as well (figures 46 A and B), but this interaction was not always reproducible and mostly rather weak. Probably vps4 interacts with filactin indirectly via vta1.

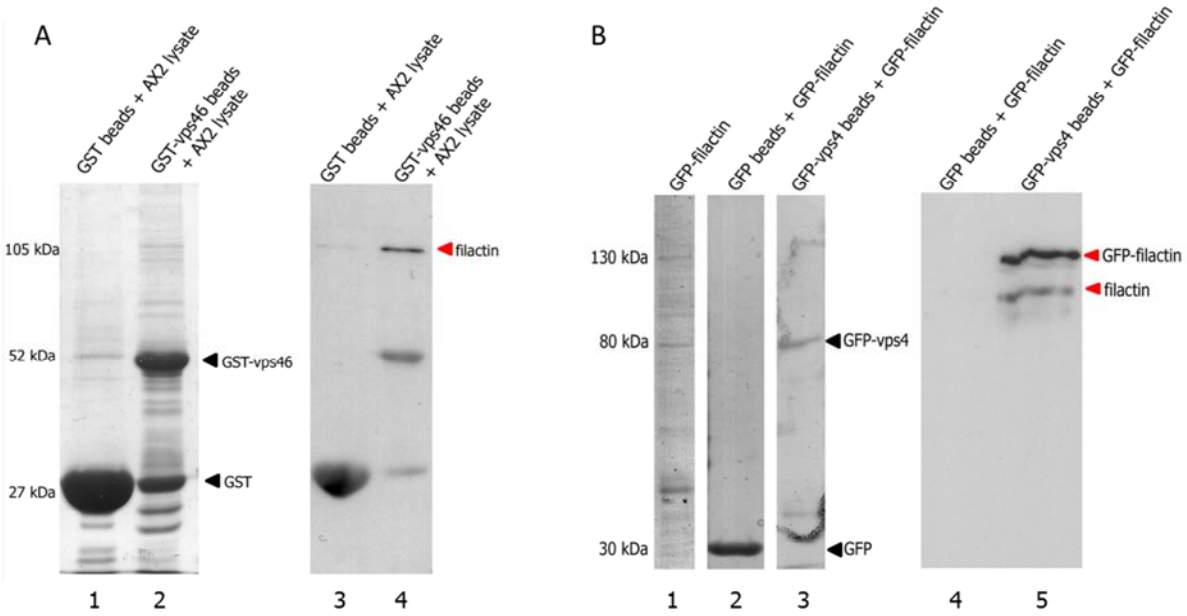

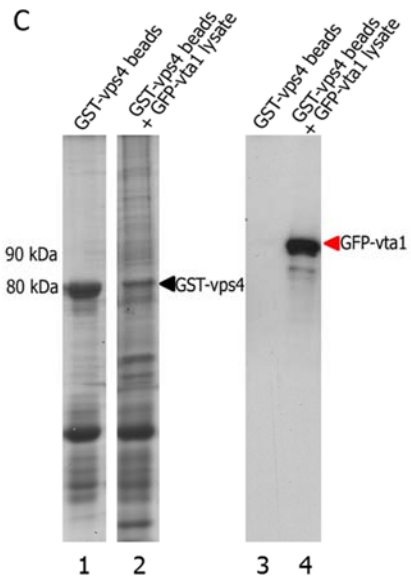

Figure 46: Filactin might interact with the ESCRT-related proteins vps4 and vps46, while vps4 is associated with vta1. The left side in each picture shows a SDS-gel stained with Coomassie Blue, the right side shows a western blot incubated with the filactin antibody 3S-55-4. A) Endogenous filactin can be pulled down with GST-vps46. GST only and GST-vps46 were incubated with AX2 lysate, centrifuged, washed and analyzed on a SDS-gel. Filactin full length could be detected weakly in the western blot (lane 4, red arrow head). B) Purified GFP-filactin can be pulled down with GFP-vps4. GFP-filactin was incubated with GFP beads and GFP-vps4 beads obtained in a GFP-trap. The beads were centrifuged, washed and analyzed on a SDS-gel. GFP-filactin and endogenous filactin could be detected in the western blot (lane 5, red arrow heads). C) GFP-vta1 can be pulled down with GST-vps4. GST-vps4 beads before and after incubation with AX2 GFP-vta1 lysate (lane 1 and 2, respectively). In the western blot incubated with GFP antibody, GFP-vta1 could be detected in the pulldown (lane 4, red arrow head).

4.1.4.2 Localization of GFP-ESCRT related proteins in *D. discoideum*

Since the interaction of the ESCRT-related proteins and filactin was determined on a biochemical basis, a putative co-localization in *D. discoideum* cells was analyzed via immunofluorescence. AX2 GFP-vta1, AX2 GFP-vps4 and AX2 GFP-vps46 cells were fixed and filactin was stained with either the N-terminal filactin antibody 3S-55-4 or the C-terminal filactin antibody 4S-59-4. GFP-vta1, GFP-vps4, GFP-vps46 and filactin co-localize occasionally, but not always (figures 47, 48, 49). Both filactin and the GFP-tagged ESCRT-related proteins vta1, vps4 and vps46 localize in vesicle-like structures but do not overlap in every case. GFP-vps4 vesicle-like structures were co-localizing with filactin most frequently (figure 48). The localization of GFP-vta1, GFP-vps4 and GFP-vps46 in a filactin KO background did not clearly alter (data not shown); vesicle-like structures were still present. Additionally, GFP-vta1 was pelletable together with filactin in the Triton-insoluble cytoskeleton (data not shown).

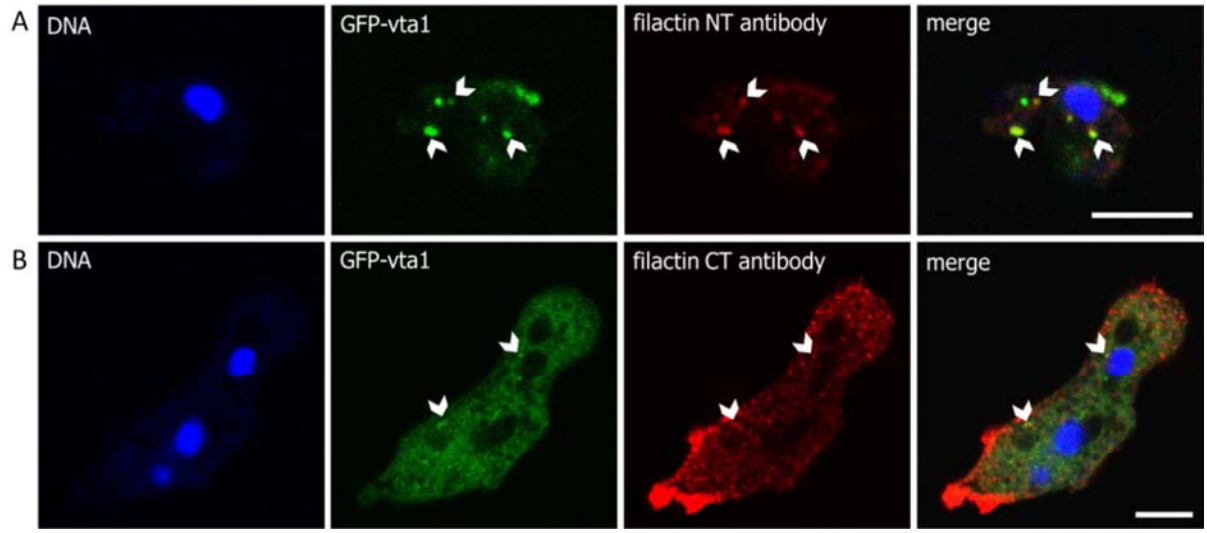

Figure 47: GFP-vta1 and filactin occasionally co-localize in *D. discoideum*. AX2 GFP-vta1 cells were fixed and filactin was labeled with the respective antibodies. GFP-vta1 structures co-localizing with filactin are indicated by white arrow heads. Scale bar, 5 µm. A) GFP-vta1 cells were incubated with the filactin antibody 3S-55-4. B) GFP-vta1 cells were incubated with the filactin antibody 4S-59-4, which shows a slight cross-reaction with conventional actin.

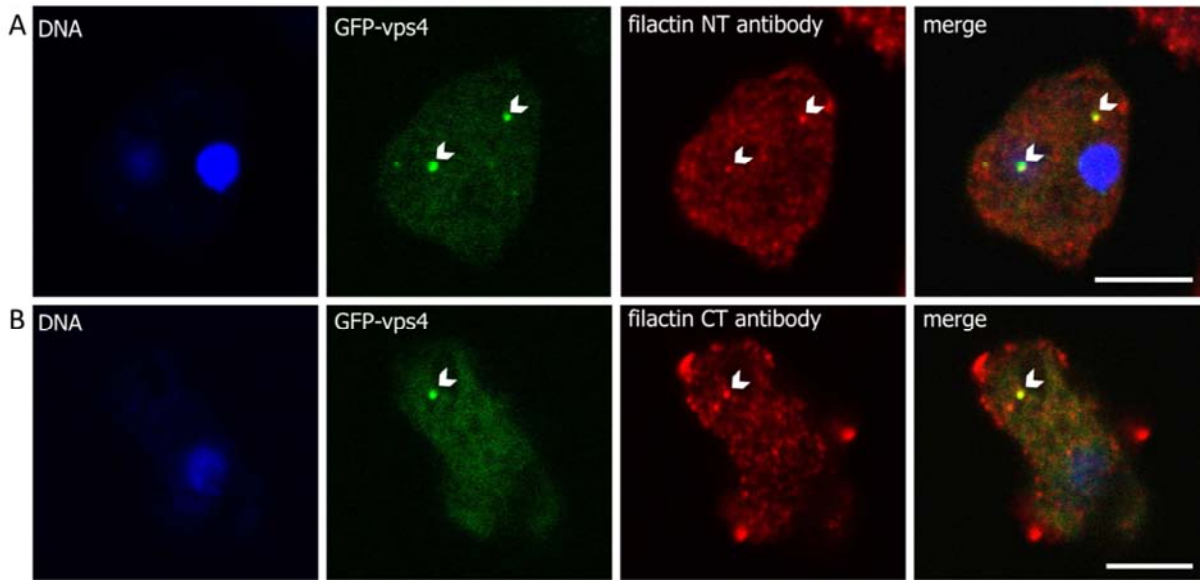

Figure 48: GFP-vps4 and filactin co-localize in *D. discoideum*. AX2 GFP-vps4 cells were fixed and filactin was labeled with the respective antibodies. GFP-vps4 structures co-localizing with filactin are indicated by white arrow heads. Scale bar, 5 µm. A) GFP-vps4 cells were incubated with the filactin antibody 3S-55-4. B) GFP-vps4 cells were incubated with the filactin antibody 4S-59-4.

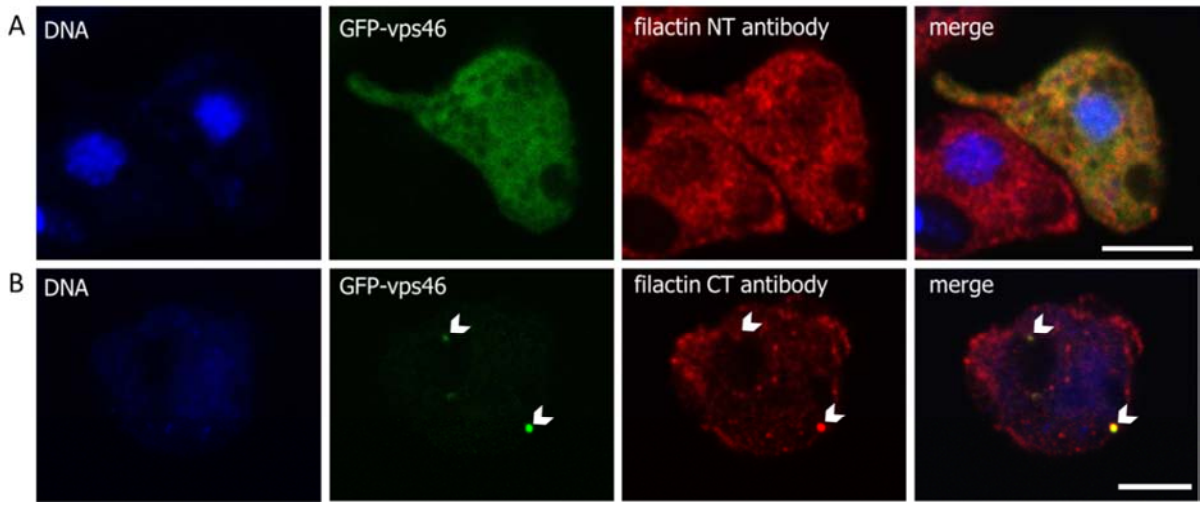

Figure 49: GFP-vps46 and filactin occasionally co-localize in *D. discoideum*. AX2 GFP-vps46 cells were fixed and filactin was labeled with the respective antibodies. GFP-vps46 structures co-localizing with filactin are indicated by white arrow heads. Scale bar, 5 µm. A) GFP-vps46 cells were incubated with the filactin antibody 3S-55-4. B) GFP-vps46 cells were incubated with the filactin antibody 4S-59-4.

4.1.4.3 Generation of a vps4 knock out construct

To properly analyze and possibly prove the involvement of filactin in the ESCRT pathway, a vps4 knock out strain was attempted. With a non-functional vps4 protein, the ESCRT-III complex cannot be recycled into the cytoplasm and accumulates on the multivesicular body. In yeast, a vps4 mutant accumulates vacuolar, endocytic and late-Golgi markers in an aberrant multilamellar pre-vacuolar compartment (Babst et al, 1997). Thus, hypothetically,

the distribution of filactin in a vps4 KO cell should alter significantly compared to the localization in a wild type cell if filactin is actually implicated in the ESCRT pathway. A construct was generated that should replace the endogenous vps4 gene in the genomic DNA of the *D. discoideum* wild type strain AX2 with a vps4 genomic sequence in which the ATPase domain is interrupted by a blasticidin resistance cassette. The construct was successfully generated and transformed in *D. discoideum* cells. Despite many attempts, no vps4 KO strain could be obtained. Verification of successful homologous recombination by PCR lead to the result that the surviving cells – if there were any – had the blasticidin resistance cassette inserted at a different region within the genome, but the vps4 sequence could not be inactivated. It seemed very unlikely that a KO of vps4 would be lethal for *D. discoideum* since vps4 KOs in yeast are viable (Babst et al, 1997) as well as dominant negative VPS4 mutants in human cells (Fujita et al, 2003; Kieffer et al, 2008; Xia et al, 2012). However, attempts to knock out vps4 by homologous recombination or down-regulate vps4 by antisense inhibition in *D. discoideum* were unsuccessful in other research groups as well (personal communication, Laurence Aubry and Paul R. Fisher). Consequently, for now, vps4 function appears to be crucial for the viability of *D. discoideum* cells and therefore, filactin could unfortunately not be analyzed in a vps4 KO background in this study.

4.1.4.4 Filactin might be involved in the autophagic pathway

Autophagy is responsible for the clearance of damaged organelles and protein aggregates as well as bulk consumption of cytoplasmic proteins during starvation. Even though there is no clear evidence yet for the implication of the ESCRT pathway in autophagy processes, several studies show that an impaired ESCRT machinery leads to the accumulation of autophagosomes in the cell (Filimonenko et al, 2007; Lee et al, 2007; Nara et al, 2002; Rusten et al, 2007). Therefore, the number of autophagosomes was analyzed in the AX2 wild type strain in comparison with the filactin KO strain. The autophagosome marker construct mRFP-ATG8 (generously supplied by Ludwig Eichinger, Universität zu Köln) was transformed into selected strains and the phenotype of the transformants was analyzed. Interestingly, an accumulation of autophagosomes was observed in the filactin KO strain compared to wild type AX2 cells (figures 50 A and B). An analysis of the autophagosome number per cell is displayed in figure 50 C. Many cells, both in AX2 and in filactin KO background, do not possess a RFP-ATG8 positive autophagosome: 37 % of the AX2 cells and 29 % of the analyzed cells of the filactin KO strain did not contain any RFP-ATG8 positive autophagosomes. On average, AX2 RFP-ATG8 and filactin KO RFP-ATG8 cells comprised 1.2

and 2.1 autophagosomes per cell, respectively. In AX2 cells, most of the cells contain none or one autophagosome (a representative cell is shown in figure 50 A). In filactin KO cells, most of the autophagosomes are present in cells with four or more autophagosomes (a representative cell is shown in figure 50 B).

A co-localization of the autophagosomes with the filactin vesicle-like structures could not be observed, neither in *D. discoideum* strains expressing both RFP-ATG8 and GFP-filactin full length, nor in immunofluorescence experiments with a polyclonal ATG8 antibody (generously supplied by Ludwig Eichinger, Universität zu Köln).

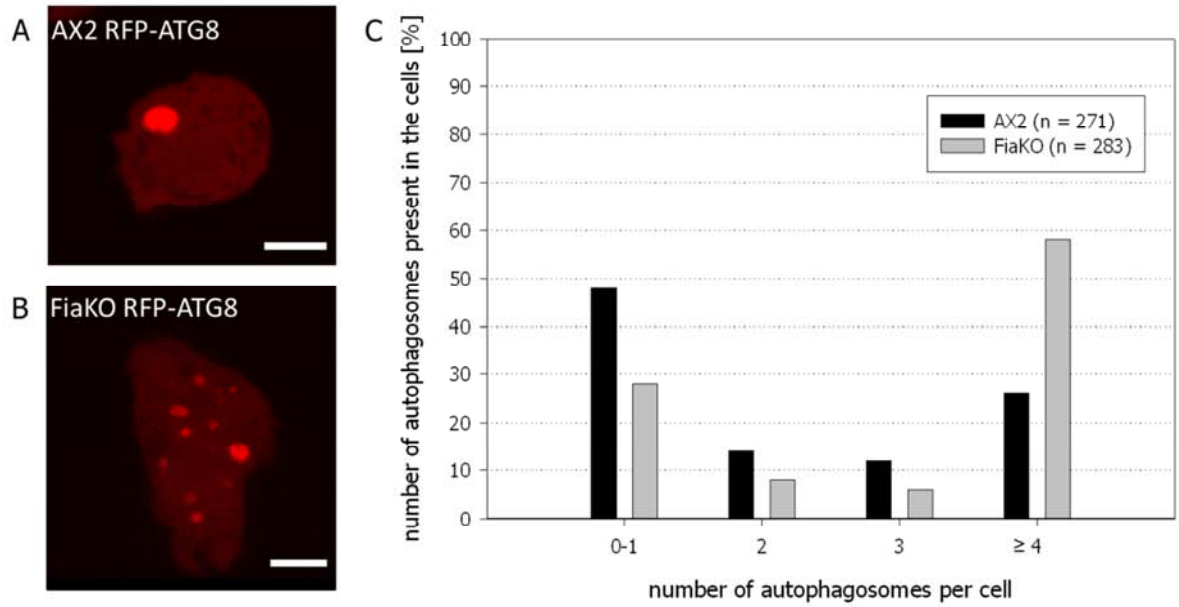

Figure 50: Autophagosomes accumulate in filactin KO cells. A) Confocal image of a living AX2 RFP-ATG8 cell which contains only one autophagosome. Autophagosomes in wild type cells usually have a diameter of 200 nm – 2 µm. Scale bar, 5 µm. B) Stack projection of confocal images of a living filactin KO RFP-ATG8 cell which contains many autophagosomes of different sizes. Scale bar, 5 µm. C) Analysis of the number of autophagosomes present in cells with 0-1, 2, 3, and not less than 4 autophagosomes in percent. Cells were fixed and the fluorescence of RFP-ATG8 was enhanced with the RFP antibody K64-372-1. For evaluation, confocal stacks were superposed and the autophagosomes in the cells were counted. The number of cells counted (n) is displayed in the upper right corner. Most of the autophagosomes in filactin KO cells are present in cells with 4 and more autophagosomes.

4.1.5 Filactin might form a tetramer via its filamin-like Ig repeat domain

The purified FLAG-filactin full length was run on a ÄKTA superose 6 gel filtration column to check the size of the protein. Filactin has a size of 105 kDa. Surprisingly, FLAG-filactin full length reproducibly elutes at a molecular weight of 400,000 (figure 51 A), suggesting a tetrameric structure. When applying a whole *D. discoideum* lysate (soluble lysate of 5 x 10^6 frozen and thawed AX2 GFP-filactin cells) on the gel filtration column, endogenous and GFP-filactin can be detected at a molecular weight between 400,000 and 40,000, indicating that in the cell, filactin is present as a tetramer, but also as monomer and even maybe as dimer or trimer.

To define more precisely which part of the protein is responsible for the tetramerization, the elution profiles of the FLAG-actin domain, the GST-Ist1-like domain and the GST-filamin repeats were analyzed on a gel filtration column. The filactin actin domain and the Ist1-like domain elute at their monomeric size, at ca. 42,000 and 50,000, respectively. In contrast, the GST-filactin filamin repeats do not elute at the expected 52,000 but at ca. 200,000 – 220,000, suggesting that this domain is responsible for the tetramerization of filactin (figure 51 B).

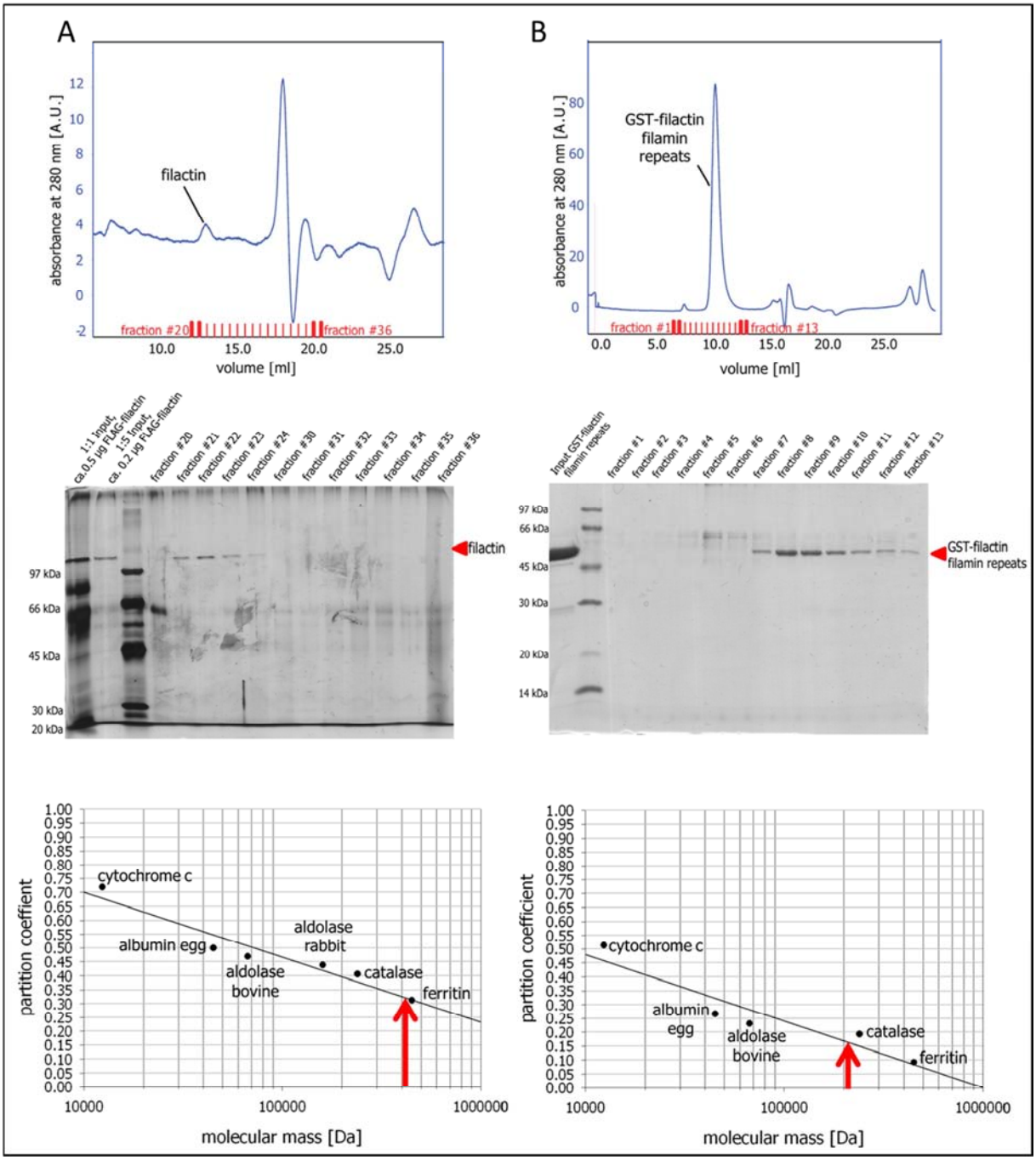

Figure 51: Filactin might form a tetramer via its filamin-like Ig repeats. Purified FLAG-filactin and GST-filactin filamin repeats were analyzed using ÄKTA superose 6 and superose 12 gel filtration columns. The upper panel shows the elution profiles (measured at 280 nm). 500 µl-fractions were collected and analyzed on a SDS-gel (middle panel). The lower panel shows the calibration curves of the columns and the measured molecular mass of the protein indicated with the red arrow. A) The peak of filactin full length appears at ca. 13.5 ml which corresponds to a partition coefficient of 0.34375, meaning that it elutes at a molecular weight of about 400,000. B) The peak of the filamin repeats appears at ca. 10.7 ml which corresponds to a partition coefficient of 0.16139, meaning that it elutes at a molecular weight of ca. 200,000-220,000.

4.1.6 Purified filactin imaged using a transmission electron microscope

To visualize the presumptive filactin tetramer, imaging of the protein with the transmission electron microscope was attempted. These experiments were carried out in the Baumeister laboratory (Max-Planck-Institut für Biochemie, Martinsried). In a negative stain, proteins and protein complexes from 100 kDa on should be visible. Filactin has a size of 105 kDa, and the tetramer would be 420 kDa. Smaller proteins only appear as a background noise. The FLAG-tagged full length filactin and the FLAG-tagged filactin actin domain were purified from Sf9 cells. Since the filactin full length protein always was contaminated by many degradation products after the purification, it was run on a ÄKTA superose 6 gel filtration column and only the fraction of a molecular weight of ca. 400,000 was kept. It was prepared for the negative stain just in G-Buffer containing 50 mM NaCl (figure 52 B), then under polymerizing conditions (figure 52 C) and together with actin under polymerizing conditions (figure 52 D). As a control, rabbit actin only was polymerized (figure 52 A). In the control, actin filaments were visible. In the sample with filactin, no distinct molecular structure could be detected. Proteins of different sizes were present, suggesting that there still occurred degradation after the purification over the gel filtration column. Also, no distinct tetrameric conformation of the protein could be assessed. When incubated in polymerization buffer, filactin seems to form aggregates (figure 52 C), more than under non-polymerizing conditions. These aggregates also remained to a lower extent when filactin was incubated with actin under polymerizing conditions, but no actin filaments were visible anymore (figure 52 D).

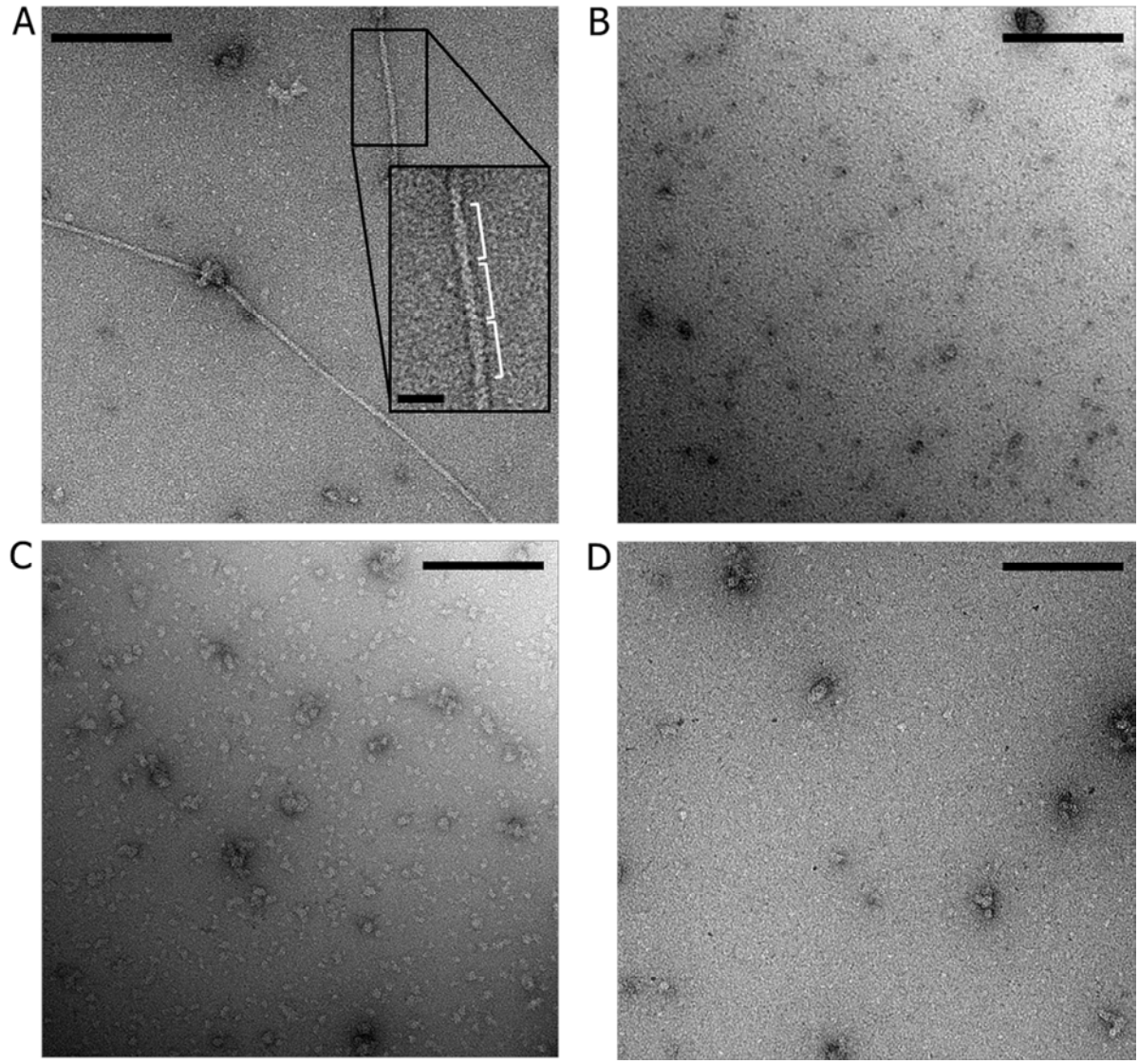

Figure 52: Purified FLAG-filactin imaged using a transmission electron microscope. Purified FLAG-filactin was fractioned on a ÄKTA superose 6 gel filtration column and the 400,000 fraction was imaged by negative stain with and without actin and under polymerizing conditions. Scale bar, 200 nm. A) Polymerized purified rabbit actin under polymerizing conditions (control). Note the two actin filaments. In the image section magnification, three helices within the filament are visible, indicated by white brackets. Scale bar in the blow-up section, 40 nm. B) Purified FLAG-filactin. Proteins of different sizes were visible, but no evident tetramer could be detected. C) Purified FLAG-filactin under polymerizing conditions. Upon addition of polymerization buffer, filactin seems to form aggregates. D) Purified FLAG-filactin with rabbit actin under polymerizing conditions. The proteins seem to form aggregates, but no filaments could be found.

Also the filactin actin domain only was imaged (figure 53). The filactin actin domain has a size of ca. 42 kDa and seems to be present as a monomer. As expected, when imaging the protein in a negative stain, only small proteins are visible that appear rather as a background noise. When incubating the protein under polymerizing conditions, it seemed to form aggregates (figure 53 B), just as it was observed for the full length protein as well (figure 52 C). When incubating the filactin actin domain together with rabbit actin, these

aggregates still were present, but apparently in a lower concentration than without actin, which is consistent with the observations for the full length filactin. Also, no actin filaments were present under that condition (figure 53 C).

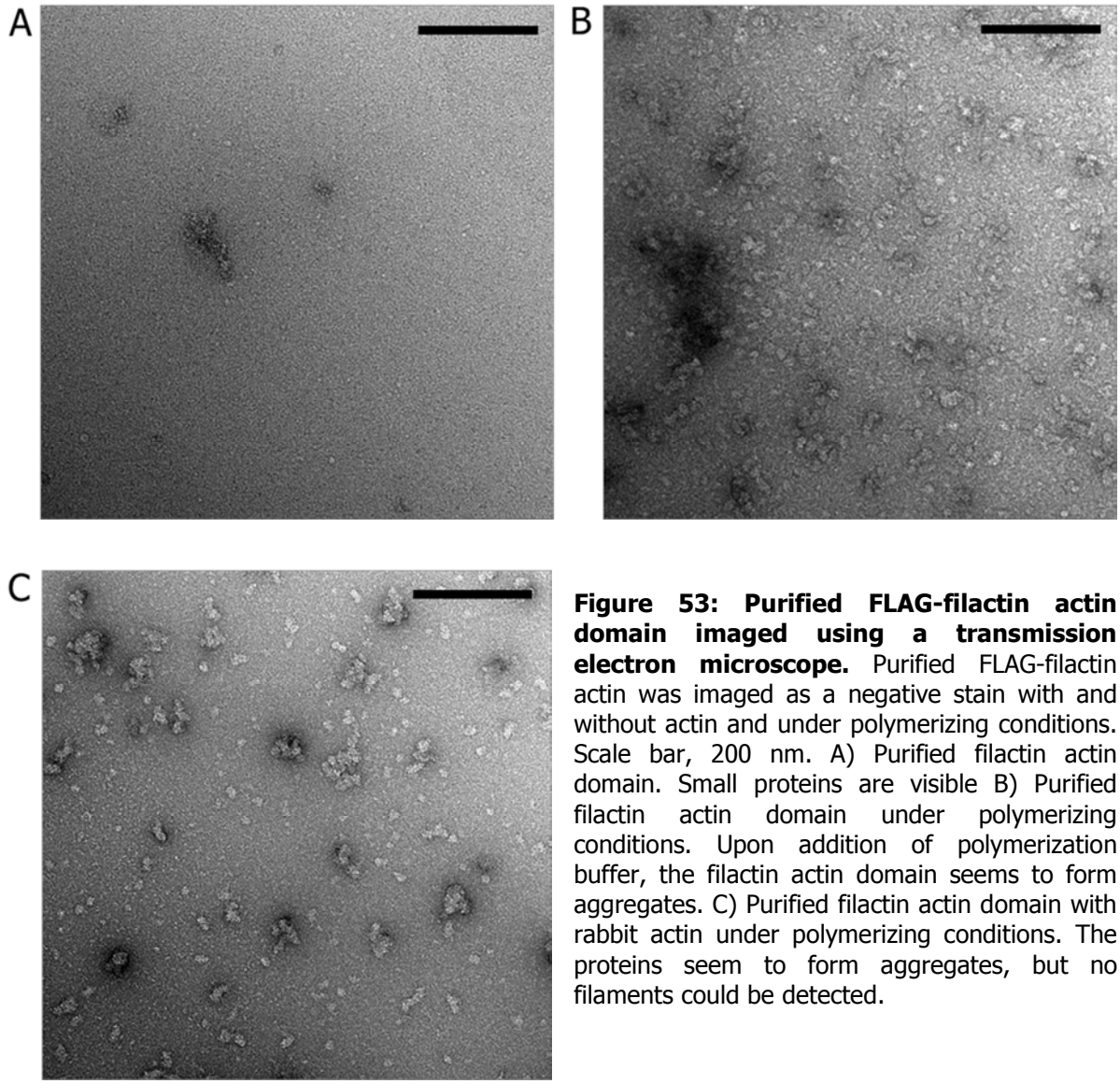

Figure 53: Purified FLAG-filactin actin domain imaged using a transmission electron microscope. Purified FLAG-filactin actin was imaged as a negative stain with and without actin and under polymerizing conditions. Scale bar, 200 nm. A) Purified filactin actin domain. Small proteins are visible B) Purified filactin actin domain under polymerizing conditions. Upon addition of polymerization buffer, the filactin actin domain seems to form aggregates. C) Purified filactin actin domain with rabbit actin under polymerizing conditions. The proteins seem to form aggregates, but no filaments could be detected.

4.2 Other actin variants in *D. discoideum*

Besides filactin, preliminary studies of few other *D. discoideum* actin variants were conducted. Act24 and act25 were chosen since they are divergent from the conventional act8 group, but not as much as e.g. filactin. The *D. discoideum* cell lines expressing GFP-act24 and GFP-act25 were provided by Annette Müller-Taubenberger. Since act24 and act25 are 82 % and 78 % identical with conventional actin, respectively, it was tested whether the act-1 antibody recognizing *D. discoideum* conventional actin (Simpson et al, 1984) would also bind to these actin variants. Western blot analysis revealed that the GFP-tagged actin variants act24 and act25 cannot be detected by the act-1 antibody (figure 54 C) even though most of the residues described to be required for the formation of the act-1 antigenic site are present (figure 55).

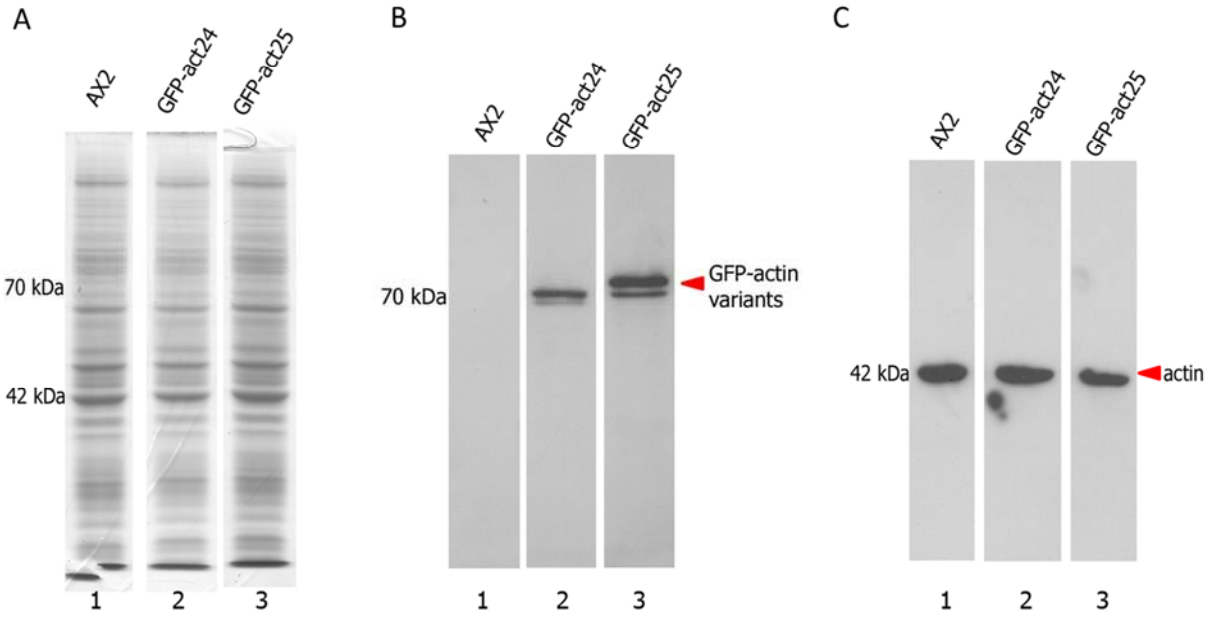

Figure 54: SDS-Page Analysis of GFP-tagged actin variants 24 and 25. Total cell lysate was applied on a SDS-gel in a concentration of 2 x 10^5 cells/lane. A) Coomassie Blue stained SDS-gel. B) Western blot incubated with the GFP antibody K3-184-2. GFP-act24 and GFP-act24 were detected at approximately 70 kDa. Note the two bands just below each other for both GFP-act24 and GFP-act25. C) Western blot incubated with the actin antibody act-1. Endogenous actin in the mutant strains is present as in the wild type strain AX2. The act-1 antibody did not recognize GFP-act24 and GFP-act25.

Simpson et al (1984) appoint amino acid 13 – 50 of *D. discoideum* actin8 to be important for act-1 binding, especially Thr42 seems to be critical. The actin variants show high homology to the act8 protein in this region (figure 55), but are still not recognized by the antibody.

Figure 55: The binding epitope of the act-1 actin antibody is conserved in the analyzed actin variants but apparently not enough to allow act-1 binding. Alignments of aa 1-60 for act8, act24 and act25 are displayed as well as aa 574-634 for filactin. Simpson et al (1984) described amino acids 13-50 of *D. discoideum* conventional actin (act8-group) to be required for act-1 binding (red box), especially the threonine at position 42 (red arrow) should be critical for the formation of the act-1 antigenic site. Particularly act24 is highly conserved in this region and differs only in two amino acids from the act8 sequence. However, the act-1 antibody can neither detect GFP-act24 nor GFP-act25 and filactin.

Another actin antibody, namely 224-236-1 (Westphal et al, 1997), was also unable to bind to GFP-act24 and GFP-act25 (figure 56 C). Furthermore, the filactin antibody which recognizes the actin domain of filactin (4S-59-4), does not bind to the actin variants act24 and act25 (data not shown).

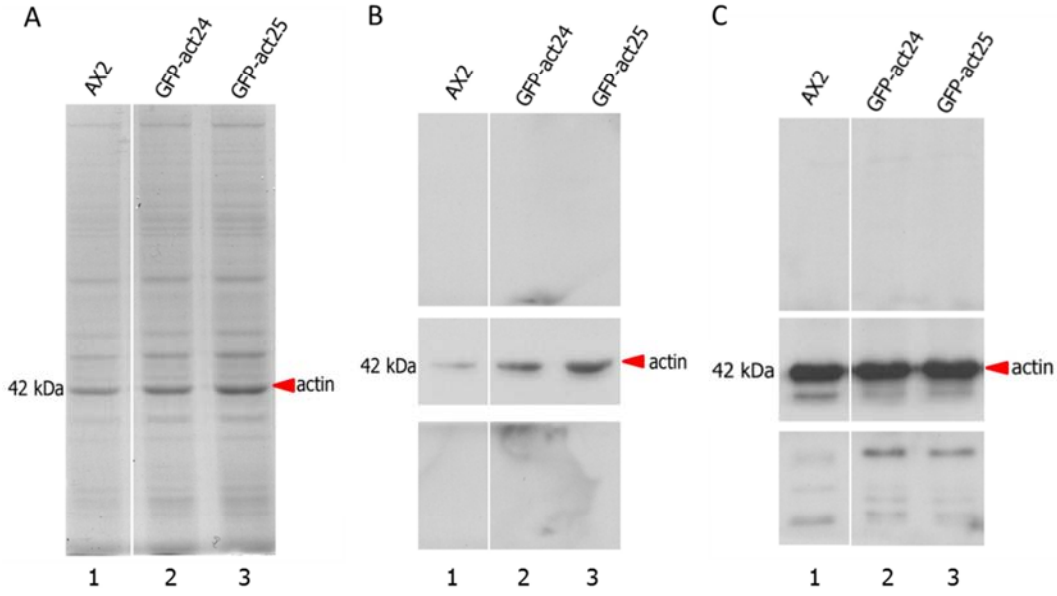

Figure 56: The actin antibodies act-1 and 224-236-1 do not recognize GFP-act24 and GFP-act25. Total cell lysate was applied on a SDS-gel in a concentration of 2 x 10^5 cells/lane. After protein transfer onto the nitrocellulose membrane, the bands of the size 42 kDa (conventional actin) were removed, so that the excess of conventional actin would not exhaust the actin antibody in solution during incubation of the membrane. A) Coomassie Blue stained SDS-gel. B) Western blot incubated with the actin antibody act-1. C) Western blot incubated with the anti-actin antibody 224-236-1.

Live-Imaging and immunofluorescence imaging showed that GFP-act24 and GFP-act25 localize to the cytoplasm and seem not to co-localize with the conventional F-actin at the cell cortex in vegetative *D. discoideum* cells (data not shown). The cell lines expressing the GFP-tagged variants did not exhibit an altered phenotype.

5. Discussion

The major goal of this work was to analyze the functions in actin dynamics of WH2 domains and selected actin variants. Analysis of the studied proteins revealed that they influence the microfilament system. The multifunctional WH2 domains in tandem can both enhance actin filament formation and disrupt F-actin in a concentration dependent manner. Filactin, an actin variant in *D. discoideum* seems to be an actin sequestering protein and to be associated with the ESCRT pathway. The first part of the discussion will elaborate the functions of WH2 domains in proteins and the second part will outline the possible functions of filactin and other actin variants.

5.1 WH2 domains are versatile regulators of actin dynamics

WH2 domains in proteins can nucleate actin polymerization, sequester actin molecules, disrupt and depolymerize actin filaments *in vitro.* These partially new findings show the intrinsic multifunctionality and versatility of that domain. In this study, WH2 domains of fly Spire and mouse CAP2 were analyzed and the WH2 domain(s) of both of these proteins showed similar characteristics. Thus, the work on these two proteins can be seen as an exemplary study for other proteins containing WH2 domains. The WH2 domain in tandem is also present in other eukaryotic proteins, such as N-WASP (two WH2 domains) and Cordon-Bleu (three WH2 domains) (Ahuja et al, 2007) but also in prokaryotic virulence factors like VopF and VopL (three WH2 domains) (Liverman et al, 2007; Tam et al, 2007).

5.1.1 Nucleation of actin polymerization and G-actin sequestering by WH2 domains

Spire nucleates actin filament formation only at substoichiometric concentrations and sequesters G-actin at stoichiometric concentrations; therefore, nucleation and sequestration by WH2 domains go hand in hand and both characteristics must be taken into account for the functions of these proteins *in vitro* and *in vivo*. First of all, for nucleation of actin polymerization by WH2 domains at least two WH2 domains in tandem are required. Single WH2 domains as present in the constructs SpireL3+D, SpireD and CAP2-WH2 show the sequestering activity only. The linker 3 situated between Spire WH2 domains C and D was previously described as an actin binding element with weak actin nucleating activity (Zuchero et al, 2009). Thus, the construct SpireL3+D should possibly be able to nucleate actin filament formation. However, in this study, the construct SpireL3+D did not exhibit any nucleating activity. Additionally, the Isothermal Titration Calorimetry (ITC) measurements

performed by Sitar et al (2011) did not identify any interaction between linker 3 and actin molecules. Two, three and four WH2 domains in series effect nucleation of actin filament formation as shown in this thesis. These data appear logical since at least two G-actin molecules need to be positioned in close proximity to act as a nucleus to which a third actin molecule can be added easily to start polymerization. It could not be concluded from our assays that a construct with three or four WH2 domains nucleates more efficiently than a construct with two WH2 domains. Theoretically, three actin molecules should act as better nucleus than two actin molecules. However, the actin bound to the WH2 domains does not adopt the F-actin conformation. WH2 domains are G-actin binding motifs. The small-angle X-ray scattering and crystallography studies performed by Sitar et al (2011) show that Spire-actin complexes form stable, straight-longitudinal configurations in which actin is loosely positioned along the WH2 domain stretch. The longitudinal architecture of the Spire–actin interaction is dominant in solution under non-polymerizing conditions (Sitar et al, 2011). The *in vitro* experiments presented by Sitar et al (2011) as well as other previous studies (Bosch et al, 2007; Ducka et al, 2010) suggest that under non-polymerizing conditions, Spire binds actin to form the sequestering/nucleating complex which remains inactive in a G-actin solution. Upon addition of polymerization buffer, the WH2 domains in tandem permit the formation of longitudinal interacting bonds, resulting in a rearrangement of the actin conformation to the filamentous form of one strand of the filament (Ducka et al, 2010). Further actin molecules are added and a two-start actin filament is generated. The WH2 domains, being G-actin binding motifs, will reduce the affinity to the emerging filament and finally release it into the solution where it acts as a nucleus for further actin polymerization. It is tempting to assume that the tandemly organized WH2 domains release, due to a decreased binding affinity, the emerging filament as soon as the ATP moieties in the nucleotide binding cleft of the individual F-actin subunit are hydrolyzed. The WH2 domains will subsequently bind *de novo* to G-actin molecules to repeat the process, leading to enhanced nucleation of actin polymerization (compare nucleation model shown in figure 57). The polymerization assays conducted with prepurified Spire-actin complexes clearly show that these are the intermediates that lead to enhanced nucleation. WH2 domains not in complex with actin would exhibit the sequestering activity at these concentrations.

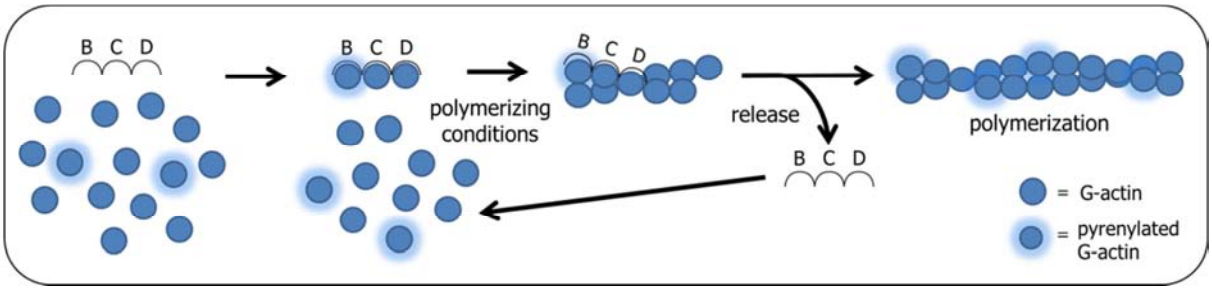

Figure 57: Working model of nucleation of actin polymerization by WH2 domains in tandem (at substoichiometric concentrations of WH2 domain constructs). WH2 domains in tandem bind to G-actin molecules forming a longitudinal sequestering/nucleating complex which remains inactive under non-polymerizing conditions. Under polymerizing conditions, the WH2-actin complex rearranges its longitudinal conformation to the filamentous form and actin filaments can be formed. The WH2 domains reduce the affinity to F-actin and release the short filament thus favoring elongation. The now 'empty' WH2 domains immediately bind to free available G-actin in solution. When all available G-actin molecules are consumed, the WH2 domains stay in complex with the remaining G-actin thus also decreasing the fluorescence at steady state.

Intriguingly, the samples in which actin polymerization was triggered by WH2 domains always show a decrease of fluorescence at steady state compared to the control. The G-actin solutions used for the *in vitro* polymerization assays usually contain about 10 % pyrenylated actin. At steady state, almost all available G-actin is polymerized, suggesting that in the other samples, some of the available monomeric actin is prevented from integration into the actin filaments. This supports the idea that the WH2 domains in tandem are dynamic nuclei that release from emerging filaments and bind available G-actin in solution. The WH2 domains have such a high affinity to actin molecules that an 'empty' WH2 stretch will immediately fill its binding sites with available G-actin and thus the WH2 domains almost only occur in complex with actin in such an assay. Once the pool of available free G-actin is exhausted in polymerization, the WH2-actin complexes will not nucleate filaments anymore but will remain bound to G-actin conformation molecules. Thus the presence of pyrenylated G-actin in solution available for polymerization is decreased which finally leads to the formation of less F-actin than in the control.

It is consistent with these assumptions that at stoichiometric concentrations of WH2 domains over actin, actin polymerization cannot be nucleated since the G-actin molecules are sequestered in the WH2-actin complex (compare model for sequestration shown in figure 58).

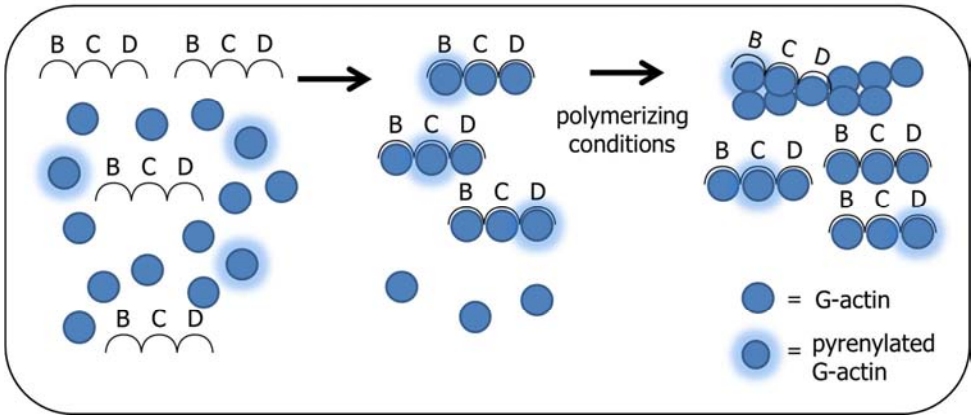

Figure 58: Working model of sequestration of actin by WH2 domains (at high concentrations of WH2 domain constructs). Substantial concentrations of WH2 domains sequester substantial concentrations of available G-actin. This reduces the amount of polymerizable G-actin and leads to a large delay of polymerization.

The hypothesis that WH2 domains in tandem are dynamic actin nuclei that release from the filaments and are not 'dead-end' WH2-actin complexes as it was suggested earlier (Bosch et al, 2007) is supported by the experiment of actin polymerization nucleation by prepurified WH2-actin complexes. In these assays, the prepurified Spire-actin complexes were generated by the use of unlabeled actin. After effected nucleation of actin polymerization by these complexes, a decrease of fluorescence at steady state is observed as well, suggesting that the unlabeled actin was released and replaced by pyrenylated actin from the solution. In case the WH2 domains would remain on the actin filaments, no decrease of fluorescence at steady state should be observed.

In conclusion, the nucleating activity by WH2 domains in tandem and the decrease of fluorescence at steady state are closely associated. The finding of this molecular mechanism of this intrinsic versatile function of WH2 domains in tandem might alter the view on WH2 domain containing proteins in general. The *in vitro* analysis of the function of WH2 domains is important and necessary, but might be insufficient to elucidate its function in living cells. *In vivo*, nucleation and sequestration by WH2 domains seem to be much more complex than observed in this study. It was shown previously that nucleation of actin polymerization by Spire depends also on cooperation with formins and profilins (Pfender et al, 2011; Quinlan et al, 2007). The nucleation of filament formation thus is regulated by other nucleating, sequestration factors and maybe unknown proteins. Sitar et al (2011) propose a model in which one formin dimer binds two molecules of Spire, and each Spire protein binds to four actin molecules thereby bringing together eight actin molecules *in vivo*. This short filament seed can then act as a nucleating complex from which Spire dissociates to allow formin-promoted actin filament elongation at the barbed end. Nevertheless, the final concentration of WH2 domain constructs in subcellular regions is not known and it is not completely clear

under which trigger a protein containing at least two WH2 domains in tandem would nucleate actin filament formation or would sequester actin molecules. Hence, the set of players required for *in vivo* function of WH2 domain containing proteins needs to be identified to understand the complexity and dynamics of these proteins.

5.1.2 Disruption of actin filaments by WH2 domains

In contrast to nucleation, the sequestering activity as well as the filament disrupting activity are attributes of all constructs, including a single WH2 domain, e.g. the SpireD construct with a sequence of only 22 amino acids. This indicates that the disintegration of actin filaments is not dependent on a concerted action of two actin binding domains as it is characteristical for the F-actin severing proteins from the gelsolin protein family (Eichinger et al, 1991; Schnuchel et al, 1995). It is intriguing that the WH2 domains being G-actin binding motifs have nonetheless such a high affinity to actin that they are able to bind the filamentous form and forcefully rip off subunits from the filament, thereby destroying the whole structure (compare model filament disruption shown in figure 59). Subsequently, the WH2 domains remain soluble with their bound actin in monomeric globular conformation. Thus, the binding affinity of single WH2 domains to actin seems to win over the process of actin filament formation.

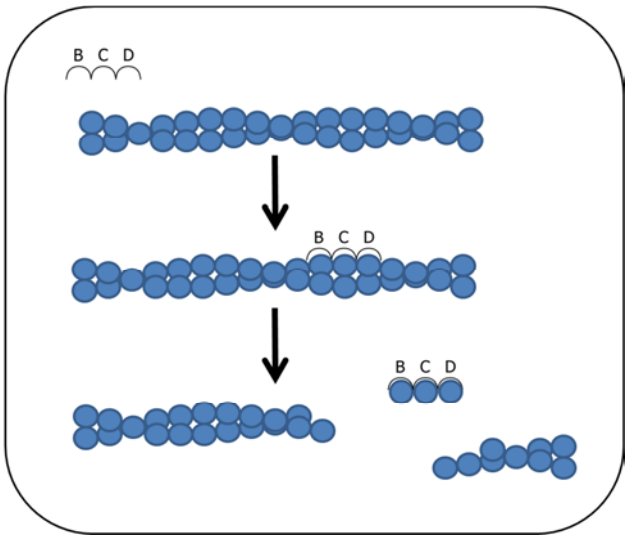

Figure 59: Working model for the disruption of actin filaments by WH2 domains. When adding WH2 domain constructs to fully polymerized actin filaments, either single WH2 domains or perhaps only a single domain arranged in a tandem, they seem to have such a high affinity to actin that they are able to bind to the filamentous form and forcefully sequester actin monomers from the filament, thereby destroying the whole structure and chopping up the filament. The actin bound to the WH2 domains most probably rearranges its conformation to the G-actin form.

The high potential of F-actin disrupting activity by 1-4 WH2 domains was shown in fluorometric assays. It is surprising how quickly the actin filaments are disrupted, resulting in drops of fluorescence to stable plateaus within seconds. In contrast to recent findings by Chen et al (2012), it could not be confirmed that SpireABCD severs more efficiently than a construct containing only two or three WH2 domains. In the assays performed in this work,

the artificial construct SpireDDD seems to chop up actin filaments most efficiently compared to the other constructs. This might be due to the high binding affinity of this domain to actin with a K_d of 0.17 µM (Sitar et al, 2011). Three domains with a strong actin binding affinity might chop up filaments more efficiently than the SpireABCD construct in which cooperative binding might play a role. Nonetheless, the single WH2 domain SpireL3D needs to be applied in much higher concentrations (about 20-fold) to reach the same effect than SpireDDD containing three WH2 domains. WH2 domains in tandem are possibly more efficient in disrupting the actin filaments because they have an entropic advantage over single domains. The force that needs to be raised to disrupt the F-actin conformation might be more efficiently established when the binding surface is bigger. The disruption of actin filaments and actin-fascin filament bundles was visualized by TIRF microscopy for the Spire constructs and on a confocal microscope for CAP2-WH2. Both constructs disrupt filaments and filament bundles until they completely disappear. Thus the affinity of WH2 domains to actin is even so high that they can disrupt cross-linked filament bundles.

WH2 domains saturated with actin do not exhibit the same F-actin disrupting activity as 'empty' WH2 domains. In fluorometric experiments, the Spire-actin complexes could not disrupt actin filaments like free WH2 domains and thus the fluorescence did not drop immediately upon addition of these constructs. However, when the fluorescence of the F-actin solution to which the Spire-actin complexes were added was measured again after some incubation time, a drop of fluorescence could be recorded. Hence, the unlabeled actin was released by the complex over time and was replaced by pyrenylated actin. These data confirm the previous finding of this study that Spire-actin complexes are dynamic nuclei for actin polymerization and do not sequester their bound actin in a 'dead-end'-manner.

The single WH2 domain of CAP2 was shown to sequester G-actin and disrupt actin filaments in this study (Peche et al, 2013). This is in agreement with earlier findings that CAP from lower eukaryotes and the other mammalian CAP - CAP1 - exert an inhibitory effect on actin polymerization (Bertling et al, 2004; Gottwald et al, 1996). CAP2 is a protein that plays a role in cardiac muscle where it localizes to the M-band and to adjacent regions of the sarcomere. Ablation of CAP2 leads to ventricular dilated cardiomyopathy in mice providing strong evidence how important this protein is for M-band and sarcomere organization. Myofibrillar organization is essential for the physiological activity of the cardiac system. To date, the turnover process of entire actin filaments in myofibrils is not entirely understood and was described to be slow (Littlefield & Fowler, 2008). In non-contractile cardiomyocytes actin filaments are very stable, whereas contractility induces rapid depolymerization of actin filaments which are not contributing to contractility (Skwarek-Maruszewska et al, 2009). These filaments might be replaced by new ones subsequently (Littlefield & Fowler, 2008;

Skwarek-Maruszewska et al, 2009). CAP2 was shown to regulate filament formation previously (Peche et al, 2007) and most probably, the lack of CAP2 leads to the disarray of the sarcomere due to the loss of its WH2 domain dependent G-actin sequestering and filament disrupting activity. CAP2 might be responsible for maintaining the length of sarcomeric actin filaments by severing them in the M-band region.

5.1.3 *D. discoideum* amoebae respond to treatment with SpireWH2 constructs

A most surprising finding of this work is the behavior of living *D. discoideum* amoebae to treatment with SpireDDD protein. The addition of SpireWH2 domains seems to exert a certain stress to the cells since the cells round up and show a disintegration of the actin cytoskeleton, a similar reaction compared to the treatment with Latrunculin A. At higher concentrations, the cells even form cytoplasmic rods which usually takes place when the cells are exposed to ATP-depletion, e.g. during the treatment with NaN_3. Interestingly, the response of the cells occurs exclusively when they encounter the 'empty' WH2 domain constructs. SpireDDD saturated with actin does not affect the amoebae. Possibly, the SpireWH2 constructs might pass the membrane of *D. discoideum* cells and disrupt the filamentous actin network. If this is a true finding, it would contradict the old dogma that proteins are not able to simply pass the membrane of cells. Even more intriguing would be the identification of a membrane receptor that would bind the WH2 domains on the surface of the *D. discoideum* membrane and trigger an intracellular response. When analyzing whether TMR-labeled SpireBCD would be able to enter AX2 GFP-cofilin overexpressing cells in preliminary experiments on a confocal microscope, no TMR-fluorescence could be detected within the treated cells (data not shown). However, the TMR-SpireBCD contains only 15 % labeled SpireBCD constructs. Thus, an investigation of the presence of WH2 domain constructs within the cells requires the generation of antibodies against these proteins.

5.2 Filactin and other actin variants

The *D. discoideum* conventional actin (act8-group) represents a nearly perfect cytoplasmic actin which is highly conserved throughout evolution (Joseph et al, 2008). The presence of the large number of actin variants in *D. discoideum* is very intriguing and raises the question whether these variants share similar activities. One could conclude that some of them have structural cytoskeletal functions, some rather have regulatory functions, some are important in a subcellular compartment or at a specific time during development in the life cycle of *D. discoideum*. Posttranslational modifications of these proteins might also play a role. Interestingly, there seem to be at least two different forms of both the GFP-act24 and GFP-act25 fusion protein in transformed *D. discoideum* cells. Possibly, more than one 'species' of a distinct actin variant (e.g. phosphorylated and unphosphorylated) are present in the cell. The investigation of actin variants on the cellular level is rather difficult because of the high similarity of the protein sequences and therefore, generating specific antibodies or KO cell lines seems to be quite a challenge. However, in this study it was discovered that two actin antibodies recognizing conventional act8-group *D. discoideum* actin (Simpson et al, 1984; Westphal et al, 1997) do not bind to at least the three tested actin variants act24, act25 and filactin. Consequently, the described binding epitope is probably too divergent in the actin variants or possibly, the different amino acids in the actin variants cause a conformational and probably antigenic change at a topologically different site within the protein. It will be interesting to analyze the many *D. discoideum* actin variants and their functions in more detail in biochemical and cell biological assays, e.g. conducting *in vitro* (polymerization) assays, generating antibodies and analyzing KO cell lines.

Filactin is the most extraordinary actin variant of *D. discoideum* with a conserved C-terminal actin domain and an extended N-terminus with a distinct domain organization. Since the actin domain of the protein has a higher homology to *bona fide* actins than to actin-related proteins (ARPs), it is classified as an actin variant.

At the beginning of this thesis, the major question was whether filactin co-polymerizes with conventional actin and whether it is able to self-polymerize as well, since the filactin actin is so similar to conventional actin. Now, with the data obtained during this work, the model changed into a different direction. Filactin, or rather the filactin actin domain seems to act as a G-actin sequestering protein, and is not integrated into filaments (figure 60 D). Furthermore, filactin probably might cap F-actin (figure 60 E). The N-terminal extension of filactin could serve as a regulator of filactins' function within the microfilament system and inhibit or activate its interaction with the actin cytoskeleton (figure 60 B). In addition, filactin seems to be present especially as a tetramer (figure 60 C) and as a monomer, and maybe as a trimer and dimer as well. In a cell, filactin co-localizes with F-

actin but is also present in the cytoplasm on vesicle-like structures. Through its N-terminal domains, filactin is associated with the ESCRT pathway (figures 60 F and G).

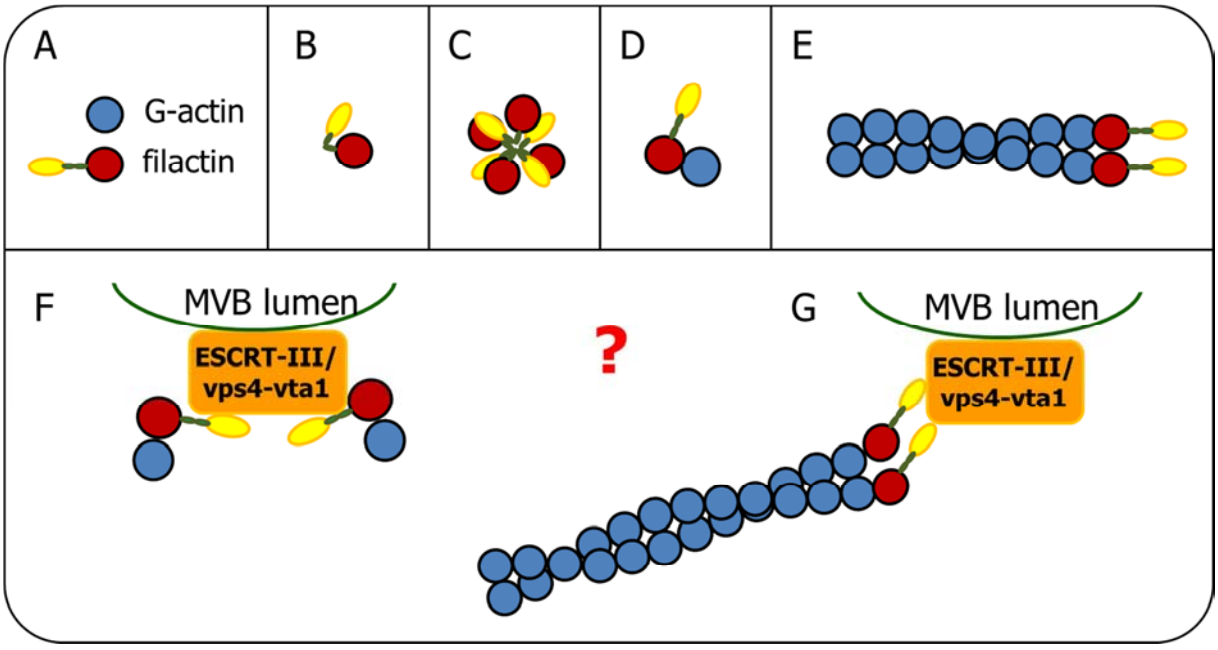

Figure 60: Working model of filactin conformation and function within the microfilament system in the cell. All the models are simple, hypothetic and undetailed depictions of possible conformations and functions of filactin. A) Depiction of G-actin and filactin as used in the following models. In filactin, the N-terminal Ist1-like domain is displayed as yellow oval, the filamin-like Ig-repeats as two small green ovals and the actin-like domain as a red circle. B) There might be an autoinhibited filactin conformation in which the access to the actin domain might be inhibited by a certain fold of the N-terminal domains. C) Filactin might be a tetramer. The tetramerization domain is located at the filamin-like Ig repeats. D) Filactin seems to act as a G-actin sequestering protein. E) Filactin possibly might act as a capping protein. However, it is unlikely that it caps the fast growing end. F) and G) Filactin is associated with the ESCRT pathway by interacting with vta1. It might sequester actin at sites of membrane scissons (F) or it might connect the ESCRT machinery to the microfilament system by capping F-actin (G).

5.2.1 The function of the filactin actin domain

In this work, the localization of filactin was analyzed with regard to the actin cytoskeleton, as well as its function in actin dynamics. The actin domain of filactin shares 64 % identity with *D. discoideum* conventional actin and 67 % identity with human β-actin. Studies prior to this thesis found filactin to co-localize with conventional actin in *D. discoideum* (Israel, 2002). Indeed, the co-localization of the 105 kDa protein with actin in the cell could be confirmed in immunofluorescence studies. Moreover, the fact that the generated antibody specific for the filactin actin domain (4S-59-4) cross-reacts with conventional actin in western blot analysis as well as in immunofluorescence studies confirms the high similarity of filactin to conventional actin.

Additionally, this study specified the actin domain of filactin to be responsible for the observed co-localization with conventional actin. The GFP-fusion constructs of the N-terminal domains do not co-localize with conventional actin but are enriched in the nucleus, even without showing the vesicle-like distribution of the full length construct. Most probably, a cooperation of the different filactin domains is necessary for localization and function of the full length protein. Interestingly, filactin is part of the stress-induced, nuclear actin rods. This is another clear indication that filactin is part of the actin cytoskeleton. Until now, only cytoskeletal proteins were identified in the rods besides actin, such as cofilin, Aip1 and coronin (Minamide et al, 2010; Nishida et al, 1987; Vandebrouck et al, 2010). All of these proteins seem to be able to pass the nuclear membrane. Small molecules and proteins of a size up to about 50 kDa can pass freely through the nuclear envelope across aqueous channels of a diameter of about 9 nm. The nuclear pores usually have a maximum diameter of about 25 nm and proteins bigger than 50 kDa need to be imported or exported in a regulated fashion. The proteins known to be implicated in the nuclear actin rods are not bigger than 65 kDa. In contrast, monomeric filactin has a molecular weight of 105 kDa. It is very intriguing that this protein can pass the nuclear membrane upon stress treatment very quickly (within 5-10 minutes) to finally be found within the rods. When treating GFP-filactin overexpressing cells with DMSO, the GFP-tagged filactin - now a protein of 130 kDa - seems to be unable to cross the nuclear envelope. The protein is found in the cytoplasm only, but the rods are still formed. Consequently, the GFP-tagged filactin might be too big to get into the nucleus. All smaller GFP-tagged filactin domain constructs used in this study were found enriched in the nucleus upon treatment with DMSO, but were clearly not part of the rods. Thus, the GFP-tag might hinder integration of the fusion protein into the rods. How filactin passes the nuclear membrane, how it influences the rod formation, how it is integrated into the actin rods and how important it is for the spatial and temporal formation, stability and biophysics of the rod remain to be elucidated.

For the first time, recombinant filactin was successfully expressed and purified in this study using the baculovirus expression system. This allowed investigation of filactin's function in actin dynamics in *in vitro* assays. The actin domain of filactin shows the characteristics of an actin sequestering protein in fluorometric, viscometric and spindown assays. However, the actin domain of filactin could also act as a minus end capping protein. It seems unlikely that the actin domain acts as a plus end capping protein, because in the dilution-induced depolymerization assay it would have slowed down the depolymerization instead of accelerating it. Possibly emerging filaments are capped at the minus end and thereby both the fluorescence signal in fluorometric assays and the viscosity of the actin solution in viscometric assays were reduced. It needs to be assessed exactly whether the

actin domain really acts as a capping protein e.g. by capping emerging filaments by known capping proteins at the minus end of the filament and subsequently investigating the influence of added filactin actin. Furthermore, a recombinant FLAG-GFP-filactin actin construct was generated in this study. The interaction of fluorescently labeled actin and filactin actin could be investigated at a TIRF microscope.

Surprisingly, the full length filactin protein does not exhibit the same characteristics as the filactin actin domain. Although the actin domain is present in this construct as well, it does not act as an actin sequestering protein in the conducted *in vitro* assays. There are several possible explanations for this phenomenon. First, the protein might not be functional after the purification since it is very sensitive to proteolytic cleavage. Second, probably the full length protein is self-inhibited but needs to be activated by certain conditions or factors. Possibly the N-terminal domains inhibit the function of the actin domain by a hairpin conformation in which the N-terminus is folded over the active sites of the actin domain. Third, the interactions of filactin with the actin cytoskeleton in *D. discoideum* are so specific that the use of rabbit muscle actin for the *in vitro* actin polymerization assays was unfavorable and the assays need to be repeated with purified *D. discoideum* actin. To further analyze the localization of full length filactin in respect to actin filaments *in vitro*, the recombinant FLAG-GFP-filactin construct generated in this work could be used in TIRF assays.

5.2.2 The function of the filactin amino-terminal domains

In this thesis, the very N-terminal domain of filactin was identified as Ist1-like domain via sequence analysis. The filactin Ist1-like domain is only homologous to amino acid 1-196 of human IST1 (366 amino acids) and supposedly has a similar fold. In human and yeast, Ist1 was described to be implicated in the ESCRT pathway, especially in the regulation of membrane scission and ESCRT-III disassembly (Dimaano et al, 2008; Entian et al, 1999). In both organisms, the Ist1 protein interacts with other proteins of the ESCRT machinery, namely CHMP1/Did2, VPS4/vps4 and LIP5/vta1 via its different domains (figure 61; Bajorek et al, 2009a; Dimaano et al, 2008; Rue et al, 2008).

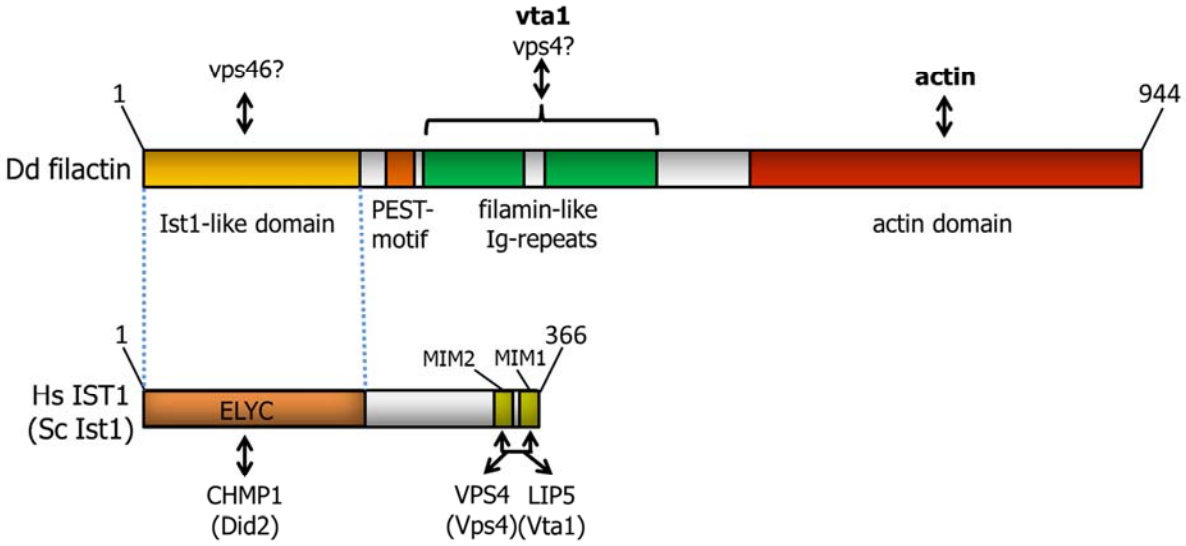

Figure 61: The proteins filactin and Hs IST1 / Sc Ist1 and their interaction partners. The Ist1-like domain of filactin is homologous to the N-terminal domain of human or yeast Ist1 (blue dashed line). *H. sapiens* IST1 and *S. cerevisiae* Ist1 have the same domain organization. The interacting proteins for human IST1 (Hs IST1) are displayed in capital letters below the both way arrows, the corresponding homologs and interacting proteins of yeast Ist1 (Sc Ist1) follow in brackets. Filactin possibly interacts with vps46, the *D. discoideum* homolog of CHMP1/Did2, via its Ist1-like domain. Filactin was clearly identified to interact with vta1 via its filamin repeats. These filamin repeats lack the MIM motifs present in ESCRT-III proteins responsible for interaction with VPS4/Vps4 and LIP5/Vta1 in human or yeast. A co-localization of vps4 and filactin was observed in this study, but the interaction domain of vps4 to filactin remains to be identified. Furthermore, filactin interacts with actin via its C-terminal actin domain.

Interestingly, even though in filactin only the N-terminal domain is present that theoretically could interact with vps46, filactin was identified to interact with vta1 in different biochemical assays. More precisely, vta1 binds to the filamin-like Ig repeats of filactin which do not show any homology to the MIM motif (MIM, MIT-interacting motif; MIT, microtubule-interacting and transport) responsible for Ist1-vta1 interaction in human and yeast. Also a co-localization of filactin and vps4 could be observed, and possibly, filactin interacts with vps46 via its Ist1-like domain.

Taken together, according to what is known about the ESCRT-III machinery in yeast and human (Azmi et al, 2006; Azmi et al, 2008; Nickerson et al, 2006; Dimaano et al, 2008; Rue et al, 2008; Yu et al, 2008), the ESCRT-III disassembly model depicted in figure 61 can be proposed in which filactin influences vps4 recruitment and assembly. This helps to trigger the last step of the ESCRT machinery in which the ESCRT-III complex after successful membrane scission is recycled back into the cytoplasm. In this model, the relation of filactin to the microfilament system is neglected for simplicity reasons. Filactin probably interacts via its Ist1-like domain with vps46 in the cytoplasm. The filactin-vps46 complex might recruit dimeric vps4 to the ESCRT-III complex. This recruitment is not crucial for vps4 function but might influence the kinetics and proper timing of vps4 recruitment to ESCRT-III, while

simultaneously inhibiting premature vps4 oligomerization into the active form until the membrane scission effected by the ESCRT-III complex is terminated. Then probably vps46 dissociates and vta1 binds to filactin and vps4. Possibly, vps46 also stays associated to filactin and the vps4-vta1 complex, since it has the potential to bind to vta1 and vps4 as well. Vta1, an assembly catalyzer of vps4, triggers the oligomerization of vps4 into the functional, dodecameric AAA ATPase. In an ATP-dependent step, vps4 disassembles the ESCRT-III complex to recycle it back into the cytoplasm. In this model, filactin triggers the vta1-vps4 interaction and therefore regulates vps4 function in *D. discoideum*. To further assess a co-localization of filactin and vta1, vps46 and vps4 *in vivo,* strains expressing GFP-filactin and RFP-vta1/RFP-vps46/RFP-vps4 should be generated.

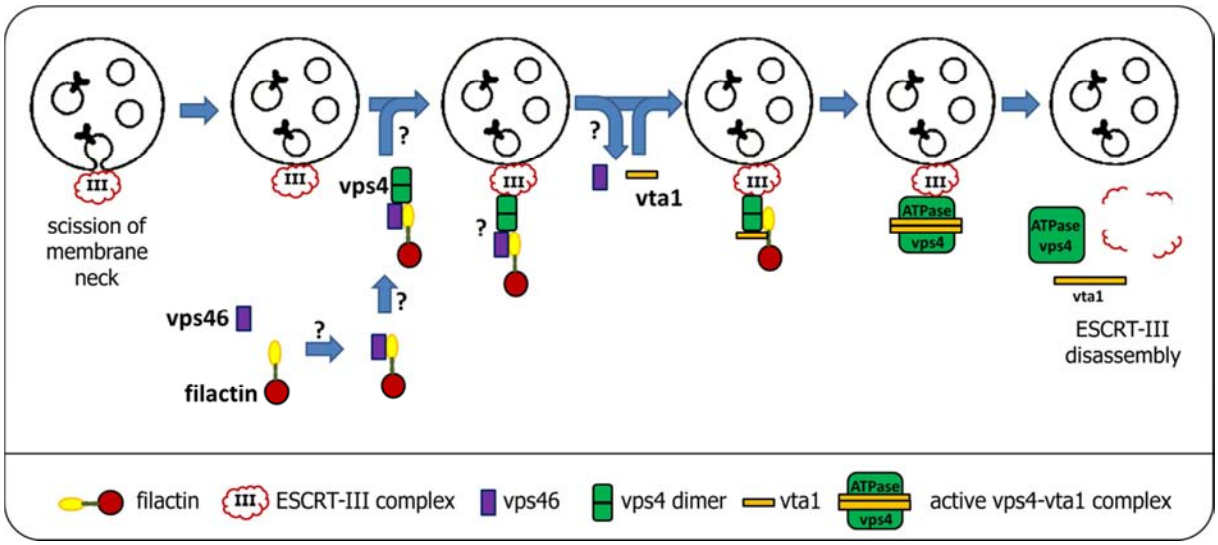

Figure 62: Working model of the implication of filactin in the ESCRT-III complex disassembly. Displayed is the hypothetical process of ESCRT-III complex disassembly from the membrane of a multivesicular body. A legend for the different components is depicted below the model. The ESCRT-III complex effects the scission of the membrane neck at the end of the ESCRT-pathway. Afterwards, it remains bound to the membrane. Filactin possibly binds with its Ist1-like domain to vps46 and recruits dimeric vps4 to the ESCRT-III complex. Once membrane scission is completed, vps46 is possibly released and vta1 recruited to the vps4 dimer. Vta1 catalyzes the assembly of the dodecameric AAA-ATPase vps4 into its active form. In an ATP-dependent step the vps4-vta1 complex disassembles the ESCRT-III complex, thereby recycling it back into the cytoplasm for another round of the ESCRT pathway.

To explore further the possible part of filactin in the ESCRT pathway, autophagy in in *D. discoideum* wild type AX2 and filactin KO cells was investigated. *D. discoideum* prove to be a suitable model to investigate autophagy processes in eukaryotic cells (Calvo-Garrido et al, 2010). Defects in the autophagic pathway are associated with a range of neurodegenerative diseases such as Alzheimer's, Huntington's and Parkinson's disease. Previous studies report that a defective ESCRT machinery leads to the accumulation of autophagosomes in the cell (Filimonenko et al, 2007; Lee et al, 2007; Nara et al, 2002;

Rusten et al, 2007). In this study, an accumulation of autophagosomes was indeed observed in the filactin KO strain compared to wildtype AX2 cells in preliminary experiments, indicating that filactin might interfere with the ESCRT machinery. Until now, there is no clear evidence of the implication of the ESCRT pathway in autophagy processes, but there are indications that have been discussed recently (Metcalf & Isaacs, 2010; Rusten & Stenmark, 2009). There are a series of hypothesis how impairing the ESCRT machinery results in the accumulation of autophagosomes. One explanation is that the ESCRT machinery is required for the closure of the phagophore neck. An autophagosome is topologically equivalent to a multivesicular body, except that it only contains a single, large intraluminal vesicle filling up the whole organelle. The closure of the phagophore neck is practically equivalent to the scission of intraluminal vesicles into the multivesicular body. Thus, it can be speculated that disruption of the ESCRT machinery leads to incomplete phagophore closure and results in multiple unsealed abnormal autophagosomes. However, according to Rusten and Stenmark (2009) the most plausible discussed model is the following: The accumulation of autophagosomes in the cell might be due to inhibition of fusion events of autophagosomes with endosomes and lysosomes. The fusion of the autophagosome with endosomes and lysosomes is a key event in the autophagic flux. The fusion of the autophagosome with a multivesicular body results in a so called amphisome, which then fuses with the lysososome in which the cargo is finally degraded. Possibly, the fusion of multivesicular bodies and the autophagosome is impaired in filactin KO cells, meaning that filactin's function might be associated with the fusion of these organelles.

How filactin connects the microfilament system with the ESCRT machinery is unknown. If filactin acts as a capping protein, it might connect F-actin to sites of membrane scission and may serve as a track for transport and 'outlet belt' of the ESCRT-III subunits back into the cytoplasm. If filactin is rather a G-actin sequestering protein, it probably might clear membrane scission sites from F-actin, as it is observed for ESCRT-mediated abscission in cytokinesis (Dambournet et al, 2011; Guizetti et al, 2011). There, actin is required for preparatory steps, but not the scission itself. A presence of F-actin at the intercellular bridge can perturb and delay cytokinesis abscission like it is the case in Lowe syndrome patients (Dambournet et al, 2011). The exact function of filactin in the ESCRT pathway needs to be investigated in more detail, as well as the connection between the microfilament system and the ESCRT pathway. Nonetheless, with the protein filactin, for the first time there is a hint that a connection exists between the actin cytoskeleton and the ESCRT pathway. Thus, actin variants might have highly specific and maybe cytoskeleton-independent subcellular functions within the cell.

References

Ahuja R, Pinyol R, Reichenbach N, Custer L, Klingensmith J, Kessels MM, Qualmann B (2007) Cordon-bleu is an actin nucleation factor and controls neuronal morphology. *Cell* **131:** 337-350

Ali MY, Krementsova EB, Kennedy GG, Mahaffy R, Pollard TD, Trybus KM, Warshaw DM (2007) Myosin Va maneuvers through actin intersections and diffuses along microtubules. *Proceedings of the National Academy of Sciences of the United States of America* **104:** 4332-4336

Arnold K, Bordoli L, Kopp J, Schwede T (2006) The SWISS-MODEL workspace: a web-based environment for protein structure homology modelling. *Bioinformatics* **22:** 195-201

Babst M, Katzmann DJ, Estepa-Sabal EJ, Meerloo T, Emr SD (2002a) Escrt-III: an endosome-associated heterooligomeric protein complex required for mvb sorting. *Developmental cell* **3:** 271-282

Babst M, Katzmann DJ, Snyder WB, Wendland B, Emr SD (2002b) Endosome-associated complex, ESCRT-II, recruits transport machinery for protein sorting at the multivesicular body. *Developmental cell* **3:** 283-289

Babst M, Sato TK, Banta LM, Emr SD (1997) Endosomal transport function in yeast requires a novel AAA-type ATPase, Vps4p. *The EMBO journal* **16:** 1820-1831

Babst M, Wendland B, Estepa EJ, Emr SD (1998) The Vps4p AAA ATPase regulates membrane association of a Vps protein complex required for normal endosome function. *The EMBO journal* **17:** 2982-2993

Bajorek M, Morita E, Skalicky JJ, Morham SG, Babst M, Sundquist WI (2009a) Biochemical analyses of human IST1 and its function in cytokinesis. *Molecular biology of the cell* **20:** 1360-1373

Bajorek M, Schubert HL, McCullough J, Langelier C, Eckert DM, Stubblefield WM, Uter NT, Myszka DG, Hill CP, Sundquist WI (2009b) Structural basis for ESCRT-III protein autoinhibition. *Nature structural & molecular biology* **16:** 754-762

Bertling E, Hotulainen P, Mattila PK, Matilainen T, Salminen M, Lappalainen P (2004) Cyclase-associated protein 1 (CAP1) promotes cofilin-induced actin dynamics in mammalian nonmuscle cells. *Molecular biology of the cell* **15:** 2324-2334

Blanc C, Charette SJ, Mattei S, Aubry L, Smith EW, Cosson P, Letourneur F (2009) *Dictyostelium* Tom1 participates to an ancestral ESCRT-0 complex. *Traffic* **10:** 161-171

Bosch M, Le KH, Bugyi B, Correia JJ, Renault L, Carlier MF (2007) Analysis of the function of Spire in actin assembly and its synergy with formin and profilin. *Molecular cell* **28:** 555-568

Calvo-Garrido J, Carilla-Latorre S, Kubohara Y, Santos-Rodrigo N, Mesquita A, Soldati T, Golstein P, Escalante R (2010) Autophagy in *Dictyostelium:* genes and pathways, cell death and infection. *Autophagy* **6:** 686-701

Campellone KG, Welch MD (2010) A nucleator arms race: cellular control of actin assembly. *Nature reviews Molecular cell biology* **11:** 237-251

Charette SJ, Cosson P (2004) Preparation of genomic DNA from *Dictyostelium discoideum* for PCR analysis. *BioTechniques* **36:** 574-575

Chen CK, Sawaya MR, Phillips ML, Reisler E, Quinlan ME (2012) Multiple forms of Spire-actin complexes and their functional consequences. *The Journal of biological chemistry* **287:** 10684-10692

Chereau D, Kerff F, Graceffa P, Grabarek Z, Langsetmo K, Dominguez R (2005) Actin-bound structures of Wiskott-Aldrich syndrome protein (WASP)-homology domain 2 and the implications for filament assembly. *Proceedings of the National Academy of Sciences of the United States of America* **102:** 16644-16649

Chisholm RL, Firtel RA (2004) Insights into morphogenesis from a simple developmental system. *Nature reviews Molecular cell biology* **5:** 531-541

Ciccarelli FD, Proukakis C, Patel H, Cross H, Azam S, Patton MA, Bork P, Crosby AH (2003) The identification of a conserved domain in both spartin and spastin, mutated in hereditary spastic paraplegia. *Genomics* **81:** 437-441

Claessens MM, Semmrich C, Ramos L, Bausch AR (2008) Helical twist controls the thickness of F-actin bundles. *Proceedings of the National Academy of Sciences of the United States of America* **105:** 8819-8822

Cleuren YT, Boonstra J (2012) Actin: Structure, Functions and Disease. In *Actin: Structure, Functions and Disease*, Consuelas VA, Minas DJ (eds), Chapter 2, pp 61 - 96. Nova Publishers

Cooper JA, Walker SB, Pollard TD (1983) Pyrene actin: documentation of the validity of a sensitive assay for actin polymerization. *Journal of muscle research and cell motility* **4:** 253-262

Czisch M, Schleicher M, Horger S, Voelter W, Holak TA (1993) Conformation of thymosin beta 4 in water determined by NMR spectroscopy. *European journal of biochemistry / FEBS* **218:** 335-344

Dagert M, Ehrlich SD (1979) Prolonged incubation in calcium chloride improves the competence of Escherichia coli cells. *Gene* **6:** 23-28

Dambournet D, Machicoane M, Chesneau L, Sachse M, Rocancourt M, El Marjou A, Formstecher E, Salomon R, Goud B, Echard A (2011) Rab35 GTPase and OCRL phosphatase remodel lipids and F-actin for successful cytokinesis. *Nature cell biology* **13:** 981-988

Devreotes PN, Zigmond SH (1988) Chemotaxis in eukaryotic cells: a focus on leukocytes and *Dictyostelium*. *Annual review of cell biology* **4:** 649-686

Dimaano C, Jones CB, Hanono A, Curtiss M, Babst M (2008) Ist1 regulates Vps4 localization and assembly. *Molecular biology of the cell* **19:** 465-474

Domazetovska A, Ilkovski B, Kumar V, Valova VA, Vandebrouck A, Hutchinson DO, Robinson PJ, Cooper ST, Sparrow JC, Peckham M, North KN (2007) Intranuclear rod myopathy: molecular pathogenesis and mechanisms of weakness. *Annals of neurology* **62:** 597-608

Ducka AM (2011) Molecular architecture of Spire-actin complexes and its implication for actin filament assembly. Dr. rer. nat Thesis, Abteilung Strukturforschung Biologische NMR-Arbeitsgruppe, Max-Planck-Institut für Biochemie

Ducka AM, Joel P, Popowicz GM, Trybus KM, Schleicher M, Noegel AA, Huber R, Holak TA, Sitar T (2010) Structures of actin-bound Wiskott-Aldrich syndrome protein homology 2 (WH2) domains of Spire and the implication for filament nucleation. *Proceedings of the National Academy of Sciences of the United States of America* **107:** 11757-11762

Eichinger L, Noegel AA, Schleicher M (1991) Domain structure in actin-binding proteins: expression and functional characterization of truncated severin. *The Journal of cell biology* **112:** 665-676

Eichinger L, Pachebat JA, Glockner G, Rajandream MA, Sucgang R, Berriman M, Song J, Olsen R, Szafranski K, Xu Q, Tunggal B, Kummerfeld S, Madera M, Konfortov BA, Rivero F, Bankier AT, Lehmann R, Hamlin N, Davies R, Gaudet P, Fey P, Pilcher K, Chen G, Saunders D, Sodergren E, Davis P, Kerhornou A, Nie X, Hall N, Anjard C, Hemphill L, Bason N, Farbrother P, Desany B, Just E, Morio T, Rost R, Churcher C, Cooper J, Haydock S, van Driessche N, Cronin A, Goodhead I, Muzny D, Mourier

T, Pain A, Lu M, Harper D, Lindsay R, Hauser H, James K, Quiles M, Madan Babu M, Saito T, Buchrieser C, Wardroper A, Felder M, Thangavelu M, Johnson D, Knights A, Loulseged H, Mungall K, Oliver K, Price C, Quail MA, Urushihara H, Hernandez J, Rabbinowitsch E, Steffen D, Sanders M, Ma J, Kohara Y, Sharp S, Simmonds M, Spiegler S, Tivey A, Sugano S, White B, Walker D, Woodward J, Winckler T, Tanaka Y, Shaulsky G, Schleicher M, Weinstock G, Rosenthal A, Cox EC, Chisholm RL, Gibbs R, Loomis WF, Platzer M, Kay RR, Williams J, Dear PH, Noegel AA, Barrell B, Kuspa A (2005) The genome of the social amoeba *Dictyostelium discoideum*. *Nature* **435:** 43-57

Entian KD, Schuster T, Hegemann JH, Becher D, Feldmann H, Guldener U, Gotz R, Hansen M, Hollenberg CP, Jansen G, Kramer W, Klein S, Kotter P, Kricke J, Launhardt H, Mannhaupt G, Maierl A, Meyer P, Mewes W, Munder T, Niedenthal RK, Ramezani Rad M, Rohmer A, Romer A, Hinnen A, et al. (1999) Functional analysis of 150 deletion mutants in *Saccharomyces cerevisiae* by a systematic approach. *Molecular & general genetics : MGG* **262:** 683-702

Faix J, Clougherty C, Konzok A, Mintert U, Murphy J, Albrecht R, Muhlbauer B, Kuhlmann J (1998) The IQGAP-related protein DGAP1 interacts with Rac and is involved in the modulation of the F-actin cytoskeleton and control of cell motility. *Journal of cell science* **111 (Pt 20):** 3059-3071

Faix J, Kreppel L, Shaulsky G, Schleicher M, Kimmel AR (2004) A rapid and efficient method to generate multiple gene disruptions in *Dictyostelium discoideum* using a single selectable marker and the Cre-loxP system. *Nucleic acids research* **32:** e143

Field J, Nikawa J, Broek D, MacDonald B, Rodgers L, Wilson IA, Lerner RA, Wigler M (1988) Purification of a RAS-responsive adenylyl cyclase complex from *Saccharomyces cerevisiae* by use of an epitope addition method. *Molecular and cellular biology* **8:** 2159-2165

Field J, Vojtek A, Ballester R, Bolger G, Colicelli J, Ferguson K, Gerst J, Kataoka T, Michaeli T, Powers S, et al. (1990) Cloning and characterization of CAP, the *S. cerevisiae* gene encoding the 70 kd adenylyl cyclase-associated protein. *Cell* **61:** 319-327

Filimonenko M, Stuffers S, Raiborg C, Yamamoto A, Malerod L, Fisher EM, Isaacs A, Brech A, Stenmark H, Simonsen A (2007) Functional multivesicular bodies are required for autophagic clearance of protein aggregates associated with neurodegenerative disease. *The Journal of cell biology* **179:** 485-500

Fujita H, Yamanaka M, Imamura K, Tanaka Y, Nara A, Yoshimori T, Yokota S, Himeno M (2003) A dominant negative form of the AAA ATPase SKD1/VPS4 impairs membrane trafficking out of endosomal/lysosomal compartments: class E vps phenotype in mammalian cells. *Journal of cell science* **116:** 401-414

Fukui Y (1978) Intranuclear actin bundles induced by dimethyl sulfoxide in interphase nucleus of *Dictyostelium*. *The Journal of cell biology* **76:** 146-157

Ghazi-Tabatabai S, Saksena S, Short JM, Pobbati AV, Veprintsev DB, Crowther RA, Emr SD, Egelman EH, Williams RL (2008) Structure and disassembly of filaments formed by the ESCRT-III subunit Vps24. *Structure* **16:** 1345-1356

Glockner G, Eichinger L, Szafranski K, Pachebat JA, Bankier AT, Dear PH, Lehmann R, Baumgart C, Parra G, Abril JF, Guigo R, Kumpf K, Tunggal B, Cox E, Quail MA, Platzer M, Rosenthal A, Noegel AA (2002) Sequence and analysis of chromosome 2 of *Dictyostelium discoideum*. *Nature* **418:** 79-85

Gottwald U, Brokamp R, Karakesisoglou I, Schleicher M, Noegel AA (1996) Identification of a cyclase-associated protein (CAP) homologue in *Dictyostelium discoideum* and characterization of its interaction with actin. *Molecular biology of the cell* **7:** 261-272

Gruenberg J, Stenmark H (2004) The biogenesis of multivesicular endosomes. *Nature reviews Molecular cell biology* **5:** 317-323

Guizetti J, Schermelleh L, Mantler J, Maar S, Poser I, Leonhardt H, Muller-Reichert T, Gerlich DW (2011) Cortical constriction during abscission involves helices of ESCRT-III-dependent filaments. *Science* **331:** 1616-1620

Halliburton WD (1887) On Muscle-Plasma. *The Journal of physiology* **8:** 133-202

Hanson PI, Roth R, Lin Y, Heuser JE (2008) Plasma membrane deformation by circular arrays of ESCRT-III protein filaments. *The Journal of cell biology* **180:** 389-402

Hurley JH, Hanson PI (2010) Membrane budding and scission by the ESCRT machinery: it's all in the neck. *Nature reviews Molecular cell biology* **11:** 556-566

Hutchinson DO, Charlton A, Laing NG, Ilkovski B, North KN (2006) Autosomal dominant nemaline myopathy with intranuclear rods due to mutation of the skeletal muscle ACTA1 gene: clinical and pathological variability within a kindred. *Neuromuscular disorders : NMD* **16:** 113-121

Israel L (2002) Domänenanalyse des Cyclase-assoziierten Proteins (CAP) und Charakterisierung von Filactin, einem neuartigen actinähnlichen Protein aus *Dictyostelium discoideum*. Dr. rer. nat Thesis, Institut für Zellbiologie, Ludwig-Maximilians-Universität, Munich

Janssen KP, Eichinger L, Janmey PA, Noegel AA, Schliwa M, Witke W, Schleicher M (1996) Viscoelastic properties of F-actin solutions in the presence of normal and mutated actin-binding proteins. *Archives of biochemistry and biophysics* **325:** 183-189

Joseph JM, Fey P, Ramalingam N, Liu XI, Rohlfs M, Noegel AA, Muller-Taubenberger A, Glockner G, Schleicher M (2008) The actinome of *Dictyostelium discoideum* in comparison to actins and actin-related proteins from other organisms. *PloS one* **3:** e2654

Kaimaktchiev V, Goebel H, Laing N, Narus M, Weeks D, Nixon R (2006) Intranuclear nemaline rod myopathy. *Muscle & nerve* **34:** 369-372

Katzmann DJ, Babst M, Emr SD (2001) Ubiquitin-dependent sorting into the multivesicular body pathway requires the function of a conserved endosomal protein sorting complex, ESCRT-I. *Cell* **106:** 145-155

Kerkhoff E (2006) Cellular functions of the Spir actin-nucleation factors. *Trends in cell biology* **16:** 477-483

Kerkhoff E, Simpson JC, Leberfinger CB, Otto IM, Doerks T, Bork P, Rapp UR, Raabe T, Pepperkok R (2001) The Spir actin organizers are involved in vesicle transport processes. *Current biology : CB* **11:** 1963-1968

Kieffer C, Skalicky JJ, Morita E, De Domenico I, Ward DM, Kaplan J, Sundquist WI (2008) Two distinct modes of ESCRT-III recognition are required for VPS4 functions in lysosomal protein targeting and HIV-1 budding. *Developmental cell* **15:** 62-73

Kouyama T, Mihashi K (1981) Fluorimetry study of N-(1-pyrenyl)iodoacetamide-labelled F-actin. Local structural change of actin protomer both on polymerization and on binding of heavy meromyosin. *European journal of biochemistry / FEBS* **114:** 33-38

Ksiazek D, Brandstetter H, Israel L, Bourenkov GP, Katchalova G, Janssen KP, Bartunik HD, Noegel AA, Schleicher M, Holak TA (2003) Structure of the N-terminal domain of the adenylyl cyclase-associated protein (CAP) from *Dictyostelium discoideum*. *Structure* **11:** 1171-1178

Laemmli UK (1970) Cleavage of structural proteins during the assembly of the head of bacteriophage T4. *Nature* **227:** 680-685

Larkin MA, Blackshields G, Brown NP, Chenna R, McGettigan PA, McWilliam H, Valentin F, Wallace IM, Wilm A, Lopez R, Thompson JD, Gibson TJ, Higgins DG (2007) Clustal W and Clustal X version 2.0. *Bioinformatics* **23:** 2947-2948

Lata S, Schoehn G, Jain A, Pires R, Piehler J, Gottlinger HG, Weissenhorn W (2008) Helical structures of ESCRT-III are disassembled by VPS4. *Science* **321:** 1354-1357

Lee JA, Beigneux A, Ahmad ST, Young SG, Gao FB (2007) ESCRT-III dysfunction causes autophagosome accumulation and neurodegeneration. *Current biology : CB* **17:** 1561-1567

Littlefield RS, Fowler VM (2008) Thin filament length regulation in striated muscle sarcomeres: pointed-end dynamics go beyond a nebulin ruler. *Seminars in cell & developmental biology* **19:** 511-519

Liverman AD, Cheng HC, Trosky JE, Leung DW, Yarbrough ML, Burdette DL, Rosen MK, Orth K (2007) Arp2/3-independent assembly of actin by Vibrio type III effector VopL. *Proceedings of the National Academy of Sciences of the United States of America* **104:** 17117-17122

MacLean-Fletcher SD, Pollard TD (1980) Viscometric analysis of the gelation of Acanthamoeba extracts and purification of two gelation factors. *The Journal of cell biology* **85:** 414-428

Makkonen M, Bertling E, Chebotareva NA, Baum J, Lappalainen P (2013) Mammalian and malaria parasite cyclase-associated proteins catalyze nucleotide exchange on G-actin through a conserved mechanism. *The Journal of biological chemistry* **288:** 984-994

Manseau LJ, Schupbach T (1989) cappuccino and spire: two unique maternal-effect loci required for both the anteroposterior and dorsoventral patterns of the Drosophila embryo. *Genes & development* **3:** 1437-1452

Mattei S, Klein G, Satre M, Aubry L (2006) Trafficking and developmental signaling: Alix at the crossroads. *European journal of cell biology* **85:** 925-936

McCoy AJ, Fucini P, Noegel AA, Stewart M (1999) Structural basis for dimerization of the Dictyostelium gelation factor (ABP120) rod. *Nature structural biology* **6:** 836-841

McHugh KM, Crawford K, Lessard JL (1991) A comprehensive analysis of the developmental and tissue-specific expression of the isoactin multigene family in the rat. *Developmental biology* **148:** 442-458

McKinney EC, Meagher RB (1998) Members of the Arabidopsis actin gene family are widely dispersed in the genome. *Genetics* **149:** 663-675

McRobbie SJ, Newell PC (1983) Changes in actin associated with the cytoskeleton following chemotactic stimulation of *dictyostelium discoideum*. *Biochemical and biophysical research communications* **115:** 351-359

Metcalf D, Isaacs AM (2010) The role of ESCRT proteins in fusion events involving lysosomes, endosomes and autophagosomes. *Biochemical Society transactions* **38:** 1469-1473

Minamide LS, Maiti S, Boyle JA, Davis RC, Coppinger JA, Bao Y, Huang TY, Yates J, Bokoch GM, Bamburg JR (2010) Isolation and characterization of cytoplasmic cofilin-actin rods. *The Journal of biological chemistry* **285:** 5450-5460

Moriyama K, Yahara I (2002) Human CAP1 is a key factor in the recycling of cofilin and actin for rapid actin turnover. *Journal of cell science* **115:** 1591-1601

Muziol T, Pineda-Molina E, Ravelli RB, Zamborlini A, Usami Y, Gottlinger H, Weissenhorn W (2006) Structural basis for budding by the ESCRT-III factor CHMP3. *Developmental cell* **10:** 821-830

Nara A, Mizushima N, Yamamoto A, Kabeya Y, Ohsumi Y, Yoshimori T (2002) SKD1 AAA ATPase-dependent endosomal transport is involved in autolysosome formation. *Cell structure and function* **27:** 29-37

Nishida E, Iida K, Yonezawa N, Koyasu S, Yahara I, Sakai H (1987) Cofilin is a component of intranuclear and cytoplasmic actin rods induced in cultured cells. *Proceedings of the National Academy of Sciences of the United States of America* **84:** 5262-5266

Noegel AA, Blau-Wasser R, Sultana H, Muller R, Israel L, Schleicher M, Patel H, Weijer CJ (2004) The cyclase-associated protein CAP as regulator of cell polarity and cAMP signaling in *Dictyostelium*. *Molecular biology of the cell* **15:** 934-945

Noegel AA, Rivero F, Albrecht R, Janssen KP, Kohler J, Parent CA, Schleicher M (1999) Assessing the role of the ASP56/CAP homologue of *Dictyostelium discoideum* and the requirements for subcellular localization. *Journal of cell science* **112 (Pt 19):** 3195-3203

Nowak KJ, Wattanasirichaigoon D, Goebel HH, Wilce M, Pelin K, Donner K, Jacob RL, Hubner C, Oexle K, Anderson JR, Verity CM, North KN, Iannaccone ST, Muller CR, Nurnberg P, Muntoni F, Sewry C, Hughes I, Sutphen R, Lacson AG, Swoboda KJ, Vigneron J, Wallgren-Pettersson C, Beggs AH, Laing NG (1999) Mutations in the skeletal muscle alpha-actin gene in patients with actin myopathy and nemaline myopathy. *Nature genetics* **23:** 208-212

O'Connell KL, Stults JT (1997) Identification of mouse liver proteins on two-dimensional electrophoresis gels by matrix-assisted laser desorption/ionization mass spectrometry of in situ enzymatic digests. *Electrophoresis* **18:** 349-359

Osborn M, Weber K (1984) Actin paracrystal induction by forskolin and by db-cAMP in CHO cells. *Experimental cell research* **150:** 408-418

Ostermeier C, Brunger AT (1999) Structural basis of Rab effector specificity: crystal structure of the small G protein Rab3A complexed with the effector domain of rabphilin-3A. *Cell* **96:** 363-374

Otto IM, Raabe T, Rennefahrt UE, Bork P, Rapp UR, Kerkhoff E (2000) The p150-Spir protein provides a link between c-Jun N-terminal kinase function and actin reorganization. *Current biology : CB* **10:** 345-348

Parent CA (2004) Making all the right moves: chemotaxis in neutrophils and *Dictyostelium*. *Current opinion in cell biology* **16:** 4-13

Peche V, Shekar S, Leichter M, Korte H, Schroder R, Schleicher M, Holak TA, Clemen CS, Ramanath YB, Pfitzer G, Karakesisoglou I, Noegel AA (2007) CAP2, cyclase-associated protein 2, is a dual compartment protein. *Cellular and molecular life sciences : CMLS* **64:** 2702-2715

Peche VS, Holak TA, Burgute BD, Kosmas K, Kale SP, Wunderlich FT, Elhamine F, Stehle R, Pfitzer G, Nohroudi K, Addicks K, Stockigt F, Schrickel JW, Gallinger J, Schleicher M, Noegel AA (2013) Ablation of cyclase-associated protein 2 (CAP2) leads to cardiomyopathy. *Cellular and molecular life sciences : CMLS* **70:** 527-543

Pfender S, Kuznetsov V, Pleiser S, Kerkhoff E, Schuh M (2011) Spire-type actin nucleators cooperate with Formin-2 to drive asymmetric oocyte division. *Current biology : CB* **21:** 955-960

Piper RC, Katzmann DJ (2007) Biogenesis and function of multivesicular bodies. *Annual review of cell and developmental biology* **23:** 519-547

Popowicz GM, Muller R, Noegel AA, Schleicher M, Huber R, Holak TA (2004) Molecular structure of the rod domain of *dictyostelium* filamin. *Journal of molecular biology* **342:** 1637-1646

Popowicz GM, Schleicher M, Noegel AA, Holak TA (2006) Filamins: promiscuous organizers of the cytoskeleton. *Trends in biochemical sciences* **31:** 411-419

Quinlan ME, Heuser JE, Kerkhoff E, Mullins RD (2005) Drosophila Spire is an actin nucleation factor. *Nature* **433:** 382-388

Quinlan ME, Hilgert S, Bedrossian A, Mullins RD, Kerkhoff E (2007) Regulatory interactions between two actin nucleators, Spire and Cappuccino. *The Journal of cell biology* **179:** 117-128

Ralston KS, Petri WA (2011) The ways of a killer: how does *Entamoeba histolytica* elicit host cell death? *Essays in biochemistry* **51:** 193-210

Raper KB (1935) *Dictyostelium discoideum*, a new species of slime mold from decaying forest leaves. *Journal of Agricultural Research* **50:** 135-147

Rechsteiner M, Rogers SW (1996) PEST sequences and regulation by proteolysis. *Trends in biochemical sciences* **21:** 267-271

Rivero F, Kuspa A, Brokamp R, Matzner M, Noegel AA (1998) Interaptin, an actin-binding protein of the alpha-actinin superfamily in *Dictyostelium discoideum*, is developmentally and cAMP-regulated and associates with intracellular membrane compartments. *The Journal of cell biology* **142:** 735-750

Rogers S, Wells R, Rechsteiner M (1986) Amino acid sequences common to rapidly degraded proteins: the PEST hypothesis. *Science* **234:** 364-368

Romans P, Firtel RA, Saxe CL, 3rd (1985) Gene-specific expression of the actin multigene family of *Dictyostelium discoideum*. *Journal of molecular biology* **186:** 337-355

Rosales-Nieves AE, Johndrow JE, Keller LC, Magie CR, Pinto-Santini DM, Parkhurst SM (2006) Coordination of microtubule and microfilament dynamics by Drosophila Rho1, Spire and Cappuccino. *Nature cell biology* **8:** 367-376

Rothbauer U, Zolghadr K, Muyldermans S, Schepers A, Cardoso MC, Leonhardt H (2008) A versatile nanotrap for biochemical and functional studies with fluorescent fusion proteins. *Molecular & cellular proteomics : MCP* **7:** 282-289

Rue SM, Mattei S, Saksena S, Emr SD (2008) Novel Ist1-Did2 complex functions at a late step in multivesicular body sorting. *Molecular biology of the cell* **19:** 475-484

Rusten TE, Stenmark H (2009) How do ESCRT proteins control autophagy? *Journal of cell science* **122:** 2179-2183

Rusten TE, Vaccari T, Lindmo K, Rodahl LM, Nezis IP, Sem-Jacobsen C, Wendler F, Vincent JP, Brech A, Bilder D, Stenmark H (2007) ESCRTs and Fab1 regulate distinct steps of autophagy. *Current biology : CB* **17:** 1817-1825

Saksena S, Sun J, Chu T, Emr SD (2007) ESCRTing proteins in the endocytic pathway. *Trends in biochemical sciences* **32:** 561-573

Saksena S, Wahlman J, Teis D, Johnson AE, Emr SD (2009) Functional reconstitution of ESCRT-III assembly and disassembly. *Cell* **136:** 97-109

Sambrook J, Russel DW (2001) *Molecular Cloning*, 3rd edition edn edn. New York: Cold Spring Harbour Laboratory.

Sameshima M, Kishi Y, Osumi M, Mahadeo D, Cotter DA (2000) Novel actin cytoskeleton: actin tubules. *Cell structure and function* **25:** 291-295

Schmoller KM, Semmrich C, Bausch AR (2011) Slow down of actin depolymerization by cross-linking molecules. *Journal of structural biology* **173:** 350-357

Schnuchel A, Wiltscheck R, Eichinger L, Schleicher M, Holak TA (1995) Structure of severin domain 2 in solution. *Journal of molecular biology* **247:** 21-27

Schwalb M, Roth R (1970) Axenic growth and development of the cellular Slime Mould, *Dictyostelium discoideum*. *Journal of general microbiology* **60:** 283-286

Sept D, McCammon JA (2001) Thermodynamics and kinetics of actin filament nucleation. *Biophysical journal* **81:** 667-674

Simpson PA, Spudich JA, Parham P (1984) Monoclonal antibodies prepared against *Dictyostelium* actin: characterization and interactions with actin. *The Journal of cell biology* **99:** 287-295

Sitar T, Gallinger J, Ducka AM, Ikonen TP, Wohlhoefler M, Schmoller KM, Bausch AR, Joel P, Trybus KM, Noegel AA, Schleicher M, Huber R, Holak TA (2011) Molecular architecture of the Spire-actin nucleus and its implication for actin filament assembly. *Proceedings of the National Academy of Sciences of the United States of America* **108:** 19575-19580

Skwarek-Maruszewska A, Hotulainen P, Mattila PK, Lappalainen P (2009) Contractility-dependent actin dynamics in cardiomyocyte sarcomeres. *Journal of cell science* **122:** 2119-2126

Sparrow JC, Nowak KJ, Durling HJ, Beggs AH, Wallgren-Pettersson C, Romero N, Nonaka I, Laing NG (2003) Muscle disease caused by mutations in the skeletal muscle alpha-actin gene (ACTA1). *Neuromuscular disorders : NMD* **13:** 519-531

Spudich JA, Watt S (1971) The regulation of rabbit skeletal muscle contraction. I. Biochemical studies of the interaction of the tropomyosin-troponin complex with actin and the proteolytic fragments of myosin. *The Journal of biological chemistry* **246:** 4866-4871

Stossel TP, Condeelis J, Cooley L, Hartwig JH, Noegel A, Schleicher M, Shapiro SS (2001) Filamins as integrators of cell mechanics and signalling. *Nature reviews Molecular cell biology* **2:** 138-145

Straub FB (1942) Actin. *Studies from the Institute of Medical Chemistry University Szeged* **2:** 3-15

Sultana H, Rivero F, Blau-Wasser R, Schwager S, Balbo A, Bozzaro S, Schleicher M, Noegel AA (2005) Cyclase-associated protein is essential for the functioning of the endo-lysosomal system and provides a link to the actin cytoskeleton. *Traffic* **6:** 930-946

Tam VC, Serruto D, Dziejman M, Brieher W, Mekalanos JJ (2007) A type III secretion system in Vibrio cholerae translocates a formin/spire hybrid-like actin nucleator to promote intestinal colonization. *Cell host & microbe* **1:** 95-107

Urushihara H, Morio T, Saito T, Kohara Y, Koriki E, Ochiai H, Maeda M, Williams JG, Takeuchi I, Tanaka Y (2004) Analyses of cDNAs from growth and slug stages of *Dictyostelium discoideum*. *Nucleic acids research* **32:** 1647-1653

Vandebrouck A, Domazetovska A, Mokbel N, Cooper ST, Ilkovski B, North KN (2010) In vitro analysis of rod composition and actin dynamics in inherited myopathies. *Journal of neuropathology and experimental neurology* **69:** 429-441

Vandekerckhove J, Weber K (1978) At least six different actins are expressed in a higher mammal: an analysis based on the amino acid sequence of the amino-terminal tryptic peptide. *Journal of molecular biology* **126:** 783-802

Vandekerckhove J, Weber K (1980) Vegetative *Dictyostelium* cells containing 17 actin genes express a single major actin. *Nature* **284:** 475-477

Watts DJ, Ashworth JM (1970) Growth of myxamoebae of the cellular slime mould *Dictyostelium discoideum* in axenic culture. *Biochemical Journal* **119:** 171-174

Wegner A (1976) Head to tail polymerization of actin. *Journal of molecular biology* **108:** 139-150

Westphal M, Jungbluth A, Heidecker M, Muhlbauer B, Heizer C, Schwartz JM, Marriott G, Gerisch G (1997) Microfilament dynamics during cell movement and chemotaxis monitored using a GFP-actin fusion protein. *Current biology : CB* **7:** 176-183

WHO (1997) Amoebiasis. *WHO Weekly Epidemiologic Record* **72:** 97–100.

Williams RL, Urbe S (2007) The emerging shape of the ESCRT machinery. *Nature reviews Molecular cell biology* **8:** 355-368

Xia J, Wang W, Li L, Liu Z, Liu M, Yang D (2012) Inhibition of HBV replication by VPS4B and its dominant negative mutant VPS4B-K180Q in vivo. *Journal of Huazhong University of Science and Technology Medical sciences = Hua zhong ke ji da xue xue bao Yi xue Ying De wen ban = Huazhong keji daxue xuebao Yixue Yingdewen ban* **32:** 311-316

Xiao J, Chen XW, Davies BA, Saltiel AR, Katzmann DJ, Xu Z (2009) Structural basis of Ist1 function and Ist1-Did2 interaction in the multivesicular body pathway and cytokinesis. *Molecular biology of the cell* **20:** 3514-3524

Yu Z, Gonciarz MD, Sundquist WI, Hill CP, Jensen GJ (2008) Cryo-EM structure of dodecameric Vps4p and its 2:1 complex with Vta1p. *Journal of molecular biology* **377:** 364-377

Zelicof A, Protopopov V, David D, Lin XY, Lustgarten V, Gerst JE (1996) Two separate functions are encoded by the carboxyl-terminal domains of the yeast cyclase-associated protein and its mammalian homologs. Dimerization and actin binding. *The Journal of biological chemistry* **271:** 18243-18252

Zuchero JB, Coutts AS, Quinlan ME, Thangue NB, Mullins RD (2009) p53-cofactor JMY is a multifunctional actin nucleation factor. *Nature cell biology* **11:** 451-459

List of Figures

List of Tables

Acknowledgements

First of all, I want to thank *Prof. Dr. Michael Schleicher* for providing an excellent, encouraging working environment. He is an outstanding supervisor, very precious colleague and friend. Special thanks for ALWAYS taking the time to answer my questions. Thank you for your apparently unlimited knowledge of science (and everything else!), your caring support, mentoring and inspiration during my work. An immeasurable part both of my professional and personal development is due to you.

Many thanks go to *Prof. Dr. Barbara Conradt* for assessing this thesis. I learned a lot from you during my Diploma thesis under your supervision which provided an excellent basis, mindset and enthusiasm to pursue this work.

I thank *Prof. Dr. Tad Holak* and his lab for inspiring discussions and providing Spire protein constructs. Many thanks also go to *Prof. Dr. Angelika Noegel*, *Prof. Dr. Jan Faix*, *Prof. Dr. Ludwig Eichinger*, *Prof. Dr. Andreas Bausch* and *Prof. Dr. Wolfgang Baumeister* for sharing precious reagents, cell lines and lab equipment.

I want to thank all lab members for creating such a great working atmosphere where I found all sorts of help, support, motivation and friends. It was a great pleasure to work with you. I am indebted to *PD Dr. Annette Müller-Taubenberger* for sharing advice, valuable reagents and cell lines. Very special thanks go to *Daniela Rieger*, my best bench mate and undisputed Actin-Queen! The past few years would not have been as much fun without you. I thank *Dr. Hellen Ishikawa-Ankerhold* for great teamwork, scientific discussions and your friendship. I sincerely thank *Dr. Meino Rohlfs*, *Dr. Matthias Samereier*, *Dr. Nagendran Ramalingam, Dr. Petros Batsios, Dr. Peter Kastner, Linda Sanftenberg*, *Heike Roth*, *Dr. Marija Vukajlovic*, *Dr. Dennis Zimmermann, Süleyman Kösem, Thi-Hieu Ho, Maria Beer, Gudrun Trommler, Marlis Fürbringer*, *Stefanie Lindholz* and *Dr. Stéphane Rolland* for their scientific and moral support.

Very special thanks go to my brother and colleague *Christoph Gallinger*. Thanks for your endless support, for providing confidence throughout all phases of my thesis and for being my best friend.

I thank the *Elite Network Of Bavaria* for generous support and providing the possibility to be an active part and elected speaker of the innovative graduate program '*Protein Dynamics in Health and Disease'*. I especially want to thank all the members of this program for stimulating scientific discussions and unforgettable times spent together during the different activities of the program. I also express my gratitude to the SFB 863 for financial support during this thesis.

Finally, very special thanks go to my parents, who always supported me in my plans. Thanks for all your love, trust and patience throughout all the years of my studies. You are the best!